©Copyright 2022

Christi W. Cho

**Characterizing the role of CYP2J2 in clear cell renal cell carcinoma and TKI-mediated cardiotoxicity**

Christi W. Cho

A dissertation

submitted in partial fulfillment of the

requirements for the degree of

Doctor of Philosophy

University of Washington

2022

Reading Committee:

Rheem A. Totah, Chair

Allan E. Rettie

William Atkins

Program Authorized to Offer Degree:

Medicinal Chemistry

University of Washington

**Abstract**

Characterizing the role of CYP2J2 in clear cell renal cell carcinoma and TKI mediated cardiotoxicity

Christi W. Cho

Chair of the Supervisory Committee:

Professor Rheem A. Totah

Department of Medicinal Chemistry

CYP2J2 is the only member of the human CYP2J family, and its expression is largely extrahepatic. The highest expression of human CYP2J2 is in the heart, where its major endogenous function as an arachidonic acid (AA) epoxygenase has been widely investigated. Unlike CYP2Cs, which are other major epoxygenases involved in AA metabolism, CYP2J2 has been shown to form an equal ratio of all four regioisomers of epoxyeicosatrienoic acids (EETs), which are associated with cardioprotection. In addition to its better-recognized role as cardioprotective compounds, EETs are promoters of tumor angiogenesis and, collectively with CYP2J2 expression, have been positively associated with promoting the neoplastic tumor phenotype in numerous cell systems (*1*). The involvement of CYPs in tumorigenesis is not a novel finding. However, a major gap remains in characterizing the role of CYPs, including CYP2J2, during the development and progression of various cancers.

The basal expression of CYP2J2 in the human kidney is low but transcriptomic studies by The Cancer Genome Atlas revealed the mRNA level of CYP2J2 is selectively overexpressed in clear cell renal cell carcinoma (ccRCC). ccRCC is the most common kidney cancer diagnosed in the U.S. and is among the top ten diagnosed cancers. Tumor angiogenesis is one major driver of ccRCC progression. Therefore, investigating CYP2J2 overexpression and EETs in ccRCC to better understand the effect on ccRCC progression would identify a novel role for CYP2J2 in kidney cancer. The current dissertation characterized the role of CYP2J2 in matched ccRCC and normal adjacent tissues and identified changes in the AA pathway using a multi-omics approach. CYP-mediated AA metabolites were also quantified to understand the implication of the altered AA pathway in ccRCC.

The cardioprotective effect of CYP2J2 and 11,12-EET against tyrosine kinase inhibitor (TKI) mediated toxicity was also investigated in this dissertation. TKIs are first- and second-line chemotherapy drugs for ccRCC, but most TKIs on the market are associated with at least one presentation of an adverse cardiac event. The cardiotoxicity of TKIs could result in poor adherence to TKI therapy or cessation of treatment resulting in poor treatment efficacy (*2*). For this study, we selected a panel of TKIs based on literature reports of cardiotoxicity which ranged from having no reported incidence of cardiotoxicity to a black box warning for sudden death due to an adverse cardiac event. The addition of exogenous 11,12-EET in primary human cardiomyocytes following the silencing of CYP2J2 mRNA expression protected the cells against TKI toxicity compared to the vehicle. We also performed transcriptomics to characterize altered pathways in the presence of 11,12-EET during TKI injury which is reported in Chapter 3. Overall,

we investigated the role of CYP2J2 and EETs in two disease states and highlight the dual effect of CYP2J2 expression in this dissertation.

**References**


1. J. G. Jiang *et al.*, Cytochrome P450 2J2 Promotes the Neoplastic Phenotype of Carcinoma Cells and Is Up-regulated in Human Tumors. *Cancer Research* **65**, 4707-4715 (2005).
2. M. Chaar, J. Kamta, S. Ait-Oudhia, Mechanisms, monitoring, and management of tyrosine kinase inhibitors–associated cardiovascular toxicities. *OncoTargets and therapy* **11**, 6227-6227 (2018).

# Table of Contents

# List of Figures

# List of Schemes

# List of Tables

# List of Supplemental Figures

# List of Abbreviations

| Abbreviation | Definition |
|---|---|
| AA | Arachidonic acid |
| AXT | Axitinib |
| ccRCC | Clear cell renal cell carcinoma |
| CBZ | Cabozantinib |
| CYP | Cytochrome P450 |
| DHET | Dihydroxyeicosatrienoic acid |
| DCM | Dilated cardiomyopathy |
| DOX | Doxorubicin |
| EGFR | Endothelial growth factor receptor |
| EET | Epoxyeicosatrienoic acid |
| ERL | Erlotinib |
| Fer-1 | Ferrostatin-1 |
| GFT | Gefitinib |
| HCM | Human cardiomyocyte |
| IMT | Imatinib |
| LNV | Lenvatinib |
| MI | Myocardial infarction |
| NAT | Normal adjacent tissue |
| NLT | Nilotinib |
| PZO | Pazopanib |
| ROS | Reactive oxygen species |
| RCC | Renal cell carcinoma |
| RTK | Receptor tyrosine kinase |
| sEH | Soluble epoxide hydrolase |
| SRF | Sorafenib |
| SNT | Sunitinib |
| TdP | Torsades de pointe |
| TKI | Tyrosine kinase inhibitor |
| VEGFR | Vascular endothelial growth factor receptor |

# Acknowledgements

The last several years have been a true test of patience, resilience, and strength. As the famous idiom goes, it takes a village to raise a child—or in this case, to train a scientist. I am grateful to everyone that influenced this journey, as it helped to shape and curate my training and individuality throughout the years. First, I would like to acknowledge my advisor, Rheem Totah, for allowing me the freedom to explore this dissertation on my own terms. I would next like to thank Ed Kelly, who was an influential figure throughout graduate school. I appreciate your scientific insight, hallway talks, and above all, your passion for science (and dogs)! And to Allan Rettie, thank you for always asking the hard questions and providing the space to think about my work throughout the years critically. Next, I would like to thank Bill Atkins for being a source of support and, most importantly, navigating the department through the pandemic. And finally, I would like to thank Cathy Yeung for being there when it mattered. Thank you to everyone for serving on my committee.

My early training in the Totah lab was influenced by Eric Evangelista, Theresa Aliwarga, Ben Maldonato, and Rob Pelletier. Thank you for everything that you've taught me and continue to teach me. I couldn't have done it without you guys. I would like to give a huge shout-out to the SOP MSC, Dale Whittington, Scott Edgar, Josefin Koehn, Neha Saxena, for your infinite help and true passion for teaching us mass spec. Thank you to the current Totah lab members for braving through the pandemic together, and a special shout out to the Kelly lab members for the friendships formed.

In addition to scientific growth, I owe my personal growth to my friends Quynh Do, Vanessa Lopez, Alex Wiley, Amy Li, and Hayli Larsen, who have each offered me endless advice, wisdom, and support—especially during these last few months. And to the rest of our cohort, Clint Voraurer, Taylor Murphree, and Tianwei Shen, we can't deny we had a lot of fun our first year. And of course, none of this would have been possible without the Med Chem staff, Sarah Lenti, Hazel Valdez, Erik Lidzbarski, Scott O'Neil, and Jeanine Kanov. Thank you for keeping everyone afloat.

Lastly, I would like to acknowledge my family, especially my mom, for always believing in me and giving me the strength to reach the end of this milestone. I'm blessed to be a part of a very big, supportive family, but I would like to especially thank my cousin Sunny for being my biggest motivator and my Aunties for their overwhelming support throughout the years. Thank you to my biggest hype group, Sakada Phal, Maribel Blas, Bianca Delgado, and Eva Kwak, for always reminding me to keep my chin up. And finally, I would like to acknowledge my fur babies, Mia and Teddy, for reminding me to take breaks and go outside often.

## Dedication

*To my mom,*

*For always being by my side.*

**This page was left intentionally blank.**

# Chapter 1

## Introduction

*Some of the studies cited within this chapter were published in a review article in Frontiers in Pharmacology. The original article can be viewed in the following link: https://doi.org/10.3389/fphar.2020.00828.*

### 1.1 Dissertation purpose and organization

The primary purpose of this dissertation is twofold: (i) to extensively characterize the expression and function of CYP2J2 in clear cell renal cell carcinoma (ccRCC) and (ii) to interrogate the cardioprotective role of CYP2J2 and epoxyeicosatrienoic acids (EETs) against tyrosine kinase inhibitor (TKI)-induced toxicity in primary human cardiomyocytes. In this investigation, we will elucidate the previously unknown role of CYP2J2 in the development and progression of ccRCC tumors while examining its better recognized function of cardioprotection against TKI injury.

Chapter 1 comprises background information and literature premise to establish a comprehensive understanding of the various systems and functions that are investigated in this dissertation. Cytochrome P450 enzymes and their critical role in drug metabolism is briefly explored followed by an in-depth review of the enzymology and functional role of CYP2J2. We then conclude this chapter with a detailed summary of two major physiological disorders, ccRCC and drug-induced cardiotoxicity, which provides the context for this study. An extensive characterization of CYP2J2 and related pathways in ccRCC is presented in Chapter 2. We utilized a multi-omics approach to characterize CYP2J2 and the arachidonic acid pathway in ccRCC tumor tissues against matched normal adjacent tissues (NAT). Subsequently, the role of

exogenous 11,12-EET and *CYP2J2* gene modulation against TKI cardiotoxicity in primary human cardiomyocytes is reported in Chapter 3. And lastly, Chapter 4 will comprise the final discussion thus concluding this dissertation.

**1.2 Overview of human cytochrome P450 enzymes**

Human cytochrome P450s (CYPs) are a superfamily of hemoproteins, monooxygenases containing 57 functional genes and 58 pseudogenes that are essential to the metabolism of a diverse range of endogenous and exogenous compounds (*1*). There are 58 CYP proteins that are classified into 18 distinct families which are then further divided into sub-families based on sequence identity (*2, 3*). CYPs convert lipid-soluble compounds (parent drug) to water-soluble compounds (metabolite) that are more readily available for excretion in a process described as phase I metabolism (*3*). Many of these reactions are oxidations (olefin epoxidation, *O*-, *N*-, *S*-dealkylations, hydroxylation) but a handful of uncommon reductive reactions (dehalogenation, denitration) have been observed (*4, 5*).

The majority of drug metabolism occurs in the liver as one of its main organ functions is detoxification. Other sites in the body that facilitate drug metabolism include the small intestine, kidney, and lung; each consisting of a unique expression pattern of CYPs (*2, 6-8*). Six isozymes are primarily responsible for hepatic clearance of ~80% of all pharmaceuticals (the remainder of which is metabolized by non-CYP drug metabolizing enzymes (DME)) (*2, 9*). CYP3A4 expression accounts for nearly a third of all CYP protein content in the liver and its active site promiscuity allows for a wide range of potential substrates (*9, 10*). CYP2D6 hepatic expression is relatively low compared to CYP3A4, however it is responsible for metabolizing

upwards of 20% of drugs (*9*). Other major CYPs that are routinely profiled during drug screening studies include CYP2C8/9, CYP1A2, CYP2C19, and CYP2E1 (*4, 9, 11*). Members of the CYP4 family also minorly participate in drug metabolism but they have been shown to have a greater substrate preference for endogenous compounds such as fatty acids (*12*).

Equally important is their role in the synthesis and catabolism of endogenous substrates that include sterols and fatty acids. Several members of the CYP1-3 families are known to oxidize both exogenous and endogenous steroids but the major enzymes responsible are the CYP7 and CYP11 enzymes. Polyunsaturated fatty acids (PUFAs) include several essential fatty acids such as arachidonic acid (AA), linoleic acid (LA), eicosapentaenoic acid (EPA), and docosahexaenoic acid (DHA). PUFAs are oxidized by several CYPs resulting in active epoxide (CYP2C and CYP2J2) or hydroxyl (CYP4F and CYP4A) metabolites and can be referred to as eicosanoids (*13, 14*). Eicosanoids are important signaling molecules that are involved in regulating the vasculature and inflammation among other important cellular processes. CYPs are currently investigated as anti-cancer targets due to a growing body of evidence of the role of eicosanoids in tumor development (*15*).

### 1.3 Cytochrome P450 2J2

#### 1.3.1 CYP2J2 structure and expression

CYP2J2 belongs to the CYP2 family which accounts for one third of all CYP protein content making it the largest and most diverse family of human CYPs (*16*). Human CYP2J2 protein has 502 amino acids with a molecular weight of 57.7 kDa, and like other CYP2 enzymes, it contains 9 introns and 8 exons (*17*). The enzyme was first identified and isolated in a human

liver cDNA library in the late 1990s and was discovered to have up to 50% sequence identity to other human CYP2 enzymes and ~80% sequence identity to rabbit *CYP2J1 (18)*. It was the first CYP2J isoform identified in the human genome, and to date, no other human CYP2J isoforms have been discovered (*18*). Human *CYP2J2* is highly conserved across different species with sequence identity of 95% in monkey, 79% in dog, 76% in bovine, and greater than 70% with various rat or mouse *Cyp2J* isoforms (*18*).

The hepatic expression of human CYP2J2 is very low hence it's contribution to hepatic drug metabolism is minor and often overlooked. But, in more recent years, there has been a growing interest in CYP2J2 drug metabolism. Lee at al., reported the volume of the active site cavity of CYP2J2 to be similar in size to that of CYP3A4 (1420 Å vs 1585 Å, respectively) (*19*). In their work, 139 compounds were screened in the same study to identify potential novel CYP2J2 substrates and interestingly, uncovered that the site of metabolism by CYP2J2 was more restricted compared to the multiple sites of metabolism by CYP3A4 for overlapping substrates. This led to the suggestion that the cavity surrounding the heme is more constrained in CYP2J2 due to a truncation in the B-4 loop that was taking up space inside of the active site cavity, which was not observed for CYP3A4 (*19*). Therefore, despite having a similar active site volume, the plasticity seems to differ resulting in a more restrictive substrate orientation for CYP2J2 metabolism.

The expression of CYP2J2 is largely extrahepatic in most species. In human, CYP2J2 gene and protein expression is highest in the heart but low basal levels have been determined in liver, kidney, and intestine (though the reported expression levels vary in the literature) (*17, 20, 21*). The bulk of the human CYP2J2 expression data has been interrogated by numerous

techniques including western blot, proteomics, RNA-seq, and RT-qPCR. Northern blot and immunocytochemistry analysis revealed rabbit CYP2J1 expression was highest in the small intestines and undetected in tissues such as kidney and liver (*18*). Some studies have reported low basal gene expression of rabbit CYP2J1 in the kidney and liver, but the data remains contentious. Similarly, RT-qPCR analysis revealed monkey CYP2J2 was highly expressed in the small intestine and low basal levels were detected in the heart despite having the highest sequence homology identity to human CYP2J2 (*18*). Rat CYP2J3 expression was found to be largely hepatic while mouse CYP2J5 expression was highest in kidney tissue (*18*).

### 1.3.2 Polymorphisms and enzyme regulation

Interindividual variation in drug metabolism often derives from genetic variations in DME enzymes that result in multiple sub-populations of poor, intermediate, extensive, and ultrarapid metabolizers (*9*). These genetic mutations are referred to as CYP polymorphisms and are generally a result of single-nucleotide polymorphisms/variants (SNPs or SNVs), copy number variations, translocations and inversions, or insertions and/or deletions (*9*). CYP2D6 is the most polymorphic enzyme with over 100 different allelic variants identified (*22*). Allelic frequency varies depending on the pharmacogenomics of the individual (a major one being ethnicity). Nonetheless, CYP2D6 polymorphisms have resulted in large interindividual variation in drug metabolism (*22*).

Ten functional allelic variants of CYP2J2 have been identified to date with the most common being CYP2J2*7 (rs890293) (*23-26*). CYP2J2*7 results from a single nucleotide substitution of thymine (T) to guanine (G) occurring at the 76$^{th}$ nucleotide upstream of the

translation start codon that results in 50% less transcriptional activity but with no clearly associated changes in functional activity (*24, 25*). The allelic frequency of the *7 variant varies from 2-17% with the lowest occurrence observed in the Han Chinese and Russian populations and the highest observance in individuals of African descent (*25*). Due to the minor role in drug metabolism, clinical implications of CYP2J2 polymorphisms have not been heavily interrogated (e.g., compared with CYP2D6). But there are a handful of studies that have linked CYP2J2*7 polymorphism to increased risk of several health anomalies (*23, 25*). For example, carriers of the SNP variant in the Russian population were associated with an increased risk in cerebral ischemia whereas carriers of African American descent were found to have a significantly lowered risk of coronary heart disease (*27, 28*). Several other studies also investigated the risk association of CYP2J2*7 to cardiovascular disease but found no significant relationship (*25*). Even so, it does not diminish the potential risk association of CYP2J2 polymorphisms and cardiovascular disease and warrants further investigation.

A handful of xenobiotics induce the expression of many CYPs resulting in increased enzyme activity. For example, rifampicin is an antibiotic prescribed to treat tuberculosis. It is also a strong inducer of CYP3A4 (also CYP2C8, CYP2C9, and CYP2C19) and activates *CYP3A4* transcription through the nuclear receptor pregnane X receptor (PXR) (*29, 30*). Other examples of xenobiotic inducers and the affected enzyme includes omeprazole (protein pump inhibitor) and CYP1A2, and phenobarbital (barbiturate) and CYP2B6 (*31, 32*). CYP2J2 expression, on the contrary, is not inducible by canonical xenobiotic inducers. Previous work from our lab interrogated CYP2J2 regulation in human cardiomyocytes and observed a dose-dependent decrease in gene expression when exposed to common antioxidants such as butylated

hydroxyanisole (BHA) and butylated hydroxytoluene (BHT) (*33*). In contrast, exposure to reactive oxygen species resulted in an increase in *CYP2J2* expression by over 3-fold (*34*). CYP2J2 expression has been observed to change under different disease states. Several studies reported preferable cardiac outputs after ischemia-reperfusion injury in mice overexpressing CYP2J2 compared to wildtype mice (*35*). Given the fact that CYP2J2 is not inducible by known CYP inducers and its relatively high expression in heart tissue, suggests a broader importance for the endogenous function of CYP2J2 in pathophysiology which will be the theme of this dissertation.

1.3.3 Xenobiotic substrates and inhibitors

CYP2J2 was identified to be the main enzyme responsible for the *O*-demethylation of astemizole (*36, 37*) and hydroxylation of ebastine (*38*) in human small intestines. The apparent kinetics of astemizole *O*-demethylation by recombinant CYP2J2 was reported to have a Km of 0.65 uM and a Vmax of 1129 pmol/nmol P450/min (*36*). This activity was then inhibited by the addition of arachidonic acid or ebastine which was concentration-dependent in small intestinal microsomes (*37*). Ebastine hydroxylation was shown to be catalyzed by both CYP4F (CYP4F2 and CYP4F12) and CYP2J2. Compared to CYP4F, CYP2J2 was observed to have a lower Km that for CYP4F12 (1.3 vs 3.0 uM, respectively) and a significantly greater Vmax (40.6 vs 0.354 nmol/min/nmol P450, respectively) suggesting CYP2J2 is the major enzyme responsible for this reaction (*38*). Like astemizole *O*-demethylation, ebastine hydroxylation was inhibited by the addition of arachidonic acid and a selective CYP2J2 antibody.

Additionally, several other drugs have been identified as CYP2J2 substrates including terfenadine (antihistamine), tamoxifen (selective estrogen receptor modulator) and cyclosporin (immunosuppressant) (*19, 39*). CYP2J2 has also been shown to metabolize ritonavir (antiretroviral protease inhibitor) and form a selective (albeit minor) metabolite although CYP3A4 and CYP2D6 are the major isoforms involved in its hepatic metabolism (*40*). Kaspera et al., has also suggested that for Individuals carrying the poor metabolizer CYP2D6 polymorphic phenotype, a metabolic switching occurs where the contribution of CYP2J2 increases from 6% to over 20% (*40*). So, despite not being a major contender in overall drug metabolism, it appears to have a major role in certain contexts.

Several potent competitive inhibitors have been identified for CYP2J2 (*41*). Lee et al., reported 42 marketed drugs that had greater than 50% inhibitory activity against CYP2J2 of which danazol was identified to be a potent inhibitor with a Ki of 20 nM. Danazol inhibition was found to be substrate-dependent exhibiting different IC50 values for different substrates (*42*). Similarly, Ren et al., screened a panel of drugs and identified telmisartan (Ki = 0.42 uM), flunarizine (Ki = 0.94 uM), and amodiaquine (Ki = 0.99 uM) to be inhibitory against CYP2J2 and in the case of telmisartan and flunarizine, they were reported to be non-substrate inhibitors (*43*). Most inhibitors of CYP2J2 were not specific but did exhibit greater selectivity over other isoforms. Lafite et al., designed and synthesized several terfenadine analogs that targeted CYP2J2 activity with high affinity and discovered two mechanism-based inhibitors in their panel (*44, 45*). More recently, Lim and colleagues reported CYP2J2 inhibition by acetylshikonin, a natural product, in renal cell carcinoma derived cells (*46*).

1.3.4 Arachidonic acid signaling pathway

Arachidonic acid (AA) is an omega-6 polyunsaturated fatty acid (20:4) that is a precursor to the synthesis of biologically active lipid signaling molecules known as the eicosanoids (Scheme 1). AA is stored esterified in the phospholipid membranes and is released by phospholipase A2 where it is subjected to one of three metabolic fates. The cyclooxygenases (COX) and lipoxygenases (LOX) form prostaglandins (which are later converted to thromboxanes) and leukotrienes, respectively, and play a major role in regulating inflammation (*47, 48*). A third pathway is mediated by a subset of CYP450 enzymes known as epoxygenases and hydroxylases (*49-51*). Epoxygenases (CYP2C8, CYP2C9, CYP2C19, and CYP2J2) oxidize one of four double bonds of AA resulting in the formation of epoxyeicosatrienoic acids (EETs) (*52*). The four regioisomers of EETs are known as 5,6-, 8,9-, 11,12-, and 14,15-EET. The CYP2Cs have been shown to preferably form 11,12- and 14,15-EET while CYP2J2 generates an equal ratio of all four regioisomers (*53, 54*). CYP2J2 is the major epoxygenase responsible for EET formation in the heart tissue (*55*). Hydroxylases (CYP4A and CYP4F) oxidize the terminal carbons (omega or omega-1) resulting in the formation of 19- or 20-hydroxyeicosatetraenoic acids (19- or 20-HETE) (*14*).

Both EETs and HETEs are biologically active and elicit their activity through endocrine, paracrine, and autocrine signaling (*56*). They are known to regulate the vasculature (EETs increase blood flow and 20-HETE decreases blood flow), inflammation (EETs are anti-inflammatory and 20-HETE is pro-inflammatory, and angiogenesis (both promote angiogenesis). In hypertension, 20-HETE has been shown to exacerbate high blood pressure (*57*) while elevated EET levels were shown to be protective (*58*). 20-HETE was also shown to elevated

vascular ROS in atherosclerosis and promote inflammation and the opposite effect was observed in the presence of EETs further exemplifying the diametric functions of both eicosanoids (*59*).

### 1.3.5 Function of CYP2J2 in the heart

Previous work from our laboratory thoroughly investigated the functional and mechanistic role of EETs in the heart. For example, Aliwarga et al. reported that *CYP2J2* transgenic mice exhibited elevated EETs levels after inducing myocardial infarction (MI) which was then associated with an overall better prognosis compared to sham or wildtype mice (*35*). In the study, EETs were shown to reduce overall infarction ratio and reactive oxygen species (ROS) in mouse cardiac tissue suggesting EETs are protective via reducing ROS levels. To further probe the potential antioxidant role of EETs, human cardiomyocytes were cultured under hypoxia in the presence and absence of *CYP2J2* expression and the addition of EETs rescued cell viability (*34*). EETs were also shown to attenuate mitochondrial dysfunction by reducing ROS levels through the induction of superoxide dismutase and catalase in carcinoma cells (*60*). Similarly, EETs were shown to reverse doxorubicin cardiotoxicity in human cardiomyocytes after silencing *CYP2J2* expression which was associated with a decrease in overall ROS levels suggesting EETs are cardioprotective by acting as antioxidants during cardiac injury (*34*). Additionally, CYP2J2 has been shown to modulate a diverse range of signaling pathways in human cardiomyocytes that included pathways involved with ion channels, extracellular matrix, and metabolism (*61*), overall highlighting its important function in the heart.

EETs are further hydrolyzed to their less active diol counterparts known as dihydroxyeicosatrienoic acids (DHETs) by soluble epoxide hydrolase (sEH). One strategy to exploit the cardioprotective properties of EETs is to prolong their half-life by targeting sEH activity and inhibiting the hydrolysis to DHETs (*62-64*). This was recently accomplished by Kitsuka et al. where the authors developed and administered a novel sEH vaccine in rats undergoing MI (*65*) The group reported significantly reduced fibrosis and infarct area that was coupled with preserved cardiac function in the vaccinated rat group compared to the unvaccinated group. The authors further confirmed that the vaccine induced neutralizing antibodies against sEH activity were correlated with an increase in EET/DHET ratio suggesting EETs activity was extended. This is not the first report of developing a therapeutic target to reduce sEH (which has been shown to be anti-hypertensive and anti-inflammatory) but developing a successful targeting agent has been challenging. For example, several urea, carbamate, or amide based chemical inhibitors of sEH are available (*66*). However, many of these compounds have been found to have poor metabolic stability and solubility making them unfit candidates for further drug development (*66*).

### 1.3.6 CYP2J2 in cancer

Several studies have reported elevated expression of CYP2J2 in tumor tissues and cancer cell lines. Jiang et al. conducted a substantial investigation by procuring 130 tumor and normal adjacent tissue samples from patients (*67*). mRNA and protein expression were measured by RT-qPCR and western blot, respectively, and immunohistochemistry (IHC) staining was conducted to determine the localization of CYP2J2. The authors reported elevated CYP2J2

mRNA and protein expression in 101 of 130 tumor pairs and the results were categorized as follows: esophageal squamous cell carcinoma (20 of 31), esophageal adenocarcinoma (4 of 4), pulmonary squamous cell carcinoma (28 of 37), pulmonary adenocarcinoma (18 of 26), small cell pulmonary carcinoma (7 of 8), breast carcinoma (5 of 5), stomach carcinoma (5 of 5), liver carcinoma (10 of 10), and colon adenocarcinoma (4 of 4). CYP2J2 expression could not be detected for the remaining 29 tumors and matched normal adjacent tissues. Interestingly, IHC staining revealed CYP2J2 protein was localized to carcinoma cells while endothelial localization was also evident to a small degree. Nonetheless, Jiang et al. suggested a potential important role for CYP2J2 in tumor development and/or progression. The authors further investigated this claim by examining CYP2J2 expression in multiple carcinoma cell lines. Importantly, CYP2J2 overexpression desensitized the cells to apoptosis favoring a positive tumor phenotype. Murine xenograft models further confirmed the results as it was reported that increased levels of CYP2J2 resulted in a larger, more rapidly growing tumor mass (*67, 68*).

**1.4 Renal cell carcinoma**

1.4.1 The tumor microenvironment and drug resistance

Previously, the cause of malignant cancer was believed to be solely due to the spread of rapidly mutated cells coupled with a downregulation of tumor suppressor genes that supported a growing tumor mass (*69*). In more recent years, however, a growing body of evidence highlights a greater role of the tumor microenvironment (TME). The TME is defined by the National Cancer Institute as *the normal cells, molecules, and blood vessels that surround and feed a tumor cell (70)*. It contains multiple cell types that include malignant cells, immune

response cells and cells responsible for providing structural support. Together, the heterogenous environment serves as a unique ecosystem that optimizes the growth of the tumor mass (*69*). Evidence in the literature suggest the tumor can communicate and influence its microenvironment through the secretion of various signaling molecules resulting in an increase in angiogenesis, and multi-drug resistance (*71-73*). Thus, improving our understanding of the tumor microenvironment and its interplay with cancerous cells may serve as a potential strategy aiding in cancer therapy.

### 1.4.2 Clear cell renal cell carcinoma: disease progression and drug therapy

Renal cell carcinoma (RCC) affects nearly 70,000 adults in the U.S. annually with men being more susceptible than woman (*74*). Several sub-types of RCC exist which include, in order of prevalence, clear cell renal cell carcinoma, papillary renal cell carcinoma, and chromophobe renal cell carcinoma (*75*). Clear cell renal cell carcinoma (ccRCC) is the most diagnosed kidney cancer accounting for nearly 80% of all cases (*76*). ccRCC is histologically distinguishable from other subtypes by its characteristic clear cell phenotype which is a result of lipid and glycogen accumulation in the cytosol (*76*). It develops from the proximal tubules in the renal cortex where most DME are expressed. The most common cause of ccRCC development is a mutation in the von Hippel-Lindau (VHL) tumor suppressor gene which causes the transcriptional activation of numerous growth factors that promote the positive tumor phenotype (*76*).

One of the main growth factors that is highly upregulated in ccRCC is the vascular endothelial growth factor A (VEGFA) (*77*). VEGFA is a growth factor responsible for regulating cell proliferation and angiogenesis through the activation of two key receptor tyrosine kinases

(RTKs): VEGFR-1 and VEGFR-2. As a result, ccRCC is a highly vascular tumor and its growth, maintenance, and metastasis are supported by promoting tumor angiogenesis. Tyrosine kinase inhibitors (TKIs) are a class of anti-angiogenic cancer drugs that target the ATP binding pocket of RTKs (such as VEGFR-1 and VEGFR-2) and prevent the activation of numerous signal transduction cascades (*78*). Since RTKs are highly upregulated in many cancers and potently promote tumor angiogenesis, a strategy to combat this is to target the receptors using small molecule tyrosine kinase inhibitors (TKIs). TKIs are multi-target drugs that are highly susceptible to acquired drug resistance so adjuvant therapy with mTOR inhibitors (e.g. everolimus) or immunotherapy (e.g. bevacizumab) is common.

### 1.4.3 Expression of CYP epoxygenases and hydroxylases in ccRCC

Several CYPs involved in arachidonic acid metabolism are expressed in the proximal tubules of healthy kidneys. For example, the expression of CYP4A11, CYP4F2, CYP4F11, and CYP4F12 were reported (and corroborated by several groups) in healthy kidneys while the expression of CYP2C8, CYP2C9, and CYP2J2 were reported to be equivocal. In ccRCC, however, most of the CYPs are downregulated in tumors *except for CYP2J2* according to RNA-seq data obtained from The Cancer Genome Atlas (TCGA). In fact, CYP2J2 was identified to be one of the top ten most differentially expressed genes in ccRCC. A recent meta-analysis conducted by Zou and colleagues reported that CYP2J2 overexpression was positively correlated with immune cell infiltration (B cells, CD8 +T cells, neutrophils) in ccRCC (*79*). High expression of CYP2J2 was also associated with a more favorable survival outcome compared to patients expressing low levels of ccRCC, thus highlighting a potential role for CYP2J2 in ccRCC progression. Regardless, the role

of EETs or HETEs in ccRCC progression have previously been explored only minimally. Alexanian et al. reported that renal adenocarcinoma cells maintained the ability to generate CYP4F mediated 20-HETE (*80*). Alternatively, inhibiting 20-HETE formation by two potent inhibitors (HET0016 and WIT002) resulted in an overall decrease in cell proliferation in two RCC derived cell lines (786-O and 786-P) while the effects in healthy primary human kidney epithelial cells were minute. WIT002 was also shown to reduce RCC tumor growth in murine xenograft models by up to 84% further suggesting an important role for 20-HETE in tumor progression (*80*).

**1.5 Drug-induced cardiotoxicity**

1.5.1 Chemotherapy drug induced cardiotoxicity and manageability

Direct injury to the heart muscle or an adverse alteration of heart electrophysiology is collectively defined as cardiotoxicity. It is one of the major complications associated with chemotherapy drugs resulting in increased morbidity and mortality (*81-83*). The most common cancer drugs associated with adverse cardiac events include taxanes (e.g. paclitaxel), 5-fluorouracil, and anthracyclines (e.g. doxorubicin) (*84*). These adverse cardiac events are commonly manifested as hypertension, left ventricular dysfunction (heart failure), arrhythmia, myocardial ischemia, and QT prolongation (*81*). Excessive QT prolongation leads to the development of Torsades de pointes (TdP) which is an abnormal heart rhythm that can cause sudden death. Sudden death from cardiotoxicity is rare, but a handful of drugs are branded with a black box warning for severe adverse cardiac events.

The exact mechanism of drug-induced cardiotoxicity is not well elucidated, but it is known that several factors, including genetic predispositions and environmental factors, are

involved (*81*). The most studied class of drugs for cardiotoxicity is the anthracyclines. Anthracyclines, derived from Streptomyces bacterium, are widely used in cancer therapy with the most recognizable in this drug class being doxorubicin (*85*). Anthracycline cardiotoxicity is further classified as acute (onset is within the first week of drug administration), early onset (within the first year) and late onset toxicity (greater than 1 year) (*85*). While risk factors associated with early and late onset anthracycline cardiotoxicity have been identified, it is not understood why acute cardiotoxicity occurs. Acute cardiotoxicity can be reversed through adjusting dose and frequency while more prolonged cardiotoxicity (depending on severity) can be managed with concomitant treatment of ACE inhibitors (*85*). Several factors, however, have been associated with anthracycline cardiotoxicity such as increased levels of reactive oxygen and reactive nitrogen species, an increase in lipid peroxidation resulting in ferroptosis, and mitochondrial dysfunction (*81-83, 86*).

### 1.5.2 Tyrosine kinase inhibitor induced cardiotoxicity

Currently, there are over 50 FDA approved TKIs on the market and nearly 75% of all TKIs are known to cause at least one adverse cardiac event (*87*). The frequency and mechanism of TKI cardiotoxicity appears to be drug specific but several common factors include mitochondrial dysfunction, increased reactive oxygen species, and disruptions of off-target kinase signal transduction (*87*). Unlike anthracycline cardiotoxicity, most TKI cardiotoxicity is acute and reversible with early detection and management. Some common cardiotoxic presentations include arrhythmia, left ventricular dysfunction, and QT prolongation though direct injury to cardiomyocytes resulting in myocardial infarction and heart failure have been observed.(*87*)

Nilotinib, approved for use in chronic myeloid leukemia, is a multi-target TKI that inhibits BCR-ABL, c-KIT, and PDGFRA. It has a black box warning for severe QT prolongation which has been reported to progress to TdP and cause sudden death in a small number of cases (*88, 89*). Several multi-target TKIs are approved for the use in metastatic ccRCC which includes sorafenib, sunitinib, cabozantinib, lenvatinib, pazopanib, and axitinib (*87*). Collectively, these TKIs target VEGF receptors 1, 2, and 3 and PDGFR while other receptor targets do not overlap (*87*). The TKIs are prescribed in combination with immunotherapy for optimal results. For example, the International Metastatic Database Consortium recommends concomitant therapy pairing cabozantinib + nivolumab, axitinib + pembrolizumab, and Lenvatinib + pembrolizumab (*90*). Nonetheless, each of the TKIs have been associated with at least one adverse cardiac event with varying degree of injury which is summarized in Chapter 3, Table I.

**1.6 Summary**

CYP2J2 and EETs have long been recognized for their cardioprotective role in the heart. But in more recent years, emerging evidence suggests a novel role for CYP2J2 expression and EETs in the development and/or progression of tumors. Transcriptomic studies by The Cancer Genome Atlas have shown the expression of CYP2J2 is significantly increased in ccRCC tumors but in other subtypes of renal cancer, CYP2J2 is not overexpressed. Therefore, we hypothesized that the selective overexpression of CYP2J2 in ccRCC is a positive driver in tumorigenesis through the subsequent increase in EET levels. We characterized CYP2J2 expression in ccRCC tumor tissues and matched normal adjacent tissues using a multi-omics approach and characterized the altered CYP mediated arachidonic acid pathway in Chapter 2. In addition, we

investigated the cardioprotective role of CYP2J2 against TKI-induced cardiotoxicity which is reported in Chapter 3.

**Figures**

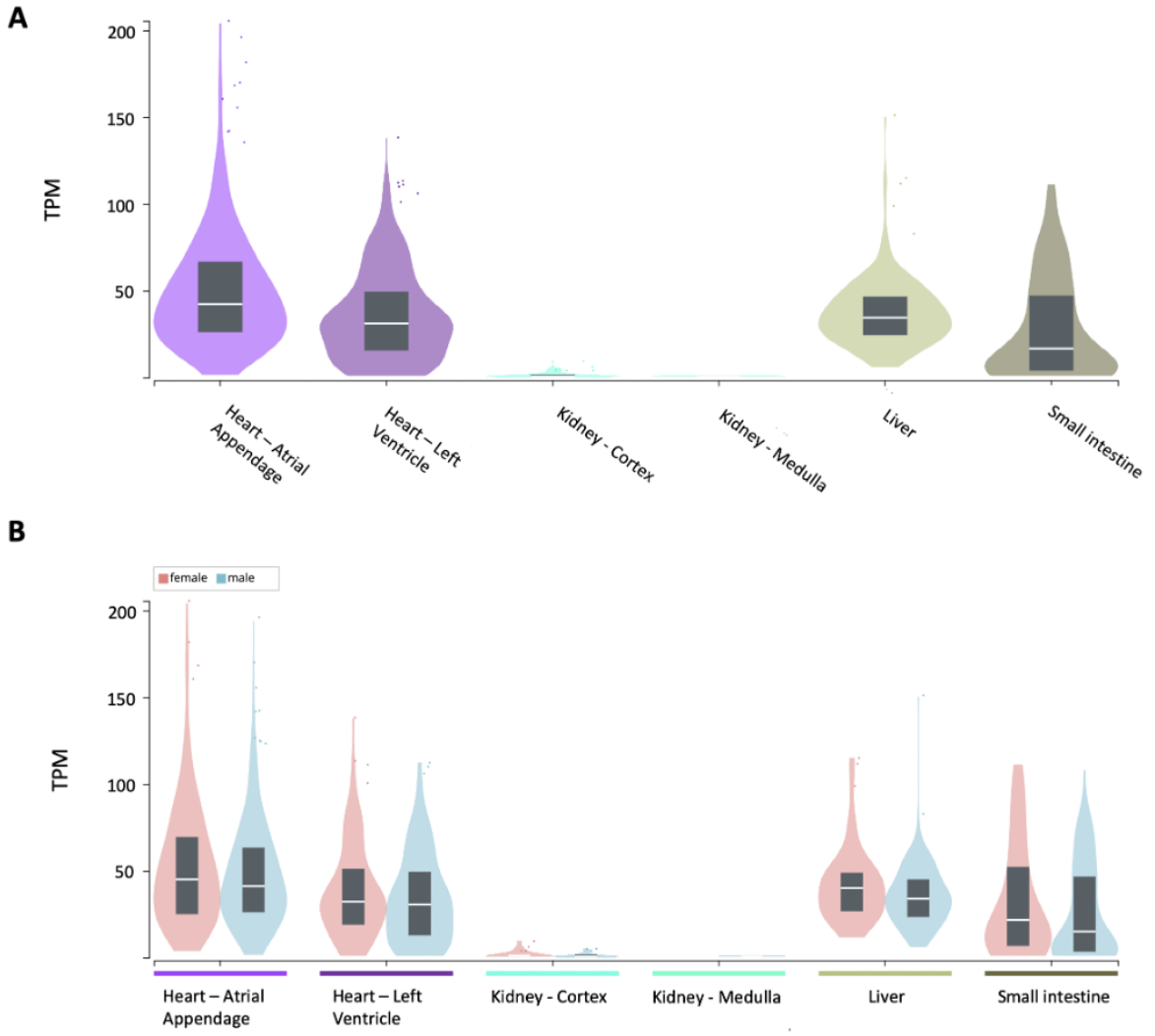


**Figure 1.1. *CYP2J2* expression in heart, kidney, liver, and small intestine tissues.** A) Total *CYP2J2* expression; B) Sex based stratification of *CYP2J2* expression. This figure was adapted from the Bulk tissue gene expression for CYP2J2 (ENSG00000134716.9) database from the GTEx Portal (dbGaP Accession phs000424.v8.p2).

**Schemes**

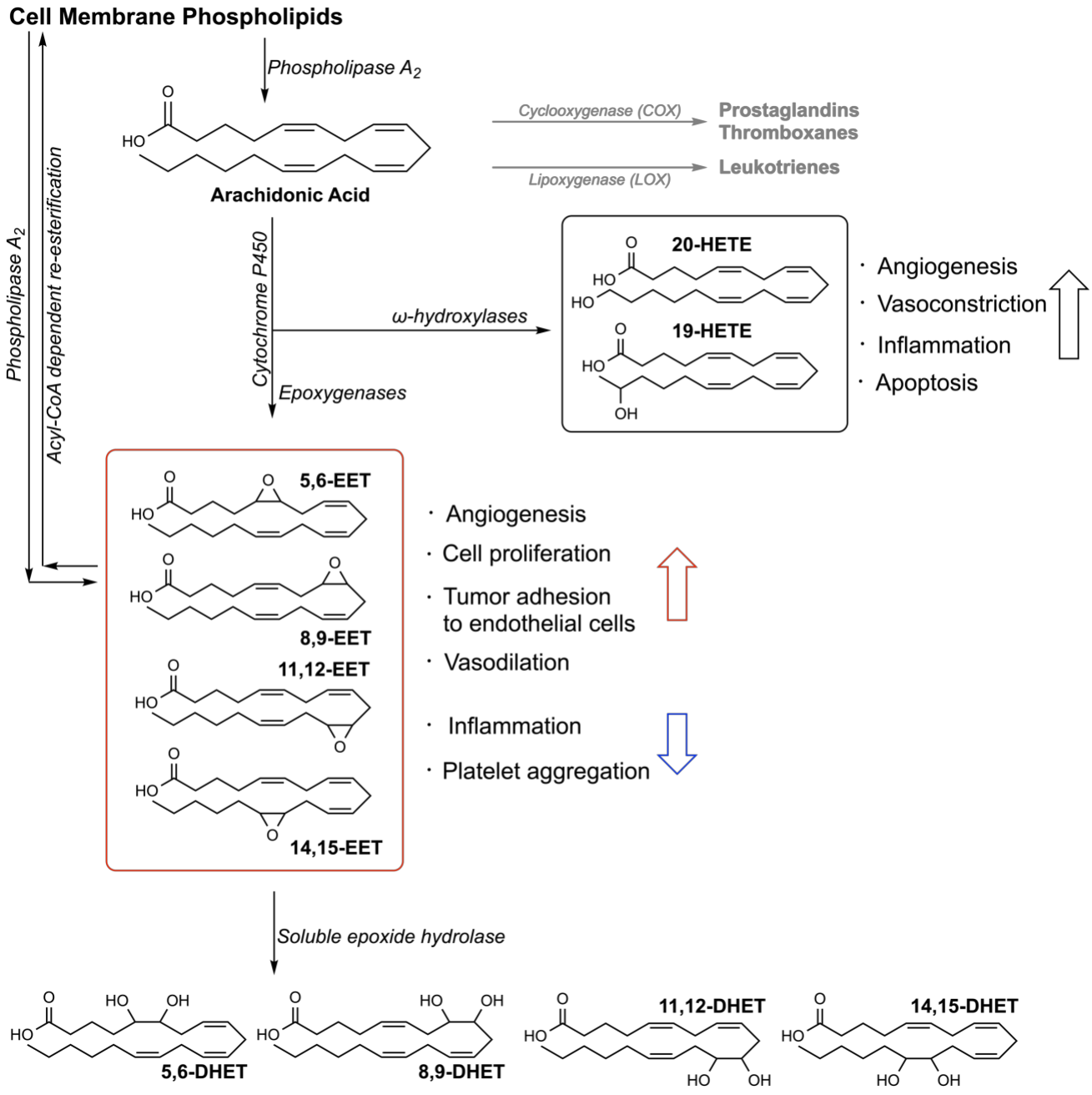


**Scheme 1. CYP mediated arachidonic acid pathway.**

**References**


1. F. P. Guengerich, Z. L. Wu, C. J. Bartleson, Function of human cytochrome P450s: characterization of the orphans. *Biochemical and biophysical research communications* **338**, 465-469 (2005).
2. F. P. Guengerich, Drug Metabolism: Cytochrome P450. *Reference Module in Biomedical Sciences*, (2021).
3. P. B. A. M. McDonnell, P. B. C. H. Dang, Basic Review of the Cytochrome P450 System. *Journal of the advanced practitioner in oncology* **4**, 263-263 (2013).
4. F. P. Guengerich, Common and uncommon cytochrome P450 reactions related to metabolism and chemical toxicity. *Chemical Research in Toxicology* **14**, 611-650 (2001).
5. J. B. Y. H. Behrendorff, Reductive Cytochrome P450 Reactions and Their Potential Role in Bioremediation. *Frontiers in Microbiology* **12**, (2021).
6. X. Ding, L. S. Kaminsky, Human extrahepatic cytochromes P450: function in xenobiotic metabolism and tissue-selective chemical toxicity in the respiratory and gastrointestinal tracts. *Annual review of pharmacology and toxicology* **43**, 149-173 (2003).
7. M. Zhao *et al.*, Cytochrome p450 enzymes and drug metabolism in humans. *International Journal of Molecular Sciences* **22**, 12808-12808 (2021).
8. M. F. Paine *et al.*, THE HUMAN INTESTINAL CYTOCHROME P450 "PIE".
9. U. M. Zanger, M. Schwab, Cytochrome P450 enzymes in drug metabolism: Regulation of gene expression, enzyme activities, and impact of genetic variation. *Pharmacology & Therapeutics* **138**, 103-141 (2013).
10. K. Venkatakrishnan, L. L. Von Moltke, D. J. Greenblatt, Human drug metabolism and the cytochromes P450: Application and relevance of in vitro models. *Journal of Clinical Pharmacology* **41**, 1149-1179 (2001).
11. M. Ingelman-Sundberg, Human drug metabolising cytochrome P450 enzymes: Properties and polymorphisms. *Naunyn-Schmiedeberg's Archives of Pharmacology* **369**, 89-104 (2004).
12. A. E. C. M. Simpson, The cytochrome P450 4 (CYP4) family. *General pharmacology* **28**, 351-359 (1997).
13. M. Sisignano, D. Steinhilber, M. J. Parnham, G. Geisslinger, Exploring CYP2J2: lipid mediators, inhibitors and therapeutic implications. *Drug Discovery Today* **25**, 1744-1753 (2020).
14. K. D. Ni, J. Y. Liu, The Functions of Cytochrome P450 ω-hydroxylases and the Associated Eicosanoids in Inflammation-Related Diseases. *Frontiers in Pharmacology* **12**, 2505-2505 (2021).
15. F. P. Guengerich, Intersection of Roles of Cytochrome P450 Enzymes with Xenobiotic and Endogenous Substrates. Relevance to Toxicity and Drug Interactions. *Chemical research in toxicology* **30**, 2-2 (2017).
16. S. M. G. Hoffman, D. R. Nelson, D. S. Keeney, Organization, structure and evolution of the CYP2 gene cluster on human chromosome 19. *Pharmacogenetics* **11**, 687-698 (2001).
17. M. Murray. (2016).

18. S. Wu, C. R. Moomaw, K. B. Tomer, J. R. Falck, D. C. Zeldin, Molecular cloning and expression of CYP2J2, a human cytochrome P450 arachidonic acid epoxygenase highly expressed in heart. *The Journal of biological chemistry* **271**, 3460-3468 (1996).
19. C. A. Lee *et al.*, Identifying a selective substrate and inhibitor pair for the evaluation of CYP2J2 activity. *Drug Metabolism and Disposition*, (2012).
20. T. C. DeLozier *et al.*, Detection of Human CYP2C8, CYP2C9, and CYP2J2 in Cardiovascular Tissues. *Drug Metabolism and Disposition* **35**, 682-688 (2007).
21. D. C. Zeldin *et al.*, CYP2J subfamily cytochrome P450s in the gastrointestinal tract: Expression, localization, and potential functional significance. *Molecular Pharmacology* **51**, 931-943 (1997).
22. M. Ingelman-Sundberg, Genetic polymorphisms of cytochrome P450 2D6 (CYP2D6): clinical consequences, evolutionary aspects and functional diversity. *The Pharmacogenomics Journal 2005 5:1* **5**, 6-13 (2004).
23. M. Spiecker *et al.*, Risk of coronary artery disease associated with polymorphism of the cytochrome P450 epoxygenase CYP2J2. *Circulation* **110**, 2132-2136 (2004).
24. L. M. King *et al.*, Cloning of CYP2J2 gene and identification of functional polymorphisms. *Molecular pharmacology* **61**, 840-852 (2002).
25. D. S. Berlin, K. Sangkuhl, T. E. Klein, R. B. Altman, PharmGKB summary: cytochrome P450, family 2, subfamily J, polypeptide 2: CYP2J2. *Pharmacogenetics and Genomics* **21**, 308-308 (2011).
26. S. S. Lee *et al.*, Identification and functional characterization of novel CYP2J2 variants: G312R variant causes loss of enzyme catalytic activity. *Pharmacogenetics and Genomics* **15**, 105-113 (2005).
27. C. R. Lee *et al.*, CYP2J2 and CYP2C8 polymorphisms and coronary heart disease risk: The Atherosclerosis Risk in Communities (ARIC) study. *Pharmacogenetics and Genomics* **17**, 349-358 (2007).
28. A. V. Polonikov *et al.*, A common polymorphism G-50T in cytochrome P450 2J2 gene is associated with increased risk of essential hypertension in a Russian population. *content.iospress.com* **24**, 119-126 (2008).
29. F. Yamashita *et al.*, Modeling of Rifampicin-Induced CYP3A4 Activation Dynamics for the Prediction of Clinical Drug-Drug Interactions from In Vitro Data. *PLoS ONE* **8**, 70330-70330 (2013).
30. J. Hakkola, J. Hukkanen, M. Turpeinen, O. Pelkonen, Inhibition and induction of CYP enzymes in humans: an update. *Archives of Toxicology* **94**, 3671-3722 (2020).
31. D. Diaz *et al.*, Omeprazole is an aryl hydrocarbon-like inducer of human hepatic cytochrome P450. *Gastroenterology* **99**, 737-747 (1990).
32. H. Martin *et al.*, Induction of cytochrome P450 2B6 and 3A4 expression by phenobarbital and cyclophosphamide in cultured human liver slices. *Pharmaceutical research* **20**, 557-568 (2003).
33. E. A. Evangelista, R. Kaspera, N. A. Mokadam, J. P. Jones, R. A. Totah, Activity, inhibition, and induction of cytochrome P450 2J2 in adult human primary cardiomyocytes. *Drug Metabolism and Disposition* **41**, 2087-2094 (2013).

34. E. A. Evangelista, R. N. Lemaitre, N. Sotoodehnia, S. A. Gharib, R. A. Totah, CYP2J2 expression in adult ventricular myocytes protects against reactive oxygen species toxicity. *Drug Metabolism and Disposition* **46**, 380-386 (2018).
35. T. Aliwarga *et al.*, Higher Epoxyeicosatrienoic Acids in Cardiomyocytes-Specific CYP2J2 Transgenic Mice Are Associated with Improved Myocardial Remodeling. *Biomedicines*, (2020).
36. S. Matsumoto, T. Hirama, T. Matsubara, K. Nagata, Y. Yamazoe, Involvement of CYP2J2 on the intestinal first-pass metabolism of antihistamine drug, astemizole. *Drug metabolism and disposition: the biological fate of chemicals* **30**, 1240-1245 (2002).
37. S. Matsumoto, T. Hirama, H. J. Kim, K. Nagata, Y. Yamazoe, In vitro inhibition of human small intestinal and liver microsomal astemizole O-demethylation: Different contribution of CYP2J2 in the small intestine and liver. *Xenobiotica* **33**, 615-623 (2003).
38. T. Hashizume *et al.*, Involvement of CYP2J2 and CYP4F12 in the Metabolism of Ebastine in Human Intestinal Microsomes. *Journal of Pharmacology and Experimental Therapeutics* **300**, 298-304 (2002).
39. M. Xu, W. Ju, H. Hao, G. Wang, P. Li, Cytochrome P450 2J2: distribution, function, regulation, genetic polymorphisms and clinical significance. *http://dx.doi.org/10.3109/03602532.2013.806537* **45**, 311-352 (2013).
40. R. Kaspera *et al.*, Investigating the contribution of CYP2J2 to ritonavir metabolism in vitro and in vivo. *Biochemical pharmacology* **91**, 109-109 (2014).
41. A. Karkhanis, Y. Hong, E. C. Y. Chan, Inhibition and inactivation of human CYP2J2: Implications in cardiac pathophysiology and opportunities in cancer therapy. *Biochemical Pharmacology* **135**, 12-21 (2017).
42. E. Lee, Z. Wu, J. C. Shon, K. H. Liu, Danazol Inhibits Cytochrome P450 2J2 Activity in a Substrate-independent Manner. *Drug metabolism and disposition: the biological fate of chemicals* **43**, 1250-1253 (2015).
43. S. Ren *et al.*, Discovery and Characterization of Novel, Potent, and Selective Cytochrome P450 2J2 Inhibitors. *Drug Metabolism and Disposition* **41**, 60-71 (2013).
44. P. Lafite *et al.*, Design and synthesis of selective, high-affinity inhibitors of human cytochrome P450 2J2. *Bioorganic & medicinal chemistry letters* **16**, 2777-2780 (2006).
45. P. Lafite, S. Dijols, D. C. Zeldin, P. M. Dansette, D. Mansuy, Selective, competitive and mechanism-based inhibitors of human cytochrome P450 2J2. *Archives of Biochemistry and Biophysics* **464**, 155-168 (2007).
46. H. M. Lim *et al.*, Acetylshikonin, A Novel CYP2J2 Inhibitor, Induces Apoptosis in RCC Cells via FOXO3 Activation and ROS Elevation. *Oxidative Medicine and Cellular Longevity* **2022**, (2022).
47. J. C. Otto, W. L. Smith, Prostaglandin endoperoxide synthases-1 and -2. *Journal of Lipid Mediators and Cell Signalling* **12**, 139-156 (1995).
48. A. R. Brash, Lipoxygenases: Occurrence, Functions, Catalysis, and Acquisition of Substrate *. *Journal of Biological Chemistry* **274**, 23679-23682 (1999).
49. J. Capdevila *et al.*, The oxidative metabolism of arachidonic acid by purified cytochromes P-450. *Biochemical and biophysical research communications* **101**, 1357-1363 (1981).

50. K. G. Proctor, J. R. Falck, J. Capdevila, Intestinal vasodilation by epoxyeicosatrienoic acids: arachidonic acid metabolites produced by a cytochrome P450 monooxygenase. *Circulation research* **60**, 50-59 (1987).
51. J. H. Capdevila, J. R. Falck, The arachidonic acid monooxygenase: from biochemical curiosity to physiological/pathophysiological significance. *Journal of lipid research* **59**, 2047-2062 (2018).
52. A. A. Spector, H. Y. Kim, Cytochrome P450 epoxygenase pathway of polyunsaturated fatty acid metabolism. *Biochimica et biophysica acta* **1851**, 356-356 (2015).
53. T. Aliwarga *et al.*, Enzymatic and free radical formation of cis- and trans-epoxyeicosatrienoic acids in vitro and in vivo. *Free Radical Biology and Medicine* **112**, 131-140 (2017).
54. M. Zeigler, D. Whittington, N. Sotoodehnia, R. N. Lemaitre, R. A. Totah, A sensitive and improved throughput UPLC-MS/MS quantitation method of total cytochrome P450 mediated arachidonic acid metabolites that can separate regio-isomers and cis/trans-EETs from human plasma. *Chemistry and physics of lipids* **216**, 162-170 (2018).
55. A. Das *et al.*, CYP2J2 Molecular Recognition: A New Axis for Therapeutic Design. *Pharmacology & therapeutics* **215**, (2020).
56. B. Wang *et al.*, Metabolism pathways of arachidonic acids: mechanisms and potential therapeutic targets. *Signal Transduction and Targeted Therapy* **6**, (2021).
57. C. Zhang *et al.*, Conflicting roles of 20-HETE in hypertension and renal end organ damage. *European Journal of Pharmacology* **833**, 190-200 (2018).
58. J. D. Imig, Epoxyeicosanoids in Hypertension. *Physiological research* **68**, 695-695 (2019).
59. J. D. Imig, Epoxyeicosatrienoic Acids and 20-Hydroxyeicosatetraenoic Acid on Endothelial and Vascular Function. *Advances in pharmacology (San Diego, Calif.)* **77**, 105-105 (2016).
60. L. Liu *et al.*, Epoxyeicosatrienoic Acids Attenuate Reactive Oxygen Species Level, Mitochondrial Dysfunction, Caspase Activation, and Apoptosis in Carcinoma Cells Treated with Arsenic Trioxide. *The Journal of Pharmacology and Experimental Therapeutics* **339**, 451-451 (2011).
61. E. A. Evangelista *et al.*, CYP2J2 Modulates Diverse Transcriptional Programs in Adult Human Cardiomyocytes. *Scientific Reports*, (2020).
62. A. R. Kompa *et al.*, Soluble epoxide hydrolase inhibition exerts beneficial anti-remodeling actions post-myocardial infarction. *International Journal of Cardiology* **167**, 210-219 (2013).
63. A. A. Spector, X. Fang, G. D. Snyder, N. L. Weintraub, Epoxyeicosatrienoic acids (EETs): metabolism and biochemical function. *Progress in Lipid Research* **43**, 55-90 (2004).
64. J. D. Imig, Cardiovascular therapeutic aspects of soluble epoxide hydrolase inhibitors. *Cardiovascular Drug Reviews* **24**, 169-188 (2006).
65. T. Kitsuka *et al.*, A novel soluble epoxide hydrolase vaccine protects murine cardiac muscle against myocardial infarction. *Scientific Reports 2022 12:1* **12**, 1-12 (2022).
66. H. Qiu *et al.*, Soluble Epoxide Hydrolase Inhibitors and Heart Failure. *Cardiovascular Therapeutics* **29**, 99-111 (2011).
67. J. G. Jiang *et al.*, Cytochrome P450 2J2 Promotes the Neoplastic Phenotype of Carcinoma Cells and Is Up-regulated in Human Tumors. *Cancer Research* **65**, 4707-4715 (2005).

68. J. G. Jiang *et al.*, Cytochrome P450 Epoxygenase Promotes Human Cancer Metastasis. *Cancer Research* **67**, 6665-6674 (2007).
69. N. M. Anderson, M. C. Simon, Tumor Microenvironment. *Current biology : CB* **30**, R921-R921 (2020).
70. .
71. A. M. Johnson, E. K. Kleczko, R. A. Nemenoff, Eicosanoids in Cancer: New Roles in Immunoregulation. *Frontiers in Pharmacology* **11**, 1756-1756 (2020).
72. A. L. Correia, M. J. Bissell, The tumor microenvironment is a dominant force in multidrug resistance. *Drug Resistance Updates* **15**, 39-49 (2012).
73. K. Khalaf *et al.*, Aspects of the Tumor Microenvironment Involved in Immune Resistance and Drug Resistance. *Frontiers in Immunology* **12**, 1764-1764 (2021).
74. R. L. Siegel, K. D. Miller, H. E. Fuchs, A. Jemal, Cancer statistics, 2022. *CA: A Cancer Journal for Clinicians* **72**, 7-33 (2022).
75. A. A. Hakimi, C. G. Pham, J. J. Hsieh, A clear picture of renal cell carcinoma. *Nature Genetics* **45**, 849-850 (2013).
76. D. J. Sanchez, M. C. Simon. (2018).
77. P. M. Wierzbicki *et al.*, Prognostic significance of VHL, HIF1A, HIF2A, VEGFA and p53 expression in patients with clear-cell renal cell carcinoma treated with sunitinib as first-line treatment. *International Journal of Oncology*, (2019).
78. R. Trenker, N. Jura, Receptor Tyrosine Kinase activation: from the ligand perspective. *Current opinion in cell biology* **63**, 174-174 (2020).
79. X. Zou, Z. Mo, CYP2J2 Is a Diagnostic and Prognostic Biomarker Associated with Immune Infiltration in Kidney Renal Clear Cell Carcinoma. *BioMed Research International* **2021**, (2021).
80. A. Alexanian *et al.*, Down-regulation of 20-HETE Synthesis and Signaling Inhibits Renal Adenocarcinoma Cell Proliferation and Tumor Growth. *Anticancer research* **29**, 3819-3819 (2009).
81. M. T. Kelleni, M. Abdelbasset, Drug Induced Cardiotoxicity: Mechanism, Prevention and Management. *Cardiotoxicity*, (2018).
82. W. Ma, S. Wei, B. Zhang, W. Li, Molecular Mechanisms of Cardiomyocyte Death in Drug-Induced Cardiotoxicity. *Frontiers in Cell and Developmental Biology* **8**, 434-434 (2020).
83. Z. V. Varga, P. Ferdinandy, L. Liaudet, P. Pacher, Drug-induced mitochondrial dysfunction and cardiotoxicity. *American Journal of Physiology - Heart and Circulatory Physiology* **309**, H1453-H1467 (2015).
84. G. M. Lanier, J. Garg, N. Shah, Cardiotoxicity of chemotherapeutic agents: incidence, treatment and prevention. *Drug safety* **22**, 1-214 (2000).
85. D. Cardinale, F. Iacopo, C. M. Cipolla, Cardiotoxicity of Anthracyclines. *Frontiers in Cardiovascular Medicine* **7**, 26-26 (2020).
86. T. Tadokoro *et al.*, Mitochondria-dependent ferroptosis plays a pivotal role in doxorubicin cardiotoxicity. *JCI insight* **5**, (2020).
87. Y. Jin *et al.*, A Comprehensive Review of Clinical Cardiotoxicity Incidence of FDA-Approved Small-Molecule Kinase Inhibitors. *Frontiers in Pharmacology* **11**, 891-891 (2020).

88. M. Chaar, J. Kamta, S. Ait-Oudhia, Mechanisms, monitoring, and management of tyrosine kinase inhibitors–associated cardiovascular toxicities. *OncoTargets and therapy* **11**, 6227-6227 (2018).
89. Z. Xu, S. Cang, T. Yang, D. Liu, Cardiotoxicity of tyrosine kinase inhibitors in chronic myelogenous leukemia therapy. *Hematology Reviews* **1**, 4-4 (2009).
90. Y. A. Vano *et al.*, First-Line Treatment of Metastatic Clear Cell Renal Cell Carcinoma: What Are the Most Appropriate Combination Therapies? *Cancers* **13**, 5548-5548 (2021).

## Chapter 2

## Multi-omics approach to characterize CYP2J2 and the altered arachidonic acid pathway in clear cell renal cell carcinoma

### 2.1 Introduction

Clear cell renal cell carcinoma (ccRCC) is the most diagnosed kidney cancer in the U.S. affecting nearly 70,000 adults annually and is in the top 10 most common cancers for both men and women (*1*). ccRCC is histologically distinct from other subtypes of kidney cancer due to its clear cell appearance which is a result of lipid and glycogen accumulation in the cytoplasm (*2*). The most common cause of ccRCC is from a mutation in the von Hippel-Lindau (VHL) tumor suppressor gene that is involved in the hypoxia pathway (*3*). *VHL* silencing promotes HIF1A mediated transcriptional activation of numerous growth factors including potent pro-angiogenic mediators such as the vascular endothelial growth factor (VEGF) (*4*). As a result, ccRCC tumors are highly vascular and the promotion of angiogenesis is a major mechanism of tumor progression and metastasis.

The early prognosis of ccRCC is generally positive and the cancer is considered "curable" with partial or total nephrectomy. However, once metastasized, the prognosis is poor and anti-angiogenic chemotherapy (e.g. multi-target tyrosine kinase inhibitors) is necessary (*5, 6*). Data from the Human Protein Atlas suggest that higher expression of CYP2J2 is associated with better prognosis in ccRCC patients, and interestingly, among other subtypes of kidney cancer, CYP2J2 overexpression is the most prominent in ccRCC tumors (Figure 2.1). CYP2J2 is a drug metabolizing enzyme that is predominately expressed in human heart tissue (*7, 8*). It is also a major epoxygenase that oxidizes arachidonic acid (AA) to form four regioisomers of bioactive epoxide metabolites known as epoxyeicosatrienoic acids (EETs) (Scheme 1) (*7, 9*).

EETs are potent autocrine and paracrine signaling compounds that are involved in the regulation of vascular function and promotion of pro-angiogenic and anti-inflammatory pathways (*10, 11*). More recently, CYP2J2 and EETs have been shown to promote the neoplastic tumor phenotype by upregulating processes involved in cell proliferation and tumor metastases while downregulating apoptotic pathways (*12-14*).

The present study demonstrated CYP2J2 mRNA and protein expression was significantly upregulated in ccRCC tumor tissues compared to histologically normal adjacent tissues (NAT), confirming previously reported literature (*15*). And while this is not a novel finding, to the best of our knowledge, the role of CYP2J2 in relation to other major CYP epoxygenases and hydroxylases within the arachidonic acid pathway in ccRCC has yet to be explored. Therefore, the present study aimed to characterize the effect of CYP2J2 overexpression in ccRCC through a multi-omics approach and explore mechanisms with an emphasis on changes in the arachidonic acid pathway.

## 2.2 Experimental

### 2.2.1 Materials

Optima grade water, acetonitrile, and acetic acid were purchased from ThermoFisher Scientific (Waltham, MA). Purelink Total RNA isolation kit, MEM Per Plus protein extraction kit, High-Capacity-RNA-to-cDNA conversion kits, Taqman FAM dye reporter assays, and any other reagents used were purchased from ThermoFisher Scientific (Waltham, MA) unless otherwise state. Heavy peptides for relative proteomics were purchased from vivitide (Gardner, MA). ccRCC tumor tissues and histologically normal adjacent tissues were sourced from patients undergoing nephrectomy at the University of Washington Medical Center (Seattle, WA) in partnership with NW Biotrust.

### 2.2.2 Procuring human kidney tissues

Matched renal cell carcinoma (RCC) tissue and NAT were collected from adult patients undergoing partial nephrectomy and sourced by NW Biotrust through the University of Washington Medical Center (UWMC). Study ethics were approved by the University of Washington IRB under FWA #00006878. The pathology of the cancerous and histologically normal tissue was examined by UWMC pathology and only confirmed ccRCC tissues were used for this study. The tissues were stored in RNALater, formalin, or flash frozen for downstream processing within 24 h of collection.

### 2.2.3 Total RNA isolation and RT-qPCR

Kidney tissue samples were stored in RNALater solution at -80°C until processing. The tissues were homogenized in Trizol reagent using a Precellys-24 cooled by a Cryolys (6800 rpm, 3x30 sec cyles, 60 sec delay) followed by RNA extraction using the PureLink RNA isolation kit

(ThermoFisher Scientific, Waltham, MA). RNA concentration and purity (A260/280) were measured using the Tecan Spark multimode microplate reader (Mannedorf, Switzerland). Total RNA was converted to cDNA via reverse transcriptase using the High-capacity-RNA-to-cDNA kit (ThermoFisher Scientific, Waltham, MA). Gene expression was measured by RT-qPCR using Taqman reporter assays (FAM dye) and normalized to the housekeeping gene *RPL13*, unless otherwise stated, following the comparative CT analysis method.

### 2.2.4 RNA-sequencing

Total RNA isolated from ccRCC tumor and matched NAT were sent to Novogene, Ltd (Sacramento, CA) for sequencing. Briefly, sample quality control (QC) was performed on the Agilent 2100 to ensure RNA integrity was <4 with a smooth baseline followed by measurement of RNA concentration and purity as determined by $A_{260/280}$ = 1.8-2.2 and $A_{260/230}$ > 1.8. Once the sample QC criteria was satisfied, library preparation and library QC was completed. The samples were then sequenced by 150 bp paired-end sequencing technique using an Illumina NovaSeq 6000 platform followed by QC of the data and data processing.

### 2.2.5 Differential gene expression and pathway analysis

Differential expression analysis was performed using the DESeq2 R package to compare the alterations in the transcriptome of ccRCC tumor tissues and matched normal adjacent tissues (NAT). Pathway analysis by iPathwayGuide using the Impact Analysis method (FDR<0.01) was performed by the University of Washington Interdisciplinary Center for Exposures, Diseases, Genomics, and Environment (EDGE).

### 2.2.6 Gene set enrichment analysis (GSEA) of differentially expressed genes

The gene list was pre-ranked according to the degree of differential expression followed by gene set enrichment analysis using GSEAPreranked. We applied GSEAPreranked using canonical curated gene sets from the Hallmark, KEGG, and Reactome pathways (FDR<0.01). The network-based enrichment mapping was visualized using the Enrichment Map plug-in application in Cytoscape. Briefly, significantly altered gene sets (FDR<0.01) were represented as individual nodes (red, upregulation; blue, downregulation) and the nodes were sorted based on biological relevance. We then performed leading edge analysis for gene sets contained within the KEGG and Reactome Arachidonic Acid Metabolism which was visualized as a two-way hierarchical cluster dendrogram.

### 2.2.7 Relative quantitative proteomics

2.2.8 Sample preparation and digestion

Healthy kidney tissues (n=6), histologically normal adjacent tissues (n=13), and ccRCC tumor tissues (n=16) were flash frozen upon receipt and stored at -80°C until processing. Membrane proteins were extracted using the Mem-PER Plus Membrane Protein Extraction Kit (ThermoFisher Scientific, Waltham, MA) following a modified manufacturer's protocol. The samples were digested using MS grade trypsin for 16 h and quenched on dry ice. A known concentration of a heavy peptide cocktail was added for relative quantification. The MS/MS transitions of each peptide is summarized in Table II.

2.2.9 LC-MS/MS

Surrogate and heavy labeled peptides were quantified using an AB Sciex 6500 tandem quadrupole mass spectrometer coupled to a Waters Acquity I-class UPLC. Chromotographic separation was achieved on a Waters Acquity CSH C18 column following a gradient of (A) 0.1% formic acid in water and (B) 0.1% formic acid in MeCN: 0-4 min 97% A, 4-8 min 87% A, 8-18 min 70% A, 18-20.5 mins 65% A, 20.5-21.1 40% A, 21.1-23.1 20% A, 23.2-27 min 97% A.

**2.2.10 EETs extraction and quantification**

Kidney tissues were homogenized in PBS with 12 uM t-AUCB using the Precellys bead beater (6800 rpm, 3x30 secs). After homogenization, the samples were centrifuged at 3,000 x g for 15 mins to pellet the membrane fraction. The supernatant was then collected and used for the extraction step. EETs and other eicosanoids were extracted under low ambient light conditions following a previously described protocol by Zeigler et al (*16*). Briefly, a modified Bligh and Dyer method was used to extract total lipids from tissue homogenate followed by saponification. The lipids were further extracted using a 96-well solid phase extraction cartridge then derivatized to create a positively molecule. The eicosanoids were then quantified in positive ionization mode on a Waters Xevo TQ-s ESI mass spectrometer coupled to a Waters Acquity I-class UPLC. The chromatographic separation was performed on a Waters Acquity BEH shield C18 column following a gradient of (A) 0.1% formic acid in water and (B) 0.1% formic acid in MeCN: 0–1 min 70% A, 1–4 min 79–69% A, 4–14.5 min 69–65% A, 14.5–16 min 10% A, 16–18 min 70% A.

## 2.3 Results

### 2.3.1 De-identified patient data for matched ccRCC tumors and normal adjacent tissues

Use of all human tissues in this study was approved by the University of Washington IRB under the protocol number FWA #00006878. The diagnoses of the tumor tissues were confirmed by UW Pathology. Patient de-identified data including final tumor diagnosis, pre-existing medical conditions, and medications are summarized in Table I.

### 2.3.2 Gene set enrichment analysis of the altered arachidonic acid pathway in ccRCC tumor tissues compared to matched histologically normal adjacent tissues

We evaluated the differential gene expression of CYP450 epoxygenases (*CYP2Cs, CYP2J2*) and hydroxylases (*CYP4A11, CYP4Fs*) in addition to genes encoding enzymes that are known to be closely related to the arachidonic acid pathway (*EPHX-2,* PLA2 isoforms, *GPX-3)* in ccRCC tumor tissues and matched histologically NAT. Total RNA of 12 matched ccRCC tumor and NAT pairs were analyzed by Novogene, Ltd using next-generation sequencing (NGS). Principal component analysis (PCA) of raw RNA-seq data revealed two distinct populations that segregated into a tumor group containing the ccRCC tumor tissue samples and a healthy group containing the NAT samples (Figure 2.2). Variability within the tumor group can be observed in the PCA plot with ccRCC tumor samples 9, 11, and 12 located outside of the main cluster but were of no major concern as tumor specimens are known to be genetically diverse (*17*). Out of a total of 24,026 genes with measured expression levels, over 10,000 differentially expressed (DE) genes were identified using the DESeq2 R package. The up-regulated genes are represented in red, and the down-regulated genes are represented in blue in the volcano plot shown in Figure

2.3. For pathway analysis, we set our significance cutoff to a p-value≤0.01 and a minimum absolute log fold change of 0.00, which narrowed down our results to 4,801 DE genes.

We conducted gene set enrichment analysis (GSEA) utilizing curated gene sets from canonical Hallmark, KEGG, and Reactome pathways that are visualized through a global circular network-based enrichment map (Figure 2.4). Each node represents a pathway that is either up-regulated (red) or down-regulated (blue) in ccRCC and the size of the node corresponds to significance level. The connectivity (gray lines) between each node was achieved based on the criteria of sharing 50% or greater genes. Pathways involved in immune response and structural remodeling were highly upregulated in ccRCC while pathways involving phase I and II drug metabolism, fatty acid metabolism, and arachidonic acid were significantly downregulated.

Leading edge analysis revealed the core subset of genes (e.g. leading edge subset) that contributed the most to the enrichment signal of the arachidonic acid pathway (Figure 2.5 A). Notably, *CYP2B6*, *CYP2C9*, *CYP4F2*, *CYP4F3*, *CYP4A11*, and *CYP4A22* were among the leading-edge genes and were significantly downregulated in ccRCC tumors. Figure 2.5 B highlights CYP450 genes involved in the AA pathway that include both leading edge and non-leading-edge genes. The non-leading edge hierarchical cluster dendrogram is presented as Figure 2.6. As expected, CYP2J2 expression is highly upregulated in ccRCC tissues, however, the expression is decreased in several tumor tissues which highlights the variability that is present within this small sample set.

We next validated the differential gene expression of key enzymes of interest involved in the AA pathway using RT-qPCR and normalizing the expression to the housekeeping gene, *RPL13* following the comparative CT method (Figure 2.7 and Figure 2.8). As expected, the expression of *CYP2J2* was significantly increased in ccRCC tumor samples while the expression

of *CYP2C8* and *CYP2C9* were downregulated, although the samples were variable (Figure 2.7 A). The relative gene expressions of *CYP4A11*, *CYP4F2*, and *CYP4F3* were significantly downregulated and *CYP4F12* was downregulated in 11 out of 12 pairs thus validating RNA-seq results (Figure 2.7 B). RT-qPCR results of *EPHX*-2, *PLA2G7*, and *POR* validated the genes were significantly reduced in ccRCC tumor tissues compared to NAT (Figure 2.8).

### 2.3.3 LC-MS/MS quantification of relative protein levels of AA pathway related enzymes

We next quantified the relative protein expression of AA pathway related enzymes by LC-MS/MS in healthy kidney tissues (n=6), histologically normal adjacent tissues (n=13), and ccRCC tumor tissues (n=16). Relative protein expression was normalized to the QC. CYP2J2 relative protein expression was significantly increased in the ccRCC tumor group compared to the healthy control group, but although the relative protein content was greater in comparison to the NAT group, the difference was not statistically significant (Figure 2.9 A). The relative protein expression of other major CYP2C epoxygenases was also quantified. CYP2C8 relative protein expression increased slightly in the NAT group compared to the healthy controls but the levels returned to baseline in the ccRCC tumor group (Figure 2.9 A). Similar trends were observed with CYP2C9 and CYP2C19 where the relative protein expression increases slightly in the NAT group compared to healthy controls then subsequently returns close to baseline in ccRCC tumor groups (Figure 2.9A). Thus, we can conclude that the relative protein expression of CYP2C8, CYP2C9, and CYP2C19 is essentially unaltered in ccRCC tumor tissues. The relative protein expression of CYP4A11 and CYP4F2 was slightly decreased in ccRCC tissues but no statistically significant changes were observed (Figure 2.9 A). The relative protein expression of soluble epoxide hydrolase (sEH), and glutathione peroxidase 3 (GPX3) was

significantly reduced in ccRCC tumors compared to NAT and/or healthy control groups (Figure 2.9 B). And finally, the relative protein expression of PLA2G4A and PLA2G12B was not significantly altered across the different population groups although a minor decrease in ccRCC tissues was observed (Figure 2.9 B).

### 2.3.4 Eicosanoid levels are altered in ccRCC tumors

Based on the transcriptomic and proteomic data showing CYP2J2 is the major AA epoxygenase expressed in ccRCC tumor tissues, and the overall altered AA pathway, we hypothesized that ccRCC tumors would contain higher levels of EETs in comparison to matched NAT. To confirm this, we extracted and quantified EETs, DHETs, and several HETEs in the tumor and NAT samples via LC-MS/MS following a previously reported protocol (*16*). Due to sample limitations, our sample pool consisted of 6 matched pairs. In 3 out of 6 pairs, all four regioisomers of *cis*-EET were significantly increased in ccRCC tumors compared to NAT with 14,15-EET being the most abundant (Figure 2.10 A). In the remaining 3 pairs that were screened, however, EETs levels were either significantly downregulated in tumors or unchanged (Figure 2.10 B). *Trans*-EETs were also either significantly upregulated or downregulated depending on the tissue pairs (Figure 2.11). DHET levels showed a similar trend where within the same tissue pairs, the levels were either significantly increased in ccRCC tumors (Figure 2.12 A) or decreased (Figure 2.12 B).

The levels of several mid-chain and terminal HETEs were also quantified. CYP4 enzymes are mainly responsible for the formation of terminal 19- and 20-HETE. In ccRCC tumor tissues, 19-HETE levels were significantly reduced in 3 out of 6 pairs, significantly increased in 1 out of 6 pairs, and unchanged in the remaining pairs (Figure 2.13 A). Interestingly,

a significant reduction in 20-HETE levels was observed in all the tissue pairs that were analyzed (Figure 2.13 B). We next quantified the expression of several mid-chain HETEs (Figure 2.14). Lipoxygenases can metabolize mid-chain carbons of AA resulting in hydroxyperoxyeicosatetraenoic acids (HPETE) which is then subsequently converted to HETEs by glutathione peroxidase (*18*). CYP1B1 is also responsible for the formation of mid-chain HETEs. In our panel, the expression pattern of mid-chain HETEs was quite variable. For instance, 5-HETE levels were significantly increased in ccRCC tissue samples in half of the pairs that were analyzed while only one pair exhibited a significant reduction in 5-HETE. Similarly, 4 out of 6 pairs saw a significant increase in 8-, 11-, and 12-HETEs while 9- and 15-HETEs were significantly increased in 3 out of 6 pairs (Figure 2.14).

## 2.4 Discussion

The present study characterized the altered CYP450 mediated arachidonic acid (AA) pathway in clear cell renal cell carcinoma (ccRCC) and quantified CYP derived eicosanoids in matched ccRCC and histologically NAT pairs. AA is found esterified in the phospholipid membranes at the *sn-2* position and once liberated by phospholipase A2 enzymes, is subjected to metabolism by several enzymatic pathways (COX, LOX, and CYP450) to produce biologically active eicosanoids (*19*). Under normal physiological conditions, AA metabolites are involved in a wide range of biological processes that govern cell proliferation, inflammation, and vascular regulation among other processes. Bioactive lipid signaling molecules (e.g. eicosanoids) derived from fatty acids were previously suggested to promote tumor cell proliferation, development, and overall metastasis, thus, metabolites of AA have garnered interest in recent years as potent mediators of tumorigenesis (*10*). However, much of the current work is focused on elucidating the role of COX and LOX mediated metabolites in cancer development but very little is known regarding the role of CYP450 mediated metabolites. Evangelista et al., summarizes the current knowledge of CYP involvement in solid tumors in this review article (*20*).

CYP2J2 expression and EETs were previously reported to promote the neoplastic tumor phenotype in several cancer cell lines (*13*) and, the expression of CYP2J2 was observed to be highly, and most variably, increased in clear cell renal cell carcinoma (ccRCC) tumors (*15*). ccRCC represents approximately 80% of all kidney cancer cases making it among the top ten most diagnosed cancers in the U.S., and while the prognosis for early stage tumors is positive, the prognosis for advanced ccRCC remains poor (*4*). CYP2J2 overexpression in ccRCC has been previously reported (*15*), but to the best of our knowledge the altered CYP mediated AA pathway, including CYP2J2 overexpression, in ccRCC had not been fully characterized. The

present study confirmed CYP2J2 mRNA and protein expressions are significantly upregulated in ccRCC tumor tissues. Enrichment mapping of transcriptomic data revealed the gene sets involved in fatty acid metabolism and fatty acid biosynthesis pathways were significantly downregulated in ccRCC. Through gene set enrichment analysis (GSEA) of the "Arachidonic acid metabolism" pathway, *EPHX-2, CYP2C8, CYP2C9*, *CYP4F2*, *CYP4F3*, *CYP4A11*, *CYP4A22* were identified to be significantly downregulated in ccRCC tumors compared to histologically NAT, which contrasts with the expression of *CYP2J2*. The pathway involving phase I and phase II drug metabolism were also significantly downregulated in ccRCC tumors which potentially explains the significant decrease in gene expression of cytochrome P450 oxidoreductase (*POR*) which is crucial to the catalytic activity of CYPs (*21*), although protein levels should be measured in the future.

Following mRNA expression, we next sought to quantify protein levels to determine whether the translation of genes correlated with the transcriptomic results. We included a healthy, non-cancerous kidney cortex control group to establish the baseline for measuring relative protein levels to stratify the findings between non-cancerous, pre-cancerous, and cancerous kidney tissues. Relative protein levels of CYP2J2 confirmed mRNA results that the expression was significantly higher in ccRCC tumor samples and in the histologically NAT samples compared to the healthy, non-cancerous group but the difference between the ccRCC samples and matched NAT was not statistically significant. Overall, these results suggest changes in CYP2J2 expression occur during the early developmental phase of ccRCC as we observed elevated CYP2J2 protein expression in the histologically NAT group as well.

Furthermore, proteomic quantification of relative protein expression of the leading-edge genes confirmed sEH was significantly decreased in ccRCC, however, the relative protein

expressions of the remaining CYPs were not significantly altered and only showed minor decreases in ccRCC. In general terms, cancer is defined as a genetic disorder that disrupts normal cell functions pertaining to proliferation and growth suggesting the alteration in CYP2J2 expression, as it pertains to ccRCC tumor development, plays a potential role in cell signaling that is positively associated with promoting the neoplastic tumor phenotype. This phenomena has been previously described by Jiang and colleagues utilizing various cancer cell models, (*13*) however, there remains a lack of understanding of the role of CYP2J2 overexpression in the AA pathway. Overall, considering that most other CYPs in the AA pathway are downregulated, a potential novel role for CYP2J2 in ccRCC development is highlighted.

In contrast to the leading-edge CYPs, the promoter region of CYP2J2 lacks a TATA box and instead contains four putative Sp1 binding regions (*22*). This is of particular interest as it not only highlights CYP2J2 as a unique enzyme within the CYPs identified in the AA pathway, but a known variant *CYP2J2*7* is associated with up to a 50% reduction in transcriptional activity compared to the wildtype enzyme as a result of a single nucleotide polymorphism in the promoter region disrupting one of the Sp1 binding sites (Scheme 2) (*22, 23*). The *7 variant exemplifies the importance of maintaining all four Sp1 binding sites within the promoter region and highlights a lesser-known role of Sp1 binding in CYP2J2 transcriptional regulation.

In cancer, Sp1 expression has been correlated with poor prognosis due to its role in regulating a wide range of oncogenes and tumor suppressor genes, and its transcriptional regulation is largely mediated by post-translational modifications (e.g. methylation, phosphorylation, acetylation, etc) (*24, 25*). A key mechanism during the initiation of a tumor phenotype is hypermethylation of the promoter DNA of tumor suppressor genes resulting in gene silencing by preventing Sp1 mediated transcriptional activation (*24*). Therefore, we hypothesized

that the promoter DNA region of CYP2J2 was demethylated in ccRCC tumors resulting in an increase in CYP2J2 transcriptional levels. By utilizing a public database (UALCAN) we confirmed our hypothesis as we observed the promoter DNA methylation of CYP2J2 was greatly reduced in ccRCC (Figure 2.15) compared to NAT which would, in turn, enhance its transcriptional activity resulting in increased expression of CYP2J2 in ccRCC (Scheme 3). Zhang and colleagues (*26*) first reported this phenomenon in hepatocellular carcinoma (HCC) but, to the best of our knowledge, the consequence of Sp1 demethylation in the promoter region of CYP2J2 in ccRCC has not been reported.

We next sought to determine a role for CYP2J2 overexpression in ccRCC and hypothesized that the formation of epoxyeicosatrienoic acids (EETs) would be favored since the AA pathway was observed to be significantly altered (Scheme 4). EETs are involved in a wide range of cellular processes that involve cell survival, angiogenesis, and anti-inflammatory pathways and more recently, EETs were suggested to be involved in promoting the tumor phenotype (*7, 12, 27*). Thus, we quantified four regioisomers of epoxyeicosatrienoic acids (EETs), dihydroxyeicosatrienoic acids (DHETs) and several mid-chain and terminal hydroxyeicosatetraenoic acids (HETEs) by LC-MS/MS to compare the eicosanoid profile in six matched ccRCC tissues and NAT pairs. The levels of all four regioisomers of EETs were significantly increased in only half of the ccRCC pairs analyzed which corresponded with an increase in DHET levels. 19-HETE decreased in the majority of ccRCC samples compared to matched NAT while 20-HETE was significantly reduced in all ccRCC samples, as would be expected from the decreased expression we observed for CYP4 genes. The expression of several mid-chain HETEs were significantly altered in ccRCC samples but compared to EETs levels, mid-chain HETEs were present in low abundance overall suggesting EETs are the major

eicosanoids present in comparison to DHETs and HETEs in ccRCC; however, a larger sample size is required to fully investigate the changes in eicosanoid levels.

Acknowledgements

We would like to acknowledge Dr. Ed Kelly for his collaboration on procuring the matched tissue samples; Dr. Sina Gharib for his expertise in transcriptomics and assistance in GSEA data analysis; the UW Edge Center and Dr. Theo Balmer for their expertise in transcriptomics, Dr. Max Zeigler for his expertise on quantifying eicosanoids, and Dr. Yuanyuan Shi for her expertise in proteomics. Additionally, the figures generated from UALCAN were previously published by Zou et al (*15*).

## Figures

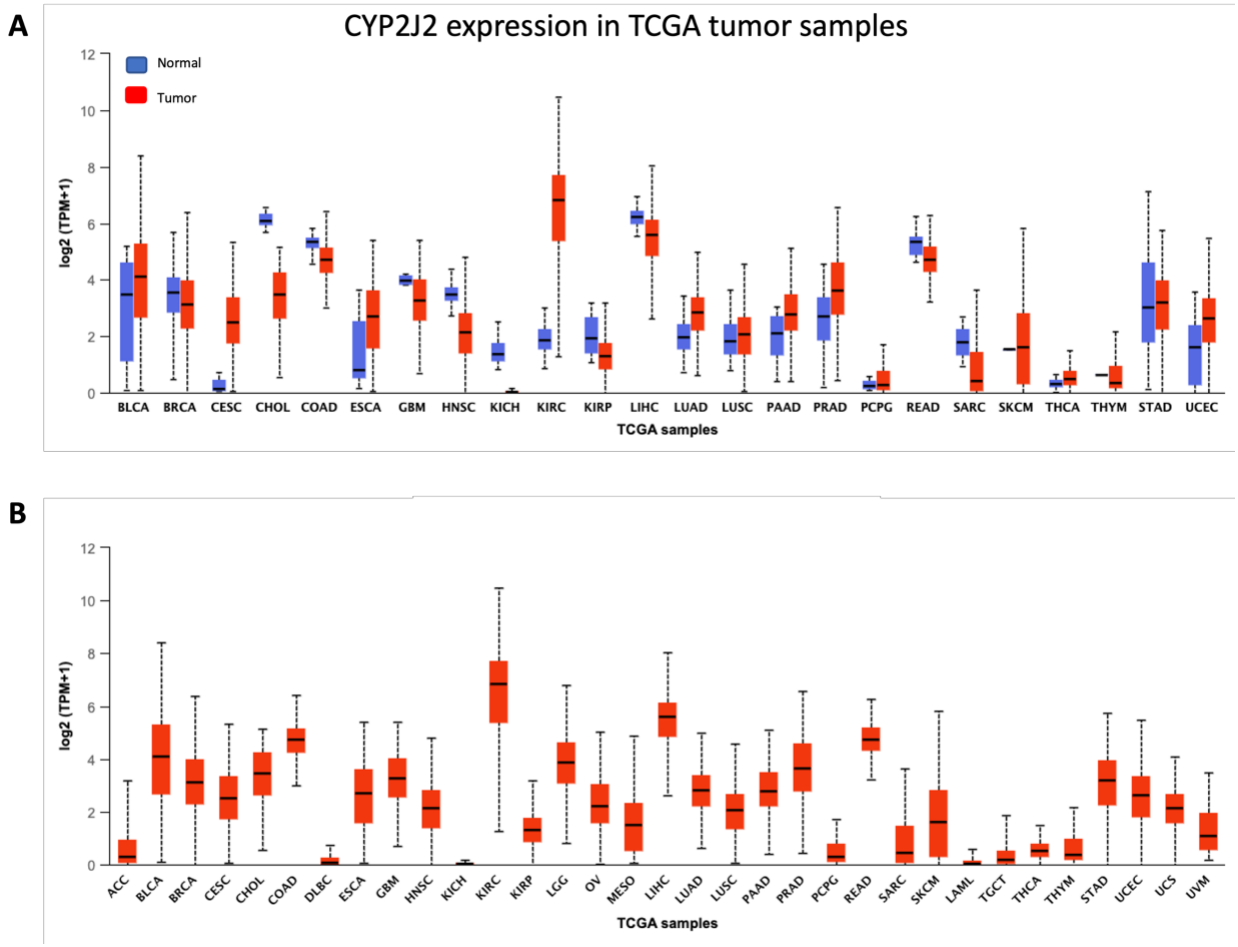


**Figure 2.1. CYP2J2 expression profile in 24 different types of cancers.** A) CYP2J2 expression in tumor tissues (red) compared to expression in normal, non-cancerous tissues (blue); B) CYP2J2 expression in only tumor tissues. The figures were adapted from the UALCAN interactive web resource (*28, 29*). *Abv., KIRC, clear cell renal cell carcinoma; TCGA, The Cancer Genome Atlas.*

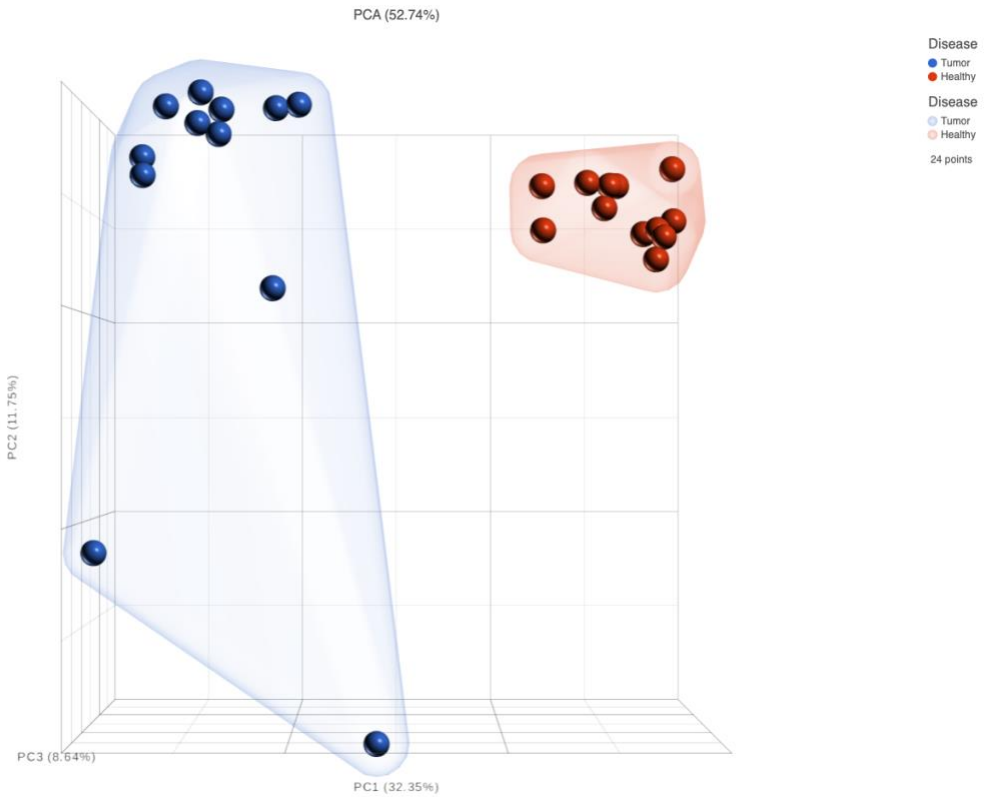


**Figure 2.2. Principal component analysis from RNA-seq results of ccRCC tumor tissues (blue) and matched normal adjacent tissues (red).** Several outliers are present in the ccRCC tumor group, however, there is a distinct segregation between the tumor tissues and normal tissues confirming the presence of two independent population groups. n=12 matched pairs.

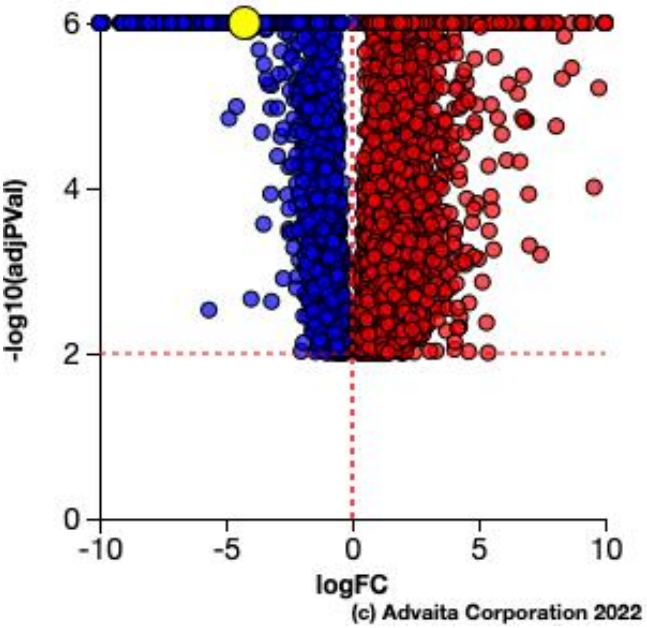


**Figure 2.3. Volcano plot of differentially expressed (DE) genes in ccRCC tissue samples compared to matched normal adjacent tissues (NAT).** Blue represents downregulated genes and red represents up-regulated genes.

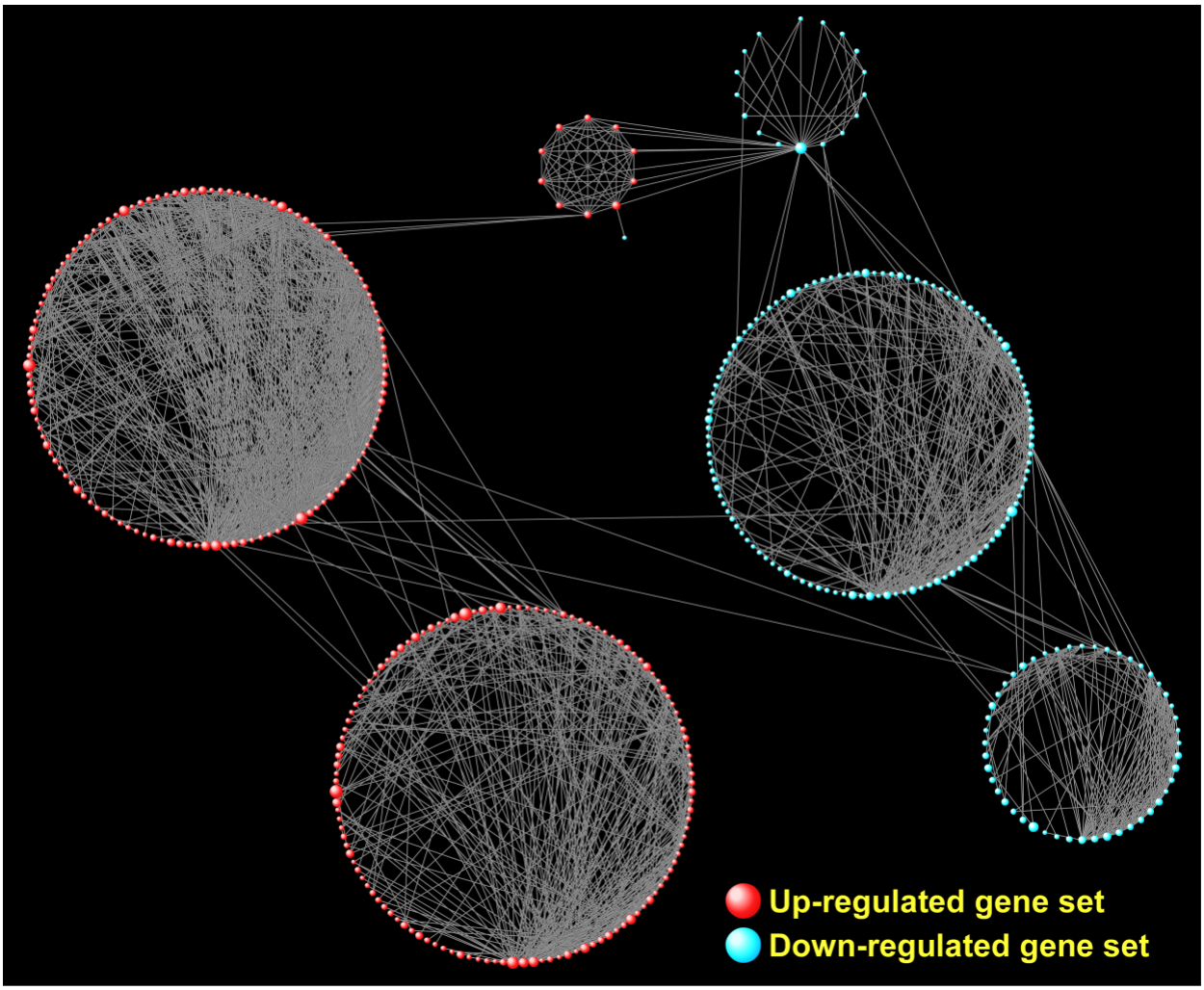


**Figure 2.4. Network-based visualization of gene set enrichment analysis (GSEA) in ccRCC tumors compared to normal adjacent tissues.** Notable modules that are highlighted in this figure are the up-regulated pathways for cellular remodeling and inflammatory processes and the downregulated arachidonic acid and phase I metabolism pathways. Red nodes represent up-regulated gene sets in ccRCC tumors and blue nodes represent down-regulated gene sets in ccRCC as compared to the normal adjacent tissues. The gray lines connecting the nodes are based on the criteria of meeting at least 50% or greater overlap between different gene set nodes. Q-value ≤ 0.01.

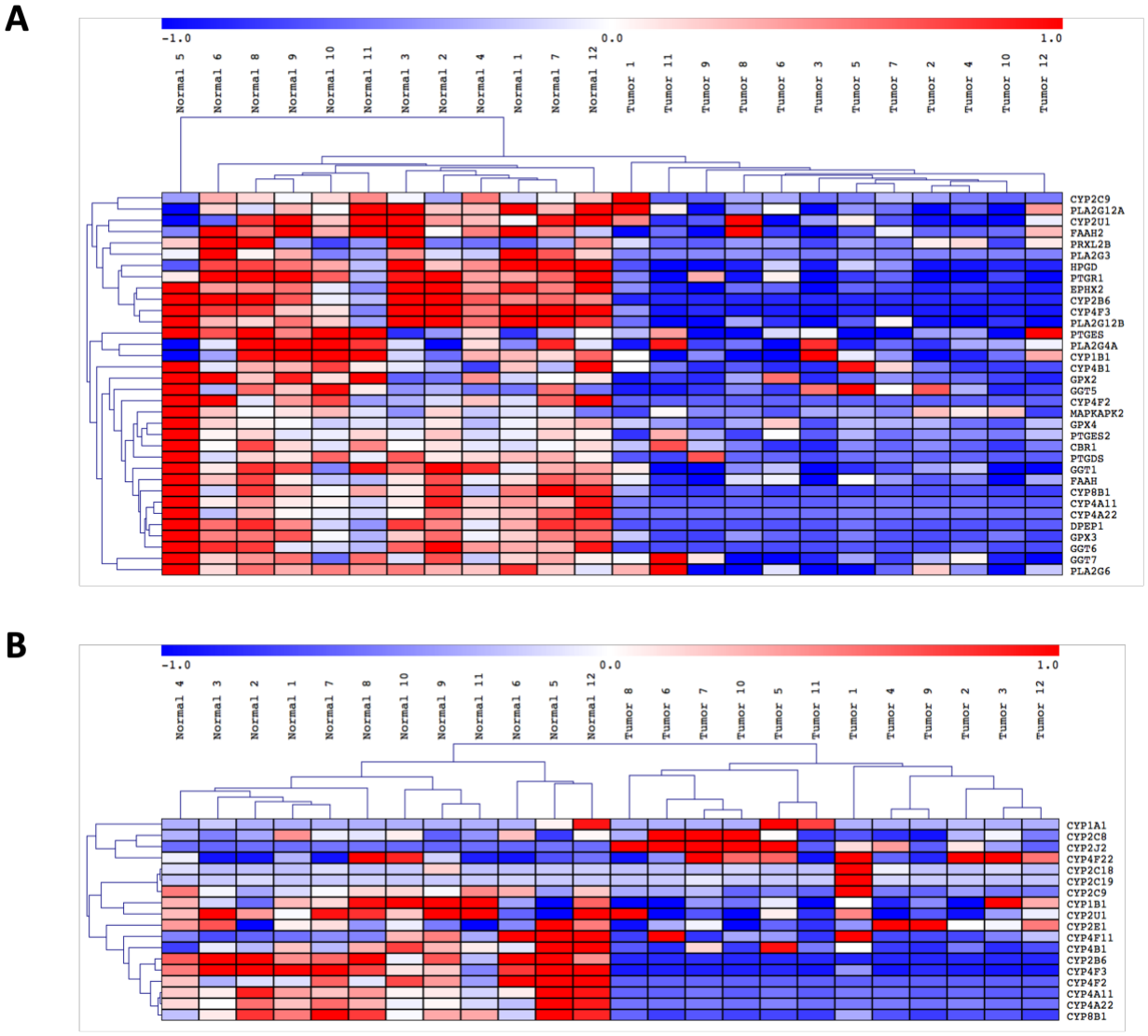


**Figure 2.5. Two-way hierarchical clustering dendrograms of differentially expressed genes involved in the arachidonic acid pathway in ccRCC tumor tissues compared to matched normal adjacent tissues.** A) Leading edge analysis of the arachidonic acid pathway from gene set enrichment analysis (GSEA) of KEGG and Reactome pathways (FDR<0.01); B) non-leading-edge analysis of CYP450s related to this pathway (FDR<0.01).

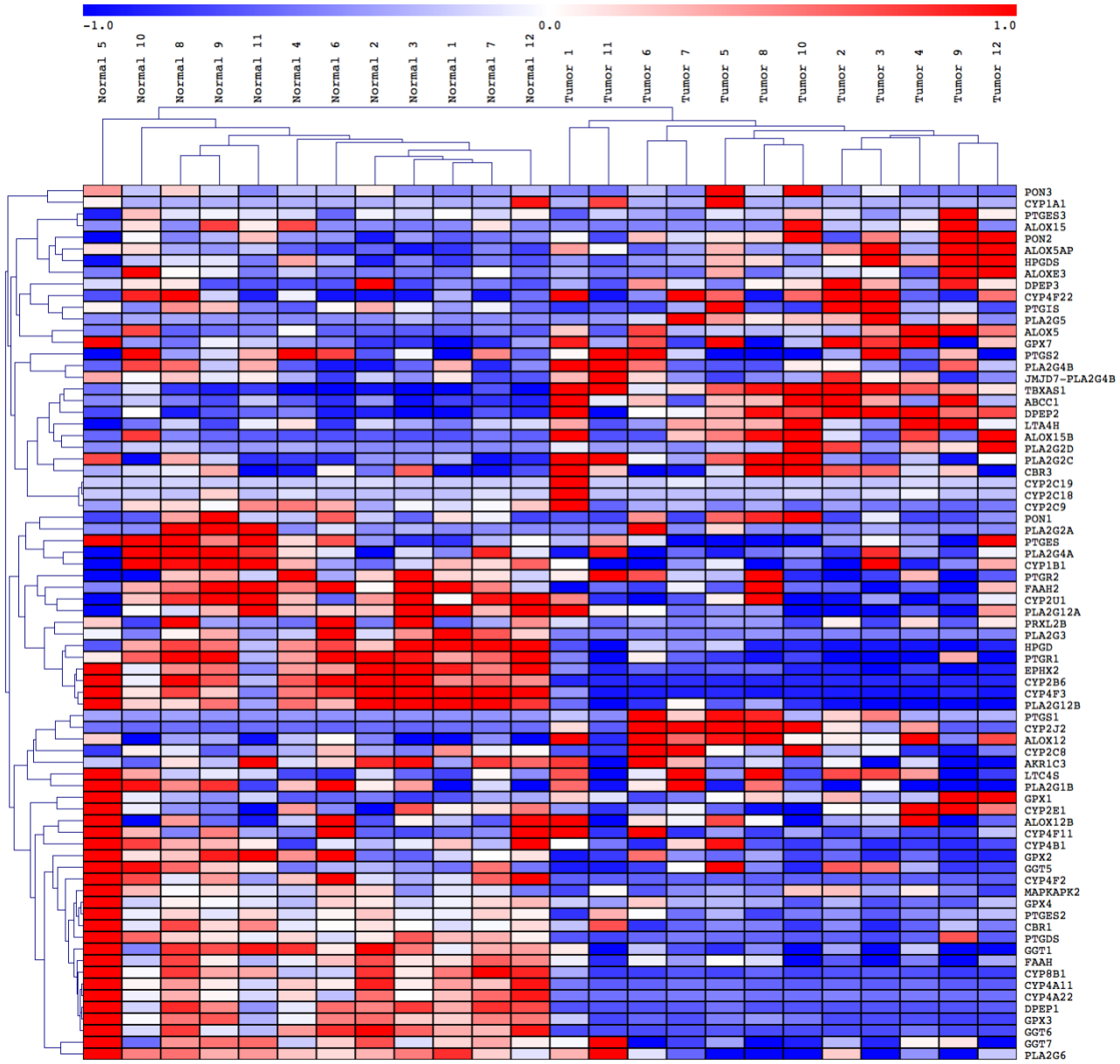


**Figure 2.6. Full gene panel of the altered arachidonic acid pathway in ccRCC presented as a two-way hierarchical cluster dendrogram (FDR<0.01)**.

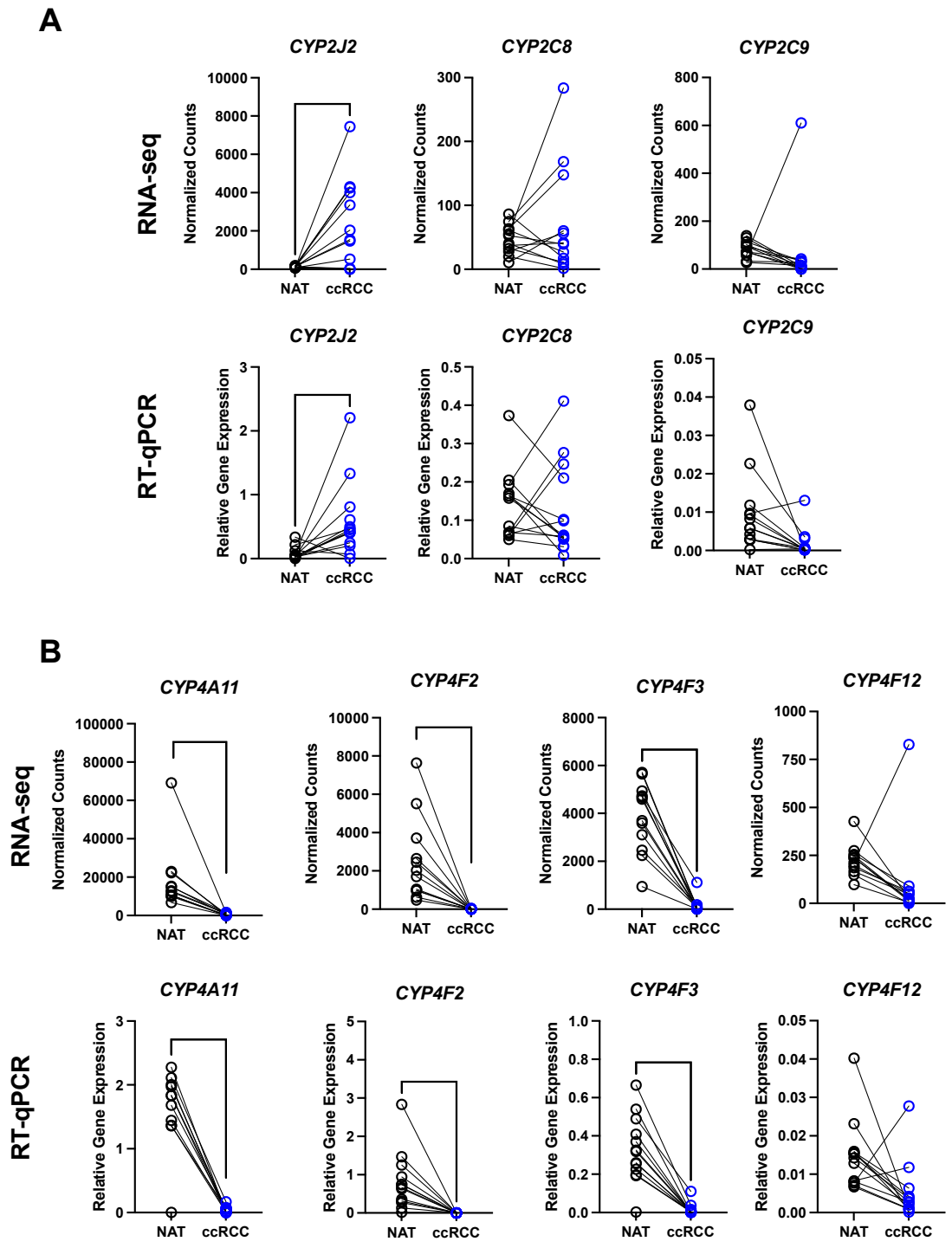


**Figure 2.7. Validation of arachidonic acid pathway related differentially expressed genes using RT-qPCR.** (A) Genes involved in AA epoxygenase activity; (B) Genes involved in AA hydroxylase activity. For RT-qPCR, gene expression is normalized to *RPL13* and all statistical analyses was performed using an unpaired t-test performed on Prism Graphpad. *$p < 0.05$, **$p < 0.01$, ***$p < 0.001$, and ****$p < 0.0001$

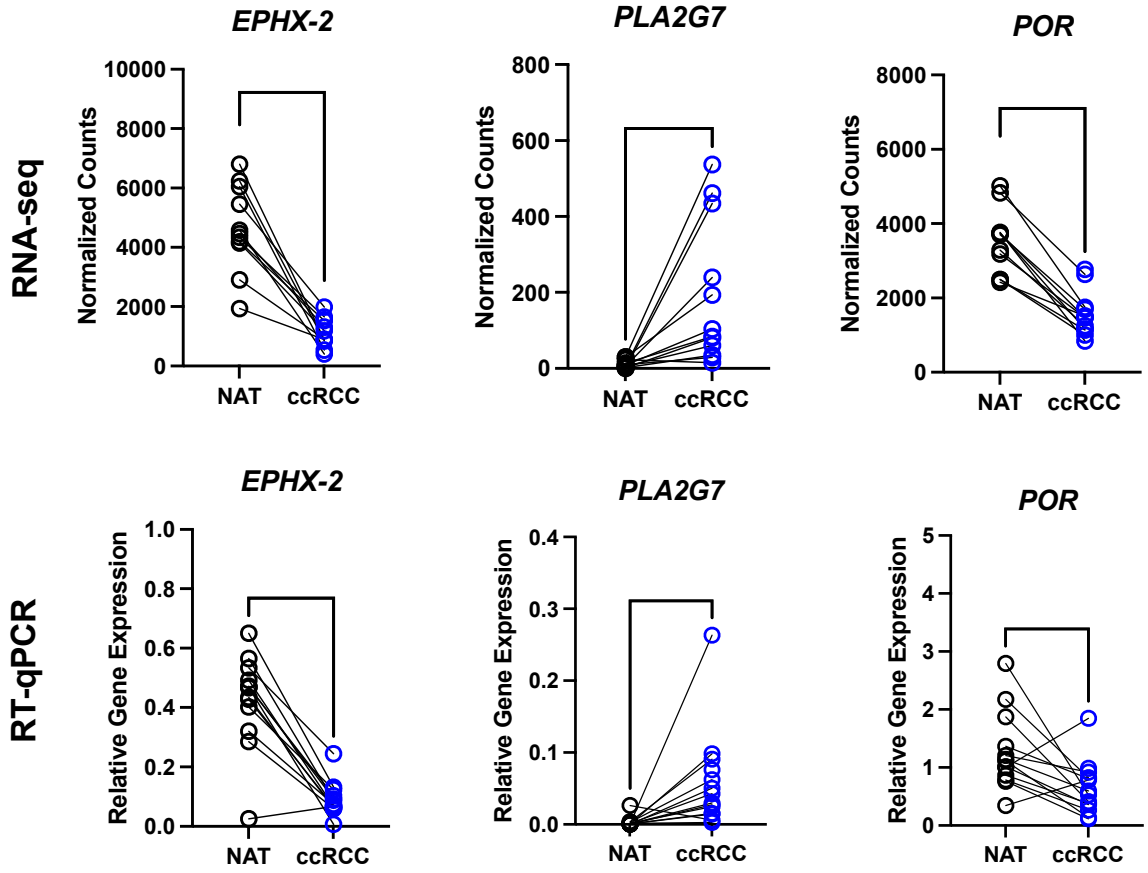


**Figure 2.8. Validation of *EPHX-2, PLA2G7*, and *POR* gene expression via RT-qPCR.** For RT-qPCR, gene expression is normalized to *RPL13,* and all statistical analyses used an unpaired t-test performed on Prism Graphpad. *$p < 0.05$, **$p < 0.01$, ***$p < 0.001$, and ****$p < 0.0001$

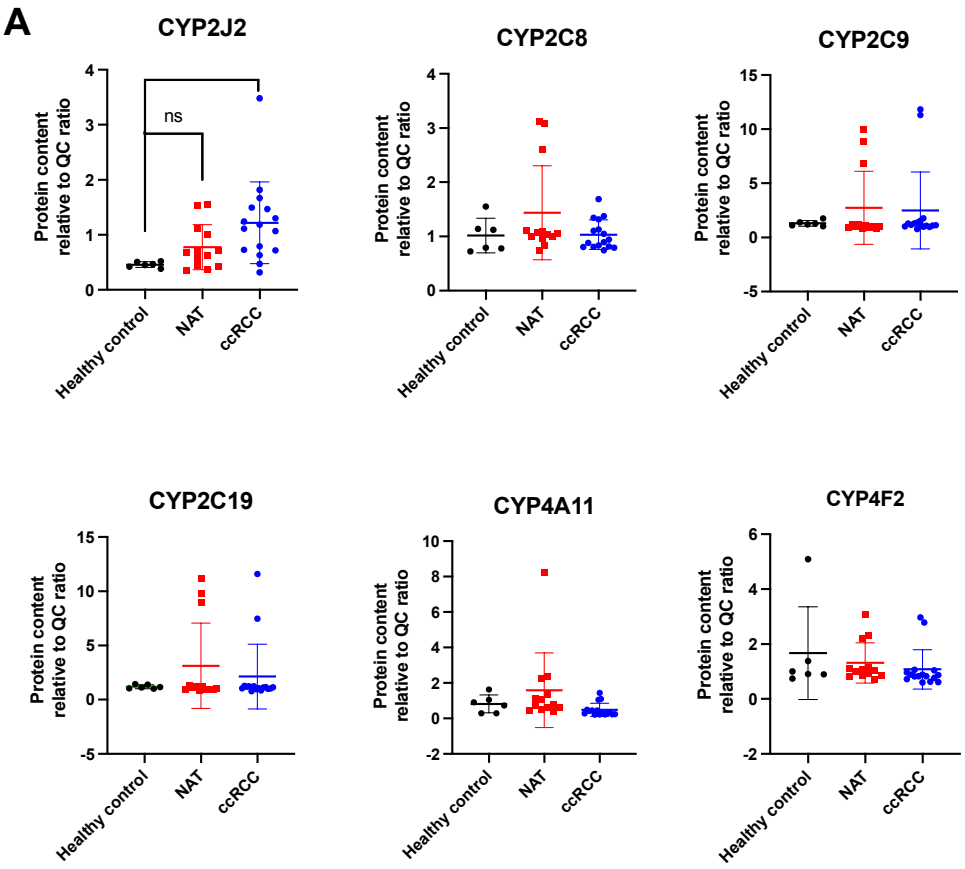
A
CYP2J2
CYP2C8
CYP2C9
CYP2C19
CYP4A11
CYP4F2
Protein content relative to QC ratio
ns
Healthy control
NAT
ccRCC

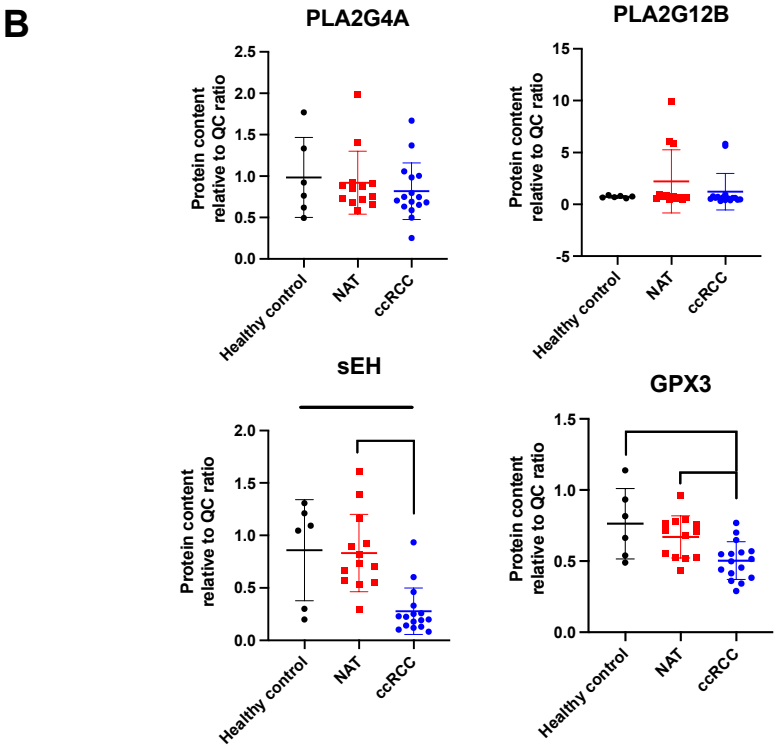
B
PLA2G4A
PLA2G12B
sEH
GPX3
Protein content relative to QC ratio
Healthy control
NAT
ccRCC

**Figure 2.9. Relative protein levels of enzymes involved in the arachidonic acid pathway in healthy (n=6), histologically normal adjacent (n=13), and ccRCC tumor tissues (n=16).** A) relative expression of cytochrome P450s; (B) relative expression of non-CYP proteins involved in the AA pathway. All data were generated from three independent tryptic digestions and are presented as mean ± SD. Statistical analysis was performed using a one-way ANOVA test on Prism Graphpad. *$p < 0.05$, **$p < 0.01$, and ***$p < 0.001$.

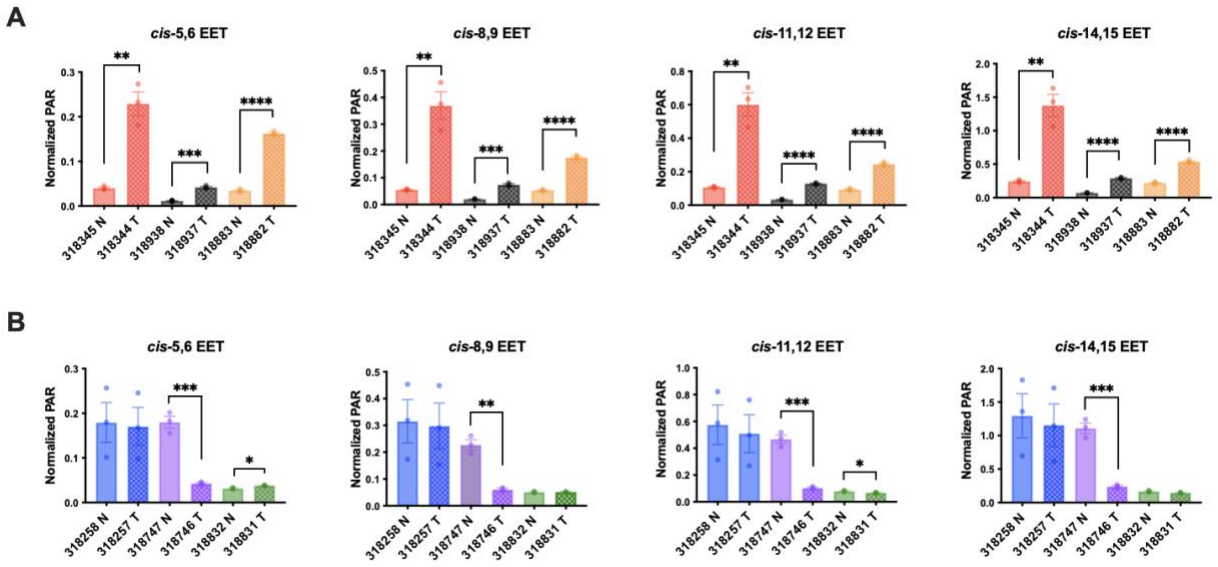


**Figure 2.10. LC-MS/MS quantification of regioisomers of EETs in ccRCC tumor tissues compared to matched normal adjacent tissues (NATs).** A) All four regioisomers of EETs are significantly upregulated in ccRCC tumor tissues. B) EETs are significantly downregulated or unchanged in ccRCC tumor tissues. Statistical analyses were performed using an unpaired t-test using the Prism Graphpad software. n=6 matched pairs. *$p < 0.05$, **$p < 0.01$, ***$p < 0.001$, and ****$p < 0.0001$

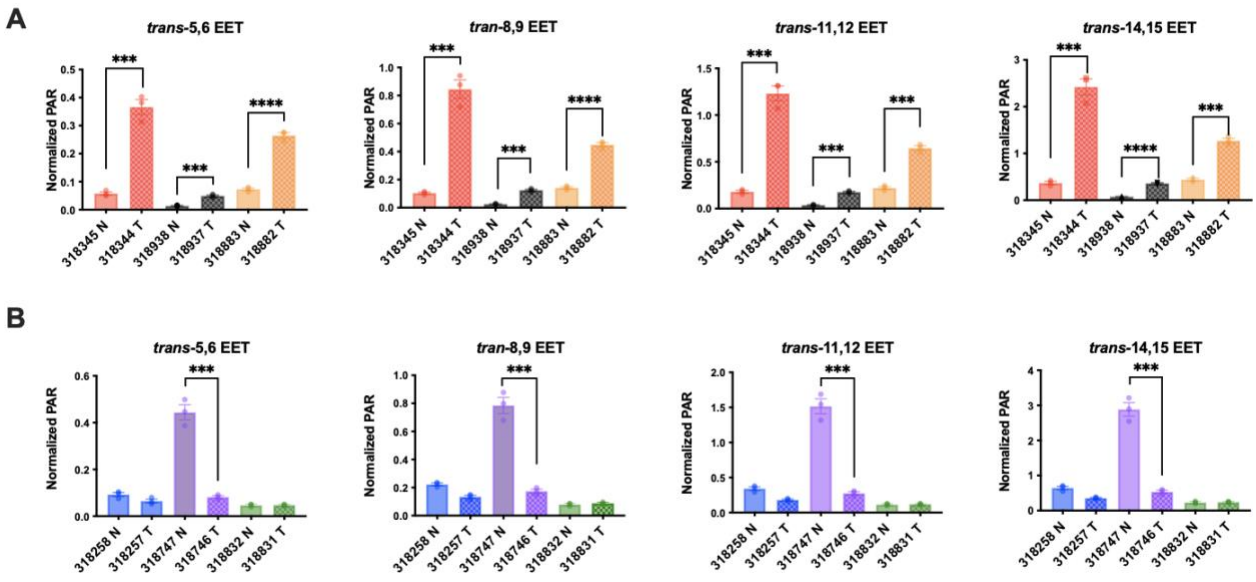


**Figure 2.11. LC-MS/MS quantification of regioisomers of EETs in ccRCC tumor tissues compared to matched normal adjacent tissues (NATs).** A) All four regioisomers of *trans*-EETs are significantly upregulated in ccRCC tumor tissues. B) *trans*-EETs are significantly downregulated or unchanged in ccRCC tumor tissues. Statistical analyses were performed using an unpaired t-test using the Prism Graphpad software. n=6 matched pairs.

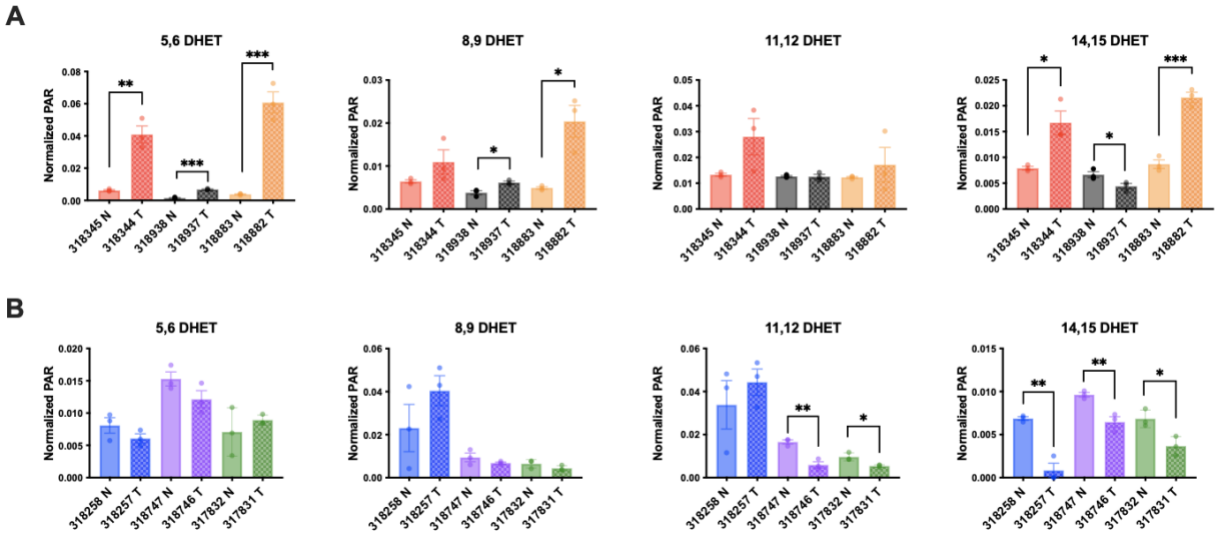


**Figure 2.12. LC-MS/MS quantification of regioisomers of EETs in ccRCC tumor tissues compared to matched normal adjacent tissues (NATs).** A) All four regioisomers of DHETs are significantly upregulated in ccRCC tumor tissues. B) DHETs are significantly downregulated or unchanged in ccRCC tumor tissues. Statistical analyses were performed using an unpaired t-test using the Prism Graphpad software. n=6 matched pairs. *$p < 0.05$, **$p < 0.01$, ***$p < 0.001$, and ****$p < 0.0001$

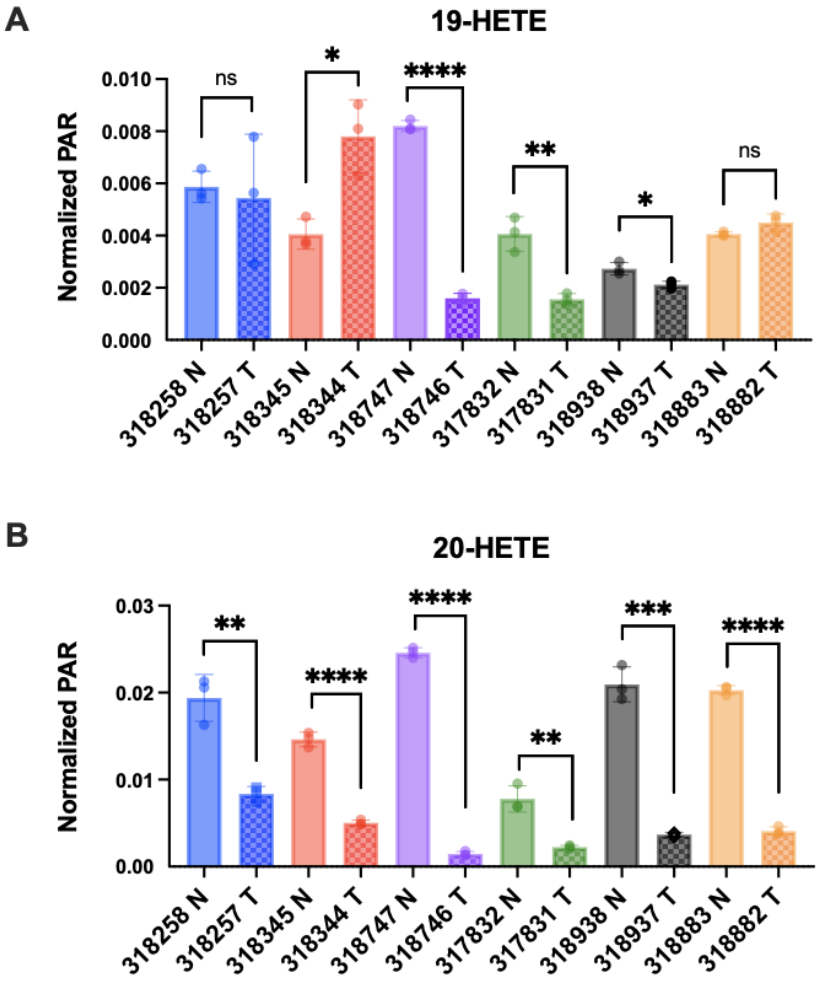


**Figure 2.13. LC-MS/MS quantification of 19- and 20-HETE levels in ccRCC tumor and normal adjacent tissues (NAT).** A) 19-HETE levels are variable between different matched pairs with several pairs exhibiting reduced levels of 19-HETE in ccRCC. B) 20-HETE levels are significantly reduced in ccRCC tumor tissues. Statistical analyses were performed using an unpaired t-test using the Prism Graphpad software. n=6 matched pairs. *$p < 0.05$, **$p < 0.01$, ***$p < 0.001$, and ****$p < 0.0001$

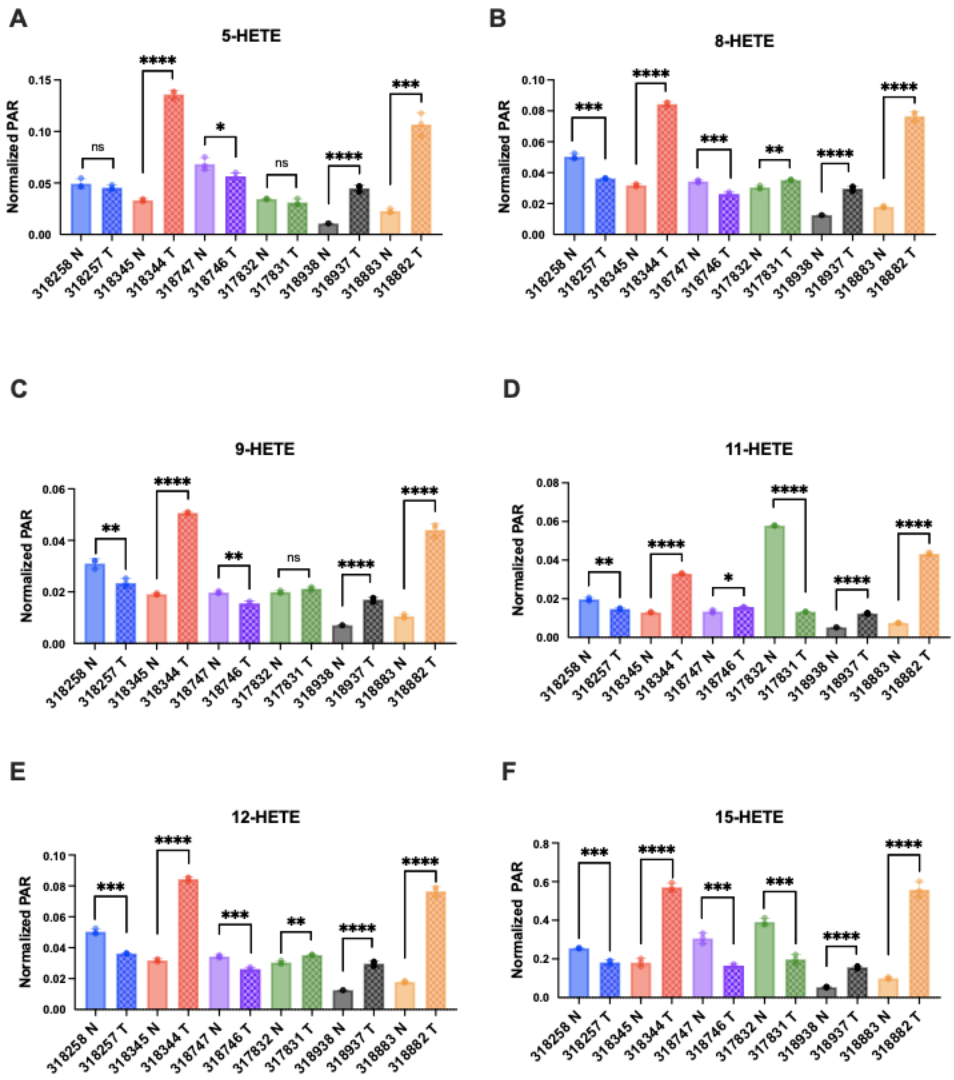


**Figure 2.14. LC-MS/MS quantification of several mid-chain HETEs in ccRCC tumor tissues compared to matched normal adjacent tissues (NAT).** A) 5-HETE; B) 8-HETE; C) 9-HETE; D) 11-HETE; E) 12-HETE; F) 15-HETE. n=6 matched pairs. Statistical analyses were performed using an unpaired t-test using the Prism Graphpad software. *$p < 0.05$, **$p < 0.01$, ***$p < 0.001$, and ****$p < 0.0001$

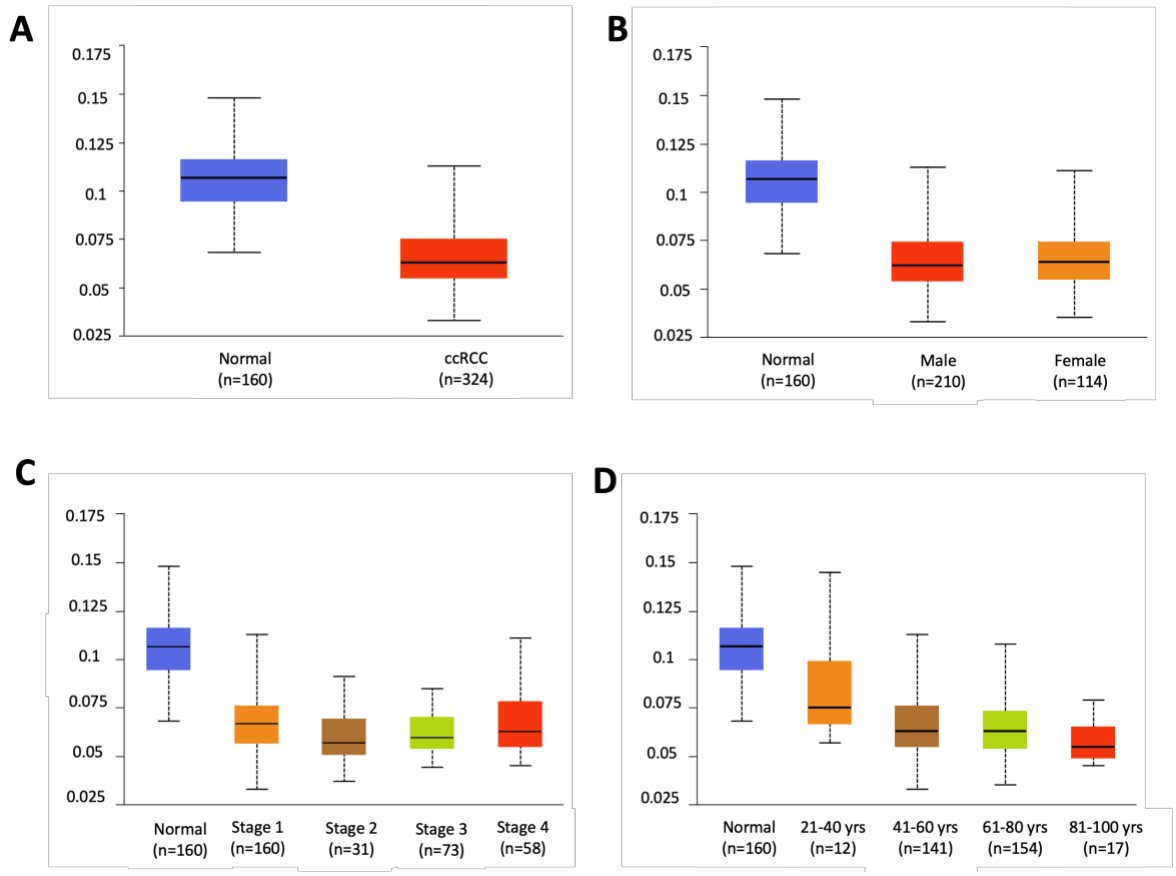


**Figure 2.15. CYP2J2 promoter DNA methylation profile in ccRCC tissues compared to normal, non-cancerous tissues.** A) Promoter DNA methylation is reduced in ccRCC tumor tissues; B) Sex based stratification of CYP2J2 promoter DNA methylation in ccRCC; C) ccRCC tumor stage-based stratification of DNA methylation of CYP2J2 promoter region; D) Age based stratification of CYP2J2 promoter DNA methylation. Figures were adapted from the UALCAN interactive web resource (*28, 29*) and were previously published by Zou et al (*15*).

## Schemes

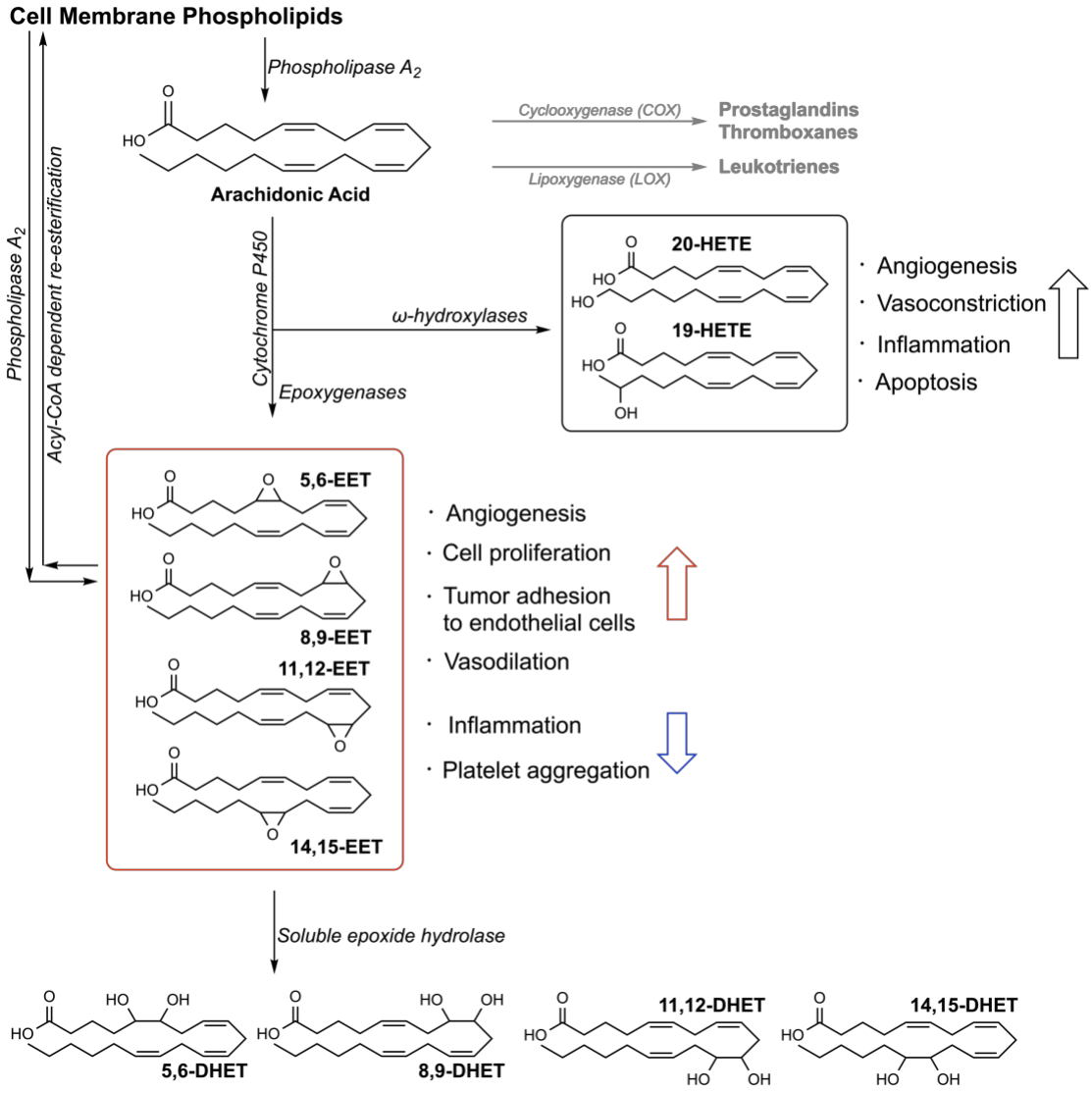


**Scheme 1. CYP mediated arachidonic acid pathway.**

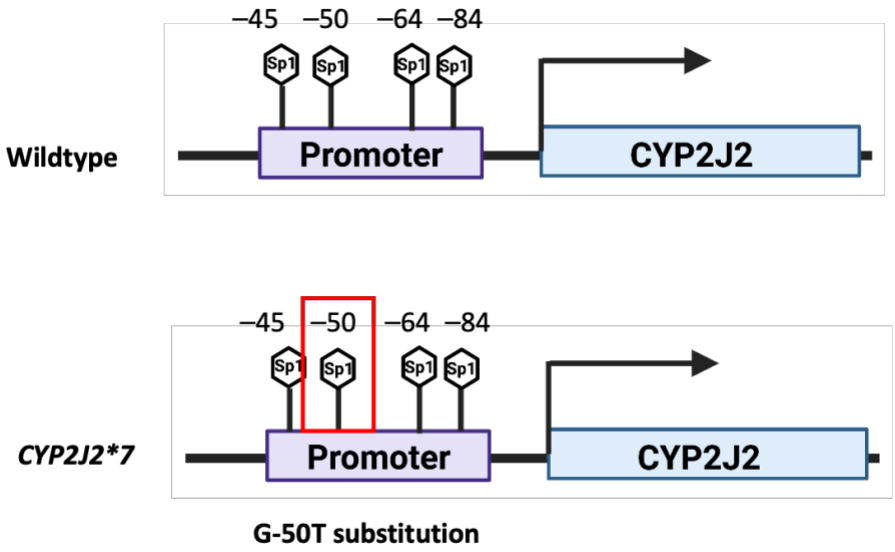


**Scheme 2. Transcriptional consequence of a loss of one Sp1 binding site in the CYP2J2*7 variant.**

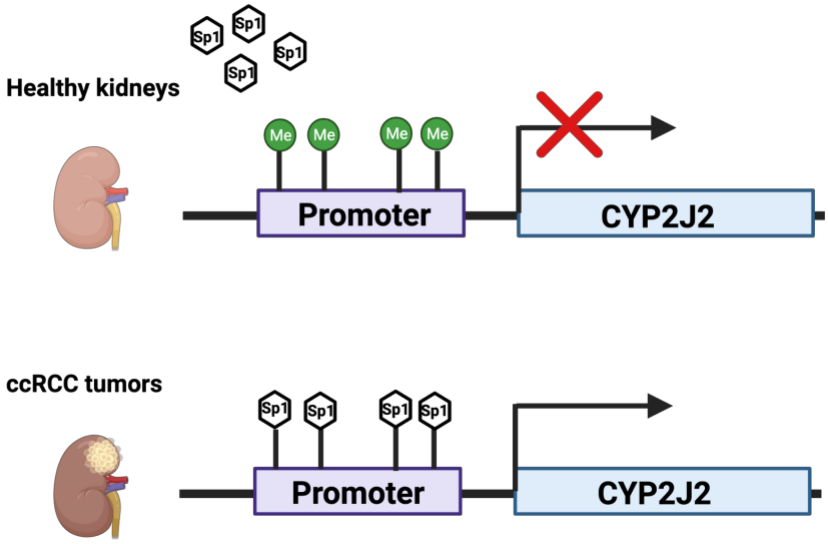


**Scheme 3. Proposed mechanism of CYP2J2 transcriptional regulation in ccRCC.** CYP2J2 is transcriptionally regulated by four putative Sp1 binding sites in the promoter region. DNA methylation prevents Sp1 from binding to the promoter region thus silencing gene expression. Compared to histologically normal adjacent tissues, CYP2J2 promoter DNA methylation is decreased in ccRCC which could explain its overexpression.

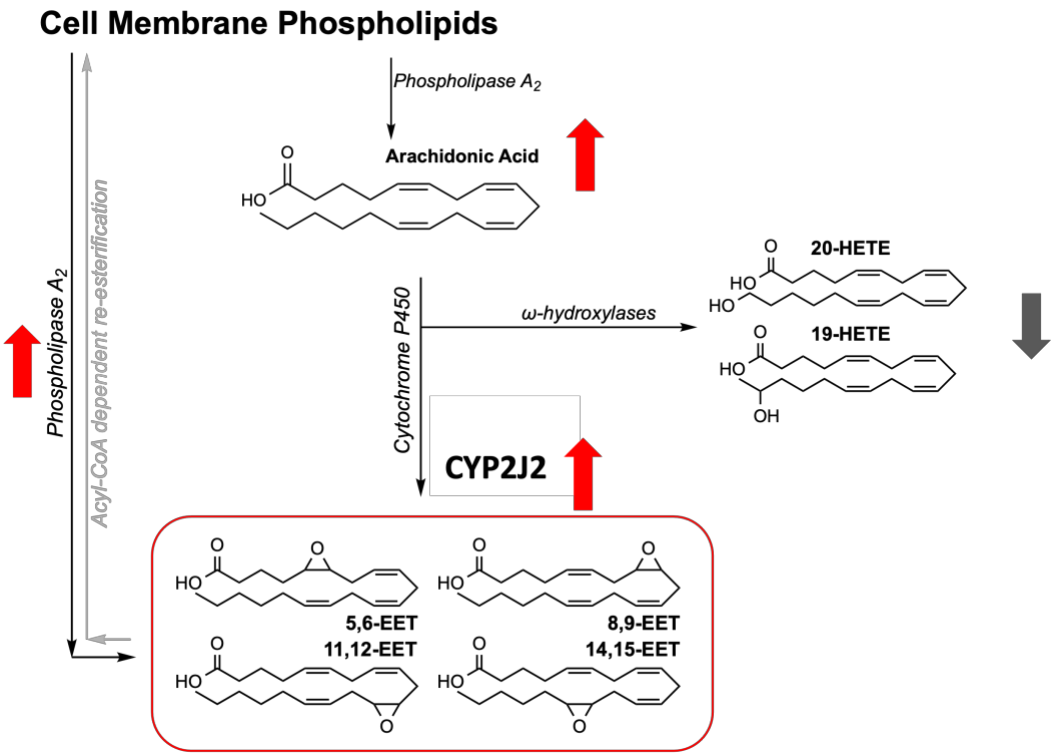


**Scheme 4. Summary of the hypothesized arachidonic acid pathway in ccRCC.**

## Tables

**Table I. Patient de-identified data.**

| Patient Information | | | | Diagnoses: clear cell renal cell carcinoma | | | |
|---|---|---|---|---|---|---|---|
| Sex | Male | 15 | | Tumor size (cm) | Mean +/- SD | 4.29 +/- 1.23 | |
| | Female | 3 | | | | | |
| Age (years) | Mean +/- SD | 63.5 +/- 12.6 | | Histological grade | G2 (9) | G3 (8) | G4 (1) |
| | Min | 31 | | | | | |
| | Max | 79 | | Tumor Necrosis* | Not detected | 3 | |
| | | | | | <5% | 1 | |
| | | | | | >5% | 6 | |

*Tumor necrosis factor was not reported for all the ccRCC tumor samples

**Table II. MS/MS transitions of peptides for relative quantitative proteomics.**

| Protein | Peptides | Parent Ion (m/z, Da) | Fragmentation (m/z, Da) |
|---|---|---|---|
| **BSA** | LVNELTEFAK.+2y9.light | 582.32 | 1050.55 |
| | LVNELTEFAK.+2y8.light | 582.32 | 951.48 |
| | LVNELTEFAK.+2y7.light | 582.32 | 837.44 |
| | LVNELTEFAK.+2y6.light | 582.32 | 708.39 |
| | LVNELTEFAK.+2y9.heavy | 586.33 | 1058.56 |
| | LVNELTEFAK.+2y8.heavy | 586.33 | 959.49 |
| | LVNELTEFAK.+2y7.heavy | 586.33 | 845.45 |
| | LVNELTEFAK.+2y6.heavy | 586.33 | 716.41 |
| | AEFVEVTK.+2y6.light | 461.75 | 722.41 |
| | AEFVEVTK.+2y5.light | 461.75 | 575.34 |
| | AEFVEVTK.+2y4.light | 461.75 | 476.27 |
| | AEFVEVTK.+2y3.light | 461.75 | 347.23 |
| | AEFVEVTK.+2y6.heavy | 465.75 | 730.42 |
| | AEFVEVTK.+2y5.heavy | 465.75 | 583.35 |
| | AEFVEVTK.+2y4.heavy | 465.75 | 484.29 |
| | AEFVEVTK.+2y3.heavy | 465.75 | 355.24 |
| **CYP2C8** | VQEEIDHVIGR.+2y9.light | 647.84 | 1067.55 |
| | VQEEIDHVIGR.+2y8.light | 647.84 | 938.51 |
| | VQEEIDHVIGR.+2y7.light | 647.84 | 809.46 |
| | VQEEIDHVIGR.+2y6.light | 647.84 | 696.38 |
| | VQEEIDHVIGR.+2y5.light | 647.84 | 581.35 |
| | VQEEIDHVIGR.+2y9.heavy | 652.85 | 1077.56 |
| | VQEEIDHVIGR.+2y8.heavy | 652.85 | 948.51 |
| | VQEEIDHVIGR.+2y7.heavy | 652.85 | 819.47 |
| | VQEEIDHVIGR.+2y6.heavy | 652.85 | 706.39 |
| | VQEEIDHVIGR.+2y5.heavy | 652.85 | 591.36 |
| | EALIDNGEEFSGR.+2y10.light | 718.84 | 1123.5 |
| | EALIDNGEEFSGR.+2y9.light | 718.84 | 1010.42 |
| | EALIDNGEEFSGR.+2y8.light | 718.84 | 895.39 |
| | EALIDNGEEFSGR.+2y7.light | 718.84 | 781.35 |
| | EALIDNGEEFSGR.+2y10.heavy | 723.84 | 1133.51 |
| | EALIDNGEEFSGR.+2y9.heavy | 723.84 | 1020.43 |
| | EALIDNGEEFSGR.+2y8.heavy | 723.84 | 905.4 |
| | EALIDNGEEFSGR.+2y7.heavy | 723.84 | 791.36 |
| **CYP2C9** | LPPGPTPLPVIGNILQIGIK.+3y10.light | 679.75 | 1068.68 |
| | LPPGPTPLPVIGNILQIGIK.+3y9.light | 679.75 | 955.59 |
| | LPPGPTPLPVIGNILQIGIK.+3y8.light | 679.75 | 898.57 |
| | LPPGPTPLPVIGNILQIGIK.+3y16+3.light | 679.75 | 558.35 |
| | LPPGPTPLPVIGNILQIGIK.+3y10.heavy | 682.43 | 1076.69 |
| | LPPGPTPLPVIGNILQIGIK.+3y9.heavy | 682.43 | 963.61 |
| | LPPGPTPLPVIGNILQIGIK.+3y8.heavy | 682.43 | 906.59 |

| | | | |
|---|---|---|---|
| | LPPGPTPLPVIGNILQIGIK.+3y16+2.heavy | 682.43 | 841.03 |
| | YIDLLPTSLPHAVTC[CAM]DIK.+3y13.light | 686.03 | 1438.74 |
| | YIDLLPTSLPHAVTC[CAM]DIK.+3y9.light | 686.03 | 1040.52 |
| | YIDLLPTSLPHAVTC[CAM]DIK.+3y16+2.light | 686.03 | 890.47 |
| | YIDLLPTSLPHAVTC[CAM]DIK.+3y13+2.light | 686.03 | 719.87 |
| | YIDLLPTSLPHAVTC[CAM]DIK.+3y13.heavy | 688.7 | 1446.75 |
| | YIDLLPTSLPHAVTC[CAM]DIK.+3y9.heavy | 688.7 | 1048.53 |
| | YIDLLPTSLPHAVTC[CAM]DIK.+3y16+2.heavy | 688.7 | 894.48 |
| | YIDLLPTSLPHAVTC[CAM]DIK.+3y13+2.heavy | 688.7 | 723.88 |
| **CYP2C19** | SNYFMPFSAGK.+2y9.light | 624.79 | 1047.5 |
| | SNYFMPFSAGK.+2y8.light | 624.79 | 884.43 |
| | SNYFMPFSAGK.+2y7.light | 624.79 | 737.37 |
| | SNYFMPFSAGK.+2y6.light | 624.79 | 606.32 |
| | SNYFMPFSAGK.+2y9.heavy | 628.8 | 1055.51 |
| | SNYFMPFSAGK.+2y8.heavy | 628.8 | 892.45 |
| | SNYFMPFSAGK.+2y7.heavy | 628.8 | 745.38 |
| | SNYFMPFSAGK.+2y6.heavy | 628.8 | 614.34 |
| | DFIDC[CAM]FLIK.+2y7.light | 585.8 | 908.49 |
| | DFIDC[CAM]FLIK.+2y6.light | 585.8 | 795.41 |
| | DFIDC[CAM]FLIK.+2y5.light | 585.8 | 680.38 |
| | DFIDC[CAM]FLIK.+2y8+2.light | 585.8 | 528.28 |
| | DFIDC[CAM]FLIK.+2y7.heavy | 589.8 | 916.51 |
| | DFIDC[CAM]FLIK.+2y6.heavy | 589.8 | 803.42 |
| | DFIDC[CAM]FLIK.+2y5.heavy | 589.8 | 688.39 |
| | DFIDC[CAM]FLIK.+2y8+2.heavy | 589.8 | 532.29 |

| Protein | Peptides | Parent Ion (m/z, Da) | Fragmentation (m/z, Da) |
|---|---|---|---|
| **CYP2J2** | VIGQGQQPSTAAR.+2y9.light | 656.85 | 915.46 |
| | VIGQGQQPSTAAR.+2y7.light | 656.85 | 730.38 |
| | VIGQGQQPSTAAR.+2y6.light | 656.85 | 602.33 |
| | VIGQGQQPSTAAR.+2y6+2.light | 656.85 | 301.67 |
| | VIGQGQQPSTAAR.+2y9.heavy | 661.86 | 925.47 |
| | VIGQGQQPSTAAR.+2y7.heavy | 661.86 | 740.39 |
| | VIGQGQQPSTAAR.+2y6.heavy | 661.86 | 612.33 |
| | VIGQGQQPSTAAR.+2y6+2.heavy | 661.86 | 306.67 |
| | LLDEVTYLEASK.+2y8.light | 690.87 | 910.49 |
| | LLDEVTYLEASK.+2y7.light | 690.87 | 811.42 |
| | LLDEVTYLEASK.+2y6.light | 690.87 | 710.37 |
| | LLDEVTYLEASK.+2y8.heavy | 694.87 | 918.5 |
| | LLDEVTYLEASK.+2y7.heavy | 694.87 | 819.43 |
| | LLDEVTYLEASK.+2y6.heavy | 694.87 | 718.39 |
| **CYP4A11** | VATALTLLR.+2y7.light | 479.31 | 787.5 |
| | VATALTLLR.+2y6.light | 479.31 | 686.46 |
| | VATALTLLR.+2y5.light | 479.31 | 615.42 |
| | VATALTLLR.+2y4.light | 479.31 | 502.33 |
| | VATALTLLR.+2y7.heavy | 484.31 | 797.51 |
| | VATALTLLR.+2y6.heavy | 484.31 | 696.46 |
| | VATALTLLR.+2y5.heavy | 484.31 | 625.43 |
| | VATALTLLR.+2y4.heavy | 484.31 | 512.34 |
| | C[CAM]AFSHQGSIQVDR.+3y9.light | 502.24 | 1039.53 |
| | C[CAM]AFSHQGSIQVDR.+3y8.light | 502.24 | 902.47 |
| | C[CAM]AFSHQGSIQVDR.+3y7.light | 502.24 | 774.41 |
| | C[CAM]AFSHQGSIQVDR.+3y6.light | 502.24 | 717.39 |
| | C[CAM]AFSHQGSIQVDR.+3y5.light | 502.24 | 630.36 |
| | C[CAM]AFSHQGSIQVDR.+3y12+2.light | 502.24 | 672.84 |
| | C[CAM]AFSHQGSIQVDR.+3y11+2.light | 502.24 | 637.32 |
| | C[CAM]AFSHQGSIQVDR.+3y10+2.light | 502.24 | 563.78 |
| | C[CAM]AFSHQGSIQVDR.+3y9.heavy | 505.57 | 1049.54 |
| | C[CAM]AFSHQGSIQVDR.+3y8.heavy | 505.57 | 912.48 |
| | C[CAM]AFSHQGSIQVDR.+3y7.heavy | 505.57 | 784.42 |
| | C[CAM]AFSHQGSIQVDR.+3y6.heavy | 505.57 | 727.4 |
| | C[CAM]AFSHQGSIQVDR.+3y5.heavy | 505.57 | 640.37 |
| | C[CAM]AFSHQGSIQVDR.+3y4.heavy | 505.57 | 527.28 |
| | C[CAM]AFSHQGSIQVDR.+3y12+2.heavy | 505.57 | 677.84 |
| | C[CAM]AFSHQGSIQVDR.+3y11+2.heavy | 505.57 | 642.32 |
| | C[CAM]AFSHQGSIQVDR.+3y10+2.heavy | 505.57 | 568.79 |
| | C[CAM]AFSHQGSIQVDR.+3y9+2.heavy | 505.57 | 525.27 |
| **CYP4F2** | SPLAFIPFSAGPR.+2y10.light | 680.37 | 1062.57 |
| | SPLAFIPFSAGPR.+2y9.light | 680.37 | 991.54 |
| | SPLAFIPFSAGPR.+2y8.light | 680.37 | 844.47 |

| | | | |
|---|---|---|---|
| | SPLAFIPFSAGPR.+2y7.light | 680.37 | 731.38 |
| | SPLAFIPFSAGPR.+2y10.heavy | 685.38 | 1072.58 |
| | SPLAFIPFSAGPR.+2y9.heavy | 685.38 | 1001.54 |
| | SPLAFIPFSAGPR.+2y8.heavy | 685.38 | 854.48 |
| | SPLAFIPFSAGPR.+2y7.heavy | 685.38 | 741.39 |
| | SVINASAAIAPK.+2y10.light | 571.33 | 955.56 |
| | SVINASAAIAPK.+2y9.light | 571.33 | 842.47 |
| | SVINASAAIAPK.+2y8.light | 571.33 | 728.43 |
| | SVINASAAIAPK.+2y7.light | 571.33 | 657.39 |
| | SVINASAAIAPK.+2y10.heavy | 575.34 | 963.57 |
| | SVINASAAIAPK.+2y9.heavy | 575.34 | 850.49 |
| | SVINASAAIAPK.+2y8.heavy | 575.34 | 736.44 |
| | SVINASAAIAPK.+2y7.heavy | 575.34 | 665.41 |
| **GPX-3** | QEPGENSEILPTLK.+2y12.light | 777.9 | 1297.7 |
| | QEPGENSEILPTLK.+2y9.light | 777.9 | 1014.58 |
| | QEPGENSEILPTLK.+2y4.light | 777.9 | 458.3 |
| | QEPGENSEILPTLK.+2y12+2.light | 777.9 | 649.35 |
| | QEPGENSEILPTLK.+2y12.heavy | 781.91 | 1305.71 |
| | QEPGENSEILPTLK.+2y9.heavy | 781.91 | 1022.6 |
| | QEPGENSEILPTLK.+2y4.heavy | 781.91 | 466.31 |
| | QEPGENSEILPTLK.+2y12+2.heavy | 781.91 | 653.36 |
| | FLVGPDGIPIMR.+2y10.light | 657.87 | 1054.57 |
| | FLVGPDGIPIMR.+2y9.light | 657.87 | 955.5 |
| | FLVGPDGIPIMR.+2y8.light | 657.87 | 898.48 |
| | FLVGPDGIPIMR.+2y4.light | 657.87 | 516.3 |
| | FLVGPDGIPIMR.+2y10.heavy | 662.87 | 1064.58 |
| | FLVGPDGIPIMR.+2y9.heavy | 662.87 | 965.51 |
| | FLVGPDGIPIMR.+2y8.heavy | 662.87 | 908.49 |
| | FLVGPDGIPIMR.+2y4.heavy | 662.87 | 526.3 |

| Protein | Peptides | Parent Ion (m/z, Da) | Fragmentation (m/z, Da) |
|---|---|---|---|
| **PLA2G4A** | GSTMEEELENITTK.+2y10.light | 791.37 | 1205.59 |
| | GSTMEEELENITTK.+2y9.light | 791.37 | 1076.55 |
| | GSTMEEELENITTK.+2y8.light | 791.37 | 947.5 |
| | GSTMEEELENITTK.+2y7.light | 791.37 | 818.46 |
| | GSTMEEELENITTK.+2y10.heavy | 795.38 | 1213.6 |
| | GSTMEEELENITTK.+2y9.heavy | 795.38 | 1084.56 |
| | GSTMEEELENITTK.+2y8.heavy | 795.38 | 955.52 |
| | GSTMEEELENITTK.+2y7.heavy | 795.38 | 826.48 |
| | IDPYVFDR.+2y7.light | 512.76 | 911.43 |
| | IDPYVFDR.+2y6.light | 512.76 | 796.4 |
| | IDPYVFDR.+2y4.light | 512.76 | 536.28 |
| | IDPYVFDR.+2y6+2.light | 512.76 | 398.7 |
| | IDPYVFDR.+2y7.heavy | 517.76 | 921.43 |
| | IDPYVFDR.+2y6.heavy | 517.76 | 806.41 |
| | IDPYVFDR.+2y4.heavy | 517.76 | 546.29 |
| | IDPYVFDR.+2y6+2.heavy | 517.76 | 403.71 |
| **PLA2G12B** | APMPRPGYKPQEPNGC[CAM]GSYFLGLK.+3y10.light | 888.77 | 1101.54 |
| | APMPRPGYKPQEPNGC[CAM]GSYFLGLK.+3y9.light | 888.77 | 1044.52 |
| | APMPRPGYKPQEPNGC[CAM]GSYFLGLK.+3y12+2.light | 888.77 | 656.82 |
| | APMPRPGYKPQEPNGC[CAM]GSYFLGLK.+3y19+3.light | 888.77 | 704.68 |
| | APMPRPGYKPQEPNGC[CAM]GSYFLGLK.+3y10.heavy | 891.44 | 1109.55 |
| | APMPRPGYKPQEPNGC[CAM]GSYFLGLK.+3y9.heavy | 891.44 | 1052.53 |
| | APMPRPGYKPQEPNGC[CAM]GSYFLGLK.+3y12+2.heavy | 891.44 | 660.83 |
| | APMPRPGYKPQEPNGC[CAM]GSYFLGLK.+3y19+3.heavy | 891.44 | 707.35 |
| | VPESMDLGIPAMTK.+2y12.light | 744.88 | 1292.62 |
| | VPESMDLGIPAMTK.+2y11.light | 744.88 | 1163.58 |
| | VPESMDLGIPAMTK.+2y9.light | 744.88 | 945.51 |
| | VPESMDLGIPAMTK.+2y5.light | 744.88 | 547.29 |
| | VPESMDLGIPAMTK.+2y12.heavy | 748.88 | 1300.64 |
| | VPESMDLGIPAMTK.+2y11.heavy | 748.88 | 1171.59 |
| | VPESMDLGIPAMTK.+2y9.heavy | 748.88 | 953.52 |
| | VPESMDLGIPAMTK.+2y5.heavy | 748.88 | 555.31 |
| **sEH** | YQIPALAQAGYR.+2y10.light | 675.86 | 1059.59 |
| | YQIPALAQAGYR.+2y9.light | 675.86 | 946.51 |
| | YQIPALAQAGYR.+2y8.light | 675.86 | 849.46 |
| | YQIPALAQAGYR.+2y7.light | 675.86 | 778.42 |

| | | |
|---|---|---|
| YQIPALAQAGYR.+2y10.heavy | 680.87 | 1069.6 |
| YQIPALAQAGYR.+2y9.heavy | 680.87 | 956.52 |
| YQIPALAQAGYR.+2y8.heavy | 680.87 | 859.47 |
| YQIPALAQAGYR.+2y7.heavy | 680.87 | 788.43 |
| GLLNDAFQK.+2y7.light | 503.27 | 835.43 |
| GLLNDAFQK.+2y6.light | 503.27 | 722.35 |
| GLLNDAFQK.+2y5.light | 503.27 | 608.3 |
| GLLNDAFQK.+2y4+2.light | 503.27 | 247.14 |
| GLLNDAFQK.+2y7.heavy | 507.28 | 843.45 |
| GLLNDAFQK.+2y6.heavy | 507.28 | 730.36 |
| GLLNDAFQK.+2y5.heavy | 507.28 | 616.32 |
| GLLNDAFQK.+2y4+2.heavy | 507.28 | 251.15 |

## References


1. R. L. Siegel, K. D. Miller, H. E. Fuchs, A. Jemal, Cancer statistics, 2022. *CA: A Cancer Journal for Clinicians* **72**, 7-33 (2022).
2. W. Du *et al.*, HIF drives lipid deposition and cancer in ccRCC via repression of fatty acid metabolism. *Nature Communications* **8**, (2017).
3. C. L. Cowey, W. K. Rathmell. (2009).
4. J. J. Hsieh *et al.*, Renal cell carcinoma. *Nature Reviews Disease Primers*, (2017).
5. A. Afriansyah, A. R. A. Hamid, C. A. Mochtar, R. Umbas, Targeted Therapy for Metastatic Renal Cell Carcinoma. *Acta medica Indonesiana* **48**, 335-347 (2016).
6. J. Bedke *et al.*, in *World Journal of Urology*. (Springer Verlag, 2017), vol. 35, pp. 179-188.
7. A. A. Spector, H. Y. Kim, Cytochrome P450 epoxygenase pathway of polyunsaturated fatty acid metabolism. *Biochimica et biophysica acta* **1851**, 356-356 (2015).
8. S. Wu, C. R. Moomaw, K. B. Tomer, J. R. Falck, D. C. Zeldin, Molecular cloning and expression of CYP2J2, a human cytochrome P450 arachidonic acid epoxygenase highly expressed in heart. *The Journal of biological chemistry* **271**, 3460-3468 (1996).
9. A. A. Spector, X. Fang, G. D. Snyder, N. L. Weintraub, Epoxyeicosatrienoic acids (EETs): metabolism and biochemical function. *Progress in Lipid Research* **43**, 55-90 (2004).
10. A. S. a. A. W. N. Arthur, Action of epoxyeicosatrienoic acids on cellular function. *American Journal of Physiology - Cell Physiology* **292**, 996-1012 , pmid = 16987999 , publisher = American Physiological Society (2007).
11. I. Fleming. (2007).
12. D. Panigrahy, E. R. Greene, A. Pozzi, D. W. Wang, D. C. Zeldin, EET signaling in cancer. *Cancer metastasis reviews* **30**, 525-525 (2011).
13. J. G. Jiang *et al.*, Cytochrome P450 2J2 Promotes the Neoplastic Phenotype of Carcinoma Cells and Is Up-regulated in Human Tumors. *Cancer Research* **65**, 4707-4715 (2005).
14. D. Wang, R. N. DuBois, in *Journal of Clinical Investigation*. (American Society for Clinical Investigation, 2012), vol. 122, pp. 19-22.
15. X. Zou, Z. Mo, CYP2J2 Is a Diagnostic and Prognostic Biomarker Associated with Immune Infiltration in Kidney Renal Clear Cell Carcinoma. *BioMed Research International* **2021**, (2021).
16. M. Zeigler, D. Whittington, N. Sotoodehnia, R. N. Lemaitre, R. A. Totah, A sensitive and improved throughput UPLC-MS/MS quantitation method of total cytochrome P450 mediated arachidonic acid metabolites that can separate regio-isomers and cis/trans-EETs from human plasma. *Chemistry and physics of lipids* **216**, 162-170 (2018).
17. E. A. Mroz, J. W. Rocco, The challenges of tumor genetic diversity. *Cancer* **123**, 917-917 (2017).
18. H. M. a. A. O. S. E.-K. Zaid, The role of mid-chain hydroxyeicosatetraenoic acids in the pathogenesis of hypertension and cardiac hypertrophy. *Archives of Toxicology 2015 90:1* **90**, 119-136 , pmid = 26525395 , publisher = Springer (2015).
19. T. Aliwarga *et al.*, Enzymatic and free radical formation of cis- and trans-epoxyeicosatrienoic acids in vitro and in vivo. *Free Radical Biology and Medicine* **112**, 131-140 (2017).

20. E. Evangelista, C. Cho, T. Aliwarga, R. A. Totah, Expression and function of eicosanoid producing cytochrome P450 enzymes in solid tumors. *Frontiers in Pharmacology*, (2020).
21. S. N. Hart *et al.*, Genetic polymorphisms in cytochrome P450 oxidoreductase influence microsomal P450-catalyzed drug metabolism. *Pharmacogenetics and Genomics* **18**, 11-24 (2008).
22. L. M. King *et al.*, Cloning of CYP2J2 gene and identification of functional polymorphisms. *Molecular pharmacology* **61**, 840-852 (2002).
23. M. Spiecker *et al.*, Risk of coronary artery disease associated with polymorphism of the cytochrome P450 epoxygenase CYP2J2. *Circulation* **110**, 2132-2136 (2004).
24. M. M. a. E. Maher, Epigenetics of renal cell carcinoma: The path towards new diagnostics and therapeutics. *Genome Medicine* **2**, 1-10 (2010).
25. A.-C. Kate Beishline and Jane, Sp1 and the 'hallmarks of cancer' ,.
26. C. Donghong Zhang and Jinli Lou and Xu Zhang and Lin Zhang and Fei Wang and Danfei Xu and Na Niu and Yidong Wang and Yue Wu and Wei, Hyperhomocysteinemia results from and promotes hepatocellular carcinoma via CYP450 metabolism by CYP2J2 DNA methylation. *Oncotarget* **8**, 15377-15392 , pmid = 28030819 , publisher = Oncotarget (2017).
27. J. G. Jiang *et al.*, Cytochrome P450 Epoxygenase Promotes Human Cancer Metastasis. *Cancer Research* **67**, 6665-6674 (2007).
28. S. C. a. B. B. a. S. A. H. B. a. C. J. C. a. I. P.-R. a. B. V. S. K. C. a. S. V. Darshan, UALCAN: A Portal for Facilitating Tumor Subgroup Gene Expression and Survival Analyses. *Neoplasia (New York, N.Y.)* **19**, 649-658 , pmid = 28732212 , publisher = Neoplasia (2017).
29. J. N. a. Z. S. Q. a. Darshan Shimoga Chandrashekar and Santhosh Kumar Karthikeyan and Praveen Kumar Korla and Henalben Patel and Ahmedur Rahman Shovon and Mohammad Athar and George, UALCAN: An update to the integrated cancer data analysis platform. *Neoplasia (New York, N.Y.)* **25**, 18-27 , pmid = 35078134 , publisher = Neoplasia (2022).

**Chapter 3**

**CYP2J2 and EET mediated cardio-protection against tyrosine kinase inhibitor toxicity**

## 3.1 Introduction

Tyrosine kinase inhibitors (TKIs) are anti-angiogenic chemotherapy drugs that target the ATP binding pocket of receptor tyrosine kinases (RTKs) (*1*). TKIs, like many chemotherapeutics, have been associated with varying adverse cardiac events with the most common presentations including QT prolongation, hypertension, left ventricular dysfunction, and arrhythmia (*1, 2*). It is estimated that 75% of all TKIs are associated with at least one adverse cardiac event (Figure 3.1, Table I) that range from minor, more manageable cases to severe cardiotoxicity resulting in sudden death (e.g. nilotinib) (*3*). It is not uncommon for patients to stop treatment due to cardiac complications. However, the exact mechanism of TKI cardiotoxicity is not well elucidated and it is believed to be a complex issue related to genetic and environmental predispositions among other factors (*4*). Regardless, non-specific target binding has been commonly associated with TKI cardiotoxicity since the molecular target of TKIs is a highly conserved region among different RTKs which could lead to the inhibition of critical RTK activity in the heart. Despite this knowledge, drug induced cardiotoxicity remains both a complex and critical issue during chemotherapy that could lead to cessation of therapy or result in high incidences of cancer and cardiovascular related co-morbidities (*2, 5-7*).

Arachidonic acid (AA) is a polyunsaturated fatty acid critical for the formation of biologically active lipid signaling molecules that are implicated in numerous cardiovascular diseases (*8*). A subset of CYP450 enzymes (CYP2Cs and CYP2J2) referred to as epoxygenases generate cardioprotective epoxide metabolites of AA known as epoxyeicosatrienoic acids (EETs)

(*9*). EETs are formed through the oxidation of one of the four double bonds of AA resulting in four regioisomers of *cis*-EETs: 14,15-, 11,12-, 8,9-, and 5,6-EETs (*8*). The half-life of EETs is presumed to be very short. The epoxides can be rapidly hydrolyzed to less active diols known as dihydroxyeicosatrienoic acids (DHETs) by soluble epoxide hydrolase (sEH) or re-esterified at the *sn-2* position in the phospholipid membranes. Once re-esterified, however, EETs can be quickly released from the membrane by phospholipase A2 in response to external stimulus (e.g. $Ca^{2+}$ influx) (*9*). In the human heart, CYP2J2 is the major isoform responsible for forming an equal ratio of all four *cis*-EETs. EETs are paracrine and autocrine modulators that are involved in a wide range of cellular processes including regulation of vascular function, promotion of anti-inflammatory and pro-angiogenic pathways, as well as inhibition of cell apoptosis (*10-12*). Most importantly, however, EETs have been examined extensively for their cardioprotective properties in numerous *in vitro* and *in vivo* systems against major adverse cardiac events such as myocardial infarction (MI), heart failure, and drug-induced toxicity (*13-17*).

In this study, we sought to investigate the role of CYP2J2 and 11,12-EET in mitigating TKI induced cardiotoxicity in two adult human ventricular derived myocyte lines. Our selection of TKIs for this study was based on two factors: (i) approval for clear cell renal cell carcinoma (ccRCC) treatment and (ii) incidence of cardiotoxicity (Table I). To assess the role of CYP2J2 against TKI cardiotoxicity, we manipulated *CYP2J2* expression in human cardiomyocytes and conditioned the cells with exogenous 11,12-EET, unless otherwise stated, prior to treatment with a panel of TKIs. Subsequently, gene set enrichment analysis of RNA-seq data was performed to elucidate the transcriptomic changes associated with TKI injury with varying CYP2J2 expression.

## 3.2 Experimental

### 3.2.1 Materials

Adult derived human ventricular myocytes, culture media and extra-cellular matrix coated flasks were purchased from Celprogen, Inc (Torrance, CA). AC16 human cardiomyocyte cell line was purchased from Sigma-Aldrich (St. Louis, MO). Axitinib, cabozantinib, erlotinib, gefitinib, nilotinib, pazopanib, lenvatinib, sorafenib, and sunitinib were purchased as the free base with a purity greater than 99% from LC Laboratories (Woburn, MA) and Toronto Research Chemicals (Ontario, Canada). CYP2J2 human siRNA oligo duplex (Locus ID 1573) and CYP2J2 (NM_000775) human untagged clone was purchased from OriGene Technologies, Inc (Rockville, MD). Lipofectamine 3000 and P3000 transfection reagents were purchased from ThermoFisher Scientific (Waltham, MA). (±)14,15-epoxy-5Z,8Z,11Z-eicosatrienoic acid, (±)11,12-epoxy-5Z,8Z,14Z-eicosatrienoic acid, (±)8,9-epoxy-5Z,11Z,14Z-eicosatrienoic acid, (±)5,6-epoxy-8Z,11Z,14Z-eicosatrienoic acid, (±)14,15-dihydroxy-5Z,8Z,11Z-eicosatrienoic acid, (±)11,12-dihydroxy-5Z,8Z,14Z-eicosatrienoic acid, (±)8,9-dihydroxy-5Z,11Z,14Z-eicosatrienoic acid, (±)5,6-dihydroxy-8Z,11Z,14Z-eicosatrienoic acid, ferrostatin-1, and (1S,3R)-RSL3 were purchased from Cayman Chemicals (Ann Arbor, MI).

### 3.2.2 Human cardiomyocytes cell culture

Primary and immortalized human ventricular cardiomyocytes were used for this study. Primary adult human ventricular derived myocytes were purchased from Celprogen, Inc (Torrance, CA). Complete media, serum free media, and extra-cellular matrix coated culture flasks and plates were obtained from Celprogen, Inc. The media was further sterile filtered

(0.22 um) prior to use. We followed previously established protocols for general cell maintenance and the cells were not used beyond passage 8 (*18*). Immortal adult human ventricular derived AC16 cardiomyocytes were purchased from Sigma-Aldrich (St. Louis, MO) and maintained in DMEM/F12 medium supplemented with 10% fetal bovine serum and 0.1% penicillin/streptomycin following manufacturer's protocol. AC16 cells were not used beyond passage 10.

### 3.2.3 TKI exposure-response curves

Human cardiomyocytes were seeded in a 48-well plate at a density of 50,000 cells/well. AC16 cells were seeded in a 96-well plate at a density of 10,000 cells/well. After seeding, the cells were allowed to attach overnight at 37°C, 5% $CO_2$. The cells were then treated with a range of TKIs (0.001-100 uM) for 24 h and viability was measured using the PrestoBlue HS cell viability reagent (ThermoFisher, Waltham, MA). The cells were incubated in the PrestoBlue HS reagent for up to 2 hours and absorbance at 570 nm with a reference wavelength at 600 nm was measured using the Tecan spark multimode plate reader (Mannedorf, Switzerland). A blank reference plate was subtracted from the sample plate and data analysis was normalized to the absorbance of the reference wavelength following the manufacturer's protocol.

### 3.2.4 Caspase 3/7 activity assay

Caspase 3/7 activity assay kit was purchased from Promega Corporation (Madison, WI). AC16 cells were treated with 10 uM of TKIs for 24 h and caspase 3/7 activity was measured to determine apoptosis following manufacturer's protocol. Luminescence was measured in relative light units (RLU) using a Tecan Infinite M200 plate reader (Mannedorf, Switzerland).

### 3.2.5 Transient *CYP2J2* gene silencing and overexpression

CYP2J2 gene silencing was achieved in the primary ventricular derived myocytes using reverse transfection of CYP2J2 siRNA oligo duplex (10 nM; Origene Technologies, Inc, Rockville, MD) and lipofectamine 3000 reagent (ThermoFisher, Waltham, MA) for 72 h. Scrambled siRNA was used as a negative control. *CYP2J2* gene expression was silenced up to 80% which was confirmed by RT-qPCR. Previous studies confirmed CYP2J2 activity decreases following gene knockdown (*18*). *CYP2J2* overexpression was achieved by reverse transfection of CYP2J2 untagged clone pCMV plasmid and transfection reagents in human cardiomyocytes for 24 h. Greater than 43,000-fold increase in *CYP2J2* gene expression was confirmed by RT-qPCR.

### 3.2.6 Total RNA isolation and RT-qPCR

Total RNA was extracted using the Magmax microarray and Magmax 96 Total RNA isolation kits (ThermoFisher, Waltham, MA) following the manufacturer's protocol. RNA $A_{260/280}$ and concentration was assessed using the Tecan spark multimode plate reader (Mannedorf, Switzerland). Reverse transcription was performed to convert total RNA to cDNA using the High-Capacity-RNA-to-cDNA conversion kit (ThermoFisher, Waltham, MA). Gene expression was quantified via RT-qPCR using Taqman reporter assays (FAM dye) and normalized to the housekeeping gene *GusB* followed by the comparative $C_T$ analysis.

### 3.2.7 TKI rescue experiments in AC16 cells

Prior to TKI treatment, AC16 cells were pre-conditioned for up to one hour with either 50 nM mixture of EETs, mixture of DHETs, or 1 uM of ferrostatin-1 in serum free media. The media was then carefully aspirated, and the cells were treated with 50 uM of TKIs for 24 h after which cell viability was measured using the PrestoBlue HS cell viability assay. Absorbance at 570 nm and 600 nm (reference wavelength) was measured on the Tecan spark multimode plate reader (Mannedorf, Switzerland). A blank reference plate was subtracted from the sample plate and data analysis was normalized to the absorbance of the reference wavelength following the manufacturer's protocol.

### 3.2.8 CYP2J2 and EETs rescue experiments in primary human cardiomyocytes

Following *CYP2J2* gene knockdown, the cells were pre-conditioned with 100 nM 11,12 EETs or ethanol in serum free media for up to one hour in the incubator at 37 ◦C, 5% $CO_2$. The media was then carefully aspirated, and the cells were treated with TKIs at varying concentrations or with DMSO for 24 h followed by the PrestoBlue HS cell viability assay. Cells from a separate set of experiments were harvested and dissolved in Trizol reagent for downstream applications. In a separate set of experiments, *CYP2J2* overexpression was achieved, and the cells were treated with TKIs for 24h and cell viability was measured and compared to the negative empty pCMV vector control.

### 3.2.9 Library preparation and mRNA-sequencing

Primary ventricular derived myocytes treated with TKIs following *CYP2J2* or scrambled siRNA gene silencing and pre-conditioning with 11,12-EET or ethanol were used for RNA-sequencing (n=3). Briefly, samples dissolved in Trizol reagent were sent to Novogene Corporation Inc. (Sacramento, CA) for RNA extraction and library preparation. First, sample quality control (QC) was performed on the Agilent 2100 to ensure RNA integrity was <4 with a smooth baseline followed by measurement of RNA concentration and purity as determined by $A_{260/280}$ = 1.8-2.2 and $A_{260/230}$ > 1.8. Once the sample QC criteria was satisfied, library preparation and library QC was completed. The samples were then sequenced by 150 bp paired-end sequencing technique using an Illumina NovaSeq 6000 platform followed by QC of the data and data processing.

### 3.2.10 Differential expression analysis

Differential expression analysis was performed using the DESeq2 R package to compare the effects of *CYP2J2* silencing and scrambled siRNA in the presence of EETs followed by TKI treatment. The false discovery rate was controlled for by adjusting the p-values using the approach of Benjamini and Hochberg (*19*). Genes with an adjusted p-value of $\leq 0.05$ were considered differentially expressed.

### 3.2.11 Gene set enrichment analysis (GSEA) of differentially expressed genes

The gene list was pre-ranked according to the degree of differential expression followed by gene set enrichment analysis using GSEAPreranked. Gene sets from the GO, KEGG,

Reactome, DO, and DisGeNET were used independently for this analysis, and the results from the KEGG analysis are reported separately due to its widespread use as a reference pathway.

## 3.3 Results

### 3.3.1 Comparing gene expression of cardiac markers and CYP2J2 related enzymes across two human cardiomyocyte cell lines to human heart tissue.

To determine TKI cardiotoxicity and EETs mediated cardioprotection, we utilized two human cardiomyocyte (HCM) cell lines. The first cell line was a pseudo-primary line derived from adult human ventricular myocytes. The cells were confirmed to express ventricular specific genes similar to human heart tissue (*20*). The second cell line used for this study was an immortalized AC16 line that was developed by fusing primary adult ventricular myocytes from human heart tissue with SV40 transformed, uridine auxotroph human fibroblasts devoid of mitochondrial DNA. As seen in Figure 3.3 A and B, the expression levels of the major cardiac markers differed greatly between the two cell lines. For example, the gene expression of *ACTN1, GJA1,* and *DES* in AC16 cells were higher than the HCMs while the expression of *TNNI3*, a cardiac muscle specific gene, was highly expressed in HCMs only. We also observed a difference in expression of *CYP2J2* and related genes (Figure 3.3 C). *CYP2J2* gene expression was undetectable in AC16 cells (FPKM < 0.1) while the expression was very low in HCMs (FPKM $\leq$ 3).

### 3.3.2 Relative TKI toxicities in primary human cardiomyocytes

The relative cytotoxicity of a panel of TKIs (Figure 3.2, Table I) was tested in primary human cardiomyocytes. The cells were incubated with a range of TKI concentrations for 24 h followed by PrestoBlue HS cell viability assay. Sorafenib (SRF) and nilotinib (NLT) were determined to be the most cytotoxic with $EC_{50}$ values of 2.5 and 1.6 uM, respectively. The $EC_{50}$ values of sunitinib (SNT), cabozantinib (CBZ), and gefitinib (GFT) ranged between 18-26 uM, hence exerting moderate cytotoxicity while lenvatinib (LNV) and axitinib (AXT) did not appear

to be cytotoxic (Figure 3.4). Due to the wide range of effect on cell viability exhibited by each TKI and the highly sensitive nature of the primary cells we decided to use a concentration of 3 uM TKI (0.5 uM NLT) for subsequent rescue experiments. The relative cytotoxicity of each TKI was also determined in immortal AC16 cells (Figure 3.5). SRF and CBZ were the most toxic in AC16s exhibiting an $EC_{50}$ value of 2 uM and 6.5 uM, respectively. SNT, LNV, and GFT exhibited moderate toxicities with $EC_{50}$ values between 18-30 uM, while IMT, PZO, and ERL exhibited very minor toxicity with $EC_{50}$ values greater than 50 uM.

### 3.3.3 TKIs induce caspase 3/7 activity in immortal AC16 cells suggesting cell death pathway is mediated in part by apoptosis

Due to the fragility of primary human cardiomyocytes, caspase 3/7 activity was only measured in AC16 cells to determine the role of apoptosis mediated cell death (Figure 3.6). AC16 cells were treated with a panel of TKIs, and caspase 3/7 activity was measured after 24 h. All the TKIs (except for ERL) significantly increased the activity of caspase 3/7 compared to the vehicle control after 24 h suggesting cell toxicity is mediated in part through apoptosis. NLT, followed closely by SRF, was identified as the most cardiotoxic TKI in the panel with caspase 3/7 activity greater than doxorubicin (DOX) which was used as a positive control for drug-induced cardiotoxicity.

### 3.3.4 AC16 cell viability was rescued from TKI injury by EETs, DHETs, and ferrostatin-1, a potent antioxidant

We compared the effects of EETs to that of DHETs and ferrostatin-1 after 50 uM TKI exposure (Figure 3.7). The cells were preconditioned for 30 mins with either a mixture of EET regioisomers, DHET regioisomers or 1 uM of ferrostatin-1 (Fer-1). Fer-1 is an antioxidant known to inhibit lipid peroxidation by scavenging alkoxyl radicals and thus is an inhibitor of ferroptosis. We included Fer-1 in this panel as SRF is known to induce ferroptosis (*21*). Therefore, we were interested in identifying whether the other TKIs in our panel activated alternative cell death pathways in addition to apoptosis. In these experiments, critical cell injury was defined as anything beyond a 70% reduction in cell viability.

EETs and DHETs significantly rescued the cell viability by nearly 15-25% after exposure to AXT while minimal changes were observed for Fer-1 (Figure 3.7 A). The vehicle control exhibited complete cell death when treated with 50 uM CBZ or DOX (Figure 3.7 B, H), however, EETs, DHETs, and Fer-1 significantly rescued viability by nearly 40% suggesting the AC16 cells can be rescued beyond critical injury as opposed to the HCMs. Interestingly, in the presence of IMT, EETs and DHETs led to a decrease in cell viability while Fer-1 rescued viability to approximately 100% (Figure 3.7 C). Cell viability against NLT was rescued to nearly 80% by EETs, DHETs, and Fer-1 (Figure 3.7 D) while minor changes in viability were observed after SRF treatment (Figure 3.7 E). SNT toxicity was significantly attenuated by EETs but not by DHETs or Fer-1 (Figure 3.7 F) while PZO exhibited minor cell toxicity which was significantly affected by EETs and Fer-1 (Figure 3.7 G).

### 3.3.5 Addition of external 11,12 EETs protect HCMs against TKI mediated cardiotoxicity

To determine whether 11,12-EETs could mitigate TKI toxicity in HCMs, we first silenced *CYP2J2* gene expression achieving up to 80% knockdown efficiency (Figure 3.8) then preconditioned the cells with 100 nM of 11,12-EETs or vehicle for at least one hour prior to TKI exposure. As seen in Figure 3.9, *CYP2J2* gene silencing increased the susceptibility to TKI injury while supplementing the cells with 11,12-EET prior to TKI exposure (0.5 uM NLT and 3 uM CBZ, SRF, and SNT) mitigated injury by up to 50% as determined by cell viability. The most profound effect was observed when adding external EETs after silencing *CYP2J2* gene expression, however, the viability of the scrambled siRNA control was also significantly preserved in some cases when compared to the vehicle. Minor cytotoxicity was observed by PZO and AXT at 10 uM which was then slightly reversed by 11,12-EET. 11,12-EET failed to rescue the cells at a higher concentration of SRF, however, suggesting EETs are not able to rescue cell viability beyond critical injury (Figure 3.10). The cells were minimally affected by TKIs ERL, IMT, LNV and GFT, hence the effect of 11,12-EETs was negligible (Figure 3.11).

### 3.3.6 Overexpression of *CYP2J2* was ineffective against TKI injury in primary human cardiomyocytes

We next investigated whether overexpressing *CYP2J2* would mitigate TKI injury. CYP2J2 overexpression in primary human cardiomyocytes was achieved through reverse transfection of pCMV-CYP2J2 expression plasmid. The gene expression of CYP2J2 was determined by RT-qPCR and CYP2J2 expression was significantly increased by over 40,000-fold compared to the empty pCMV vector control. pCMV-CYP2J2-transfected HCMs were treated with TKIs, however it failed

to mitigate injury as determined by changes in cell viability (Figure 3.12). In contrast to silencing *CYP2J2* gene expression, it appears the effect of overexpressing *CYP2J2* is negligible.

### 3.3.8 Hypertrophic responses are triggered following CYP2J2 silencing and TKI treatment in primary human cardiomyocytes

Transcriptomic analysis of the RNA-seq data summarizing altered genes after exogenous 11,12-EET rescue against CBZ, SRF, and NLT toxicity in HCMs revealed 567, 441, and 234 unique expressions, respectively (Figure 3.13). A hierarchically clustered heatmap revealed the expression pattern of differentially expressed genes (DEGs) of all experimental conditions and controls (Figure 3.14). Gene set enrichment analysis (GSEA) using the KEGG pathways revealed the data set pertaining to hypertrophy and dilated cardiomyopathies were highly enriched in *CYP2J2* silenced cells treated with CBZ and following 11,12-EET rescue compared to scrambled siRNA treated cells (Figure 3.15 and 3.16, respectively). These pathways were also enriched after SRF treatment but not NLT treatment. Figures 3.15 and 3.16 A and B reveal the enrichment plot and heatmaps to visualize gene expression patterns, respectively, which is representative of both CBZ and SRF treatment.

**3.4 Discussion**

Drug-induced cardiotoxicity is perhaps the most detrimental consequence of cancer therapy leading to increases in morbidity and mortality even after successfully achieving complete remission (*22*). Dose management and reducing the overall exposure to chemotherapy drugs is one strategy to combat cancer and cardiovascular co-morbidities. However, under circumstances where other treatment options are limited, reducing dosage and/or frequency remains a delicate decision especially when the therapy is effective against the tumor (*22-25*). Considering the prevalence of cancer and cardiovascular co-morbidities, and the lack of approved strategies to prevent cardiovascular toxicity, the present study focused on the role of cardioprotective CYP2J2 and EETs against TKI cardiotoxicity. We conducted the study using two human ventricular derived myocytes, one primary and one immortal line, as the gene expression of primary human cardiomyocytes (HCMs) most closely resembled human heart tissue (*20*), however, the cell line was exceptionally fragile and resulted in high variability due to difficulties in cell culture maintenance. Thus, we sought to utilize a robust cell line (AC16) to supplement this study.

Initial dosage screenings suggest the TKIs in our panel exhibit varying degrees of toxicity ranging from very minor to potent toxicities (Figure 3.4-3.5). Some differences in the cytotoxicity of TKIs in the different cell types were observed, however. For example, in primary human cardiomyocytes, lenvatinib exerted minor cell toxicity ($EC_{50}$ > 500 uM) while the $EC_{50}$ value in immortal AC16 cells was roughly 10-fold less (Figure 3.4 G and 3.5 C) overall highlighting the variation in two different cell models. Nonetheless, broad inclusion of a panel

of TKIs allowed us to interrogate the role of CYP2J2 and EETs from a global perspective to better understand the functional value in an *in vitro* human heart model.

Initially, we determined the TKIs in our panel induced caspase 3/7 activity to varying degrees in AC16 cells suggesting apoptosis was a major cell death pathway that is being activated (Figure 3.6). The presence of EETs and DHETs rescued cell viability against TKI mediated cell death which was often comparable to the effects of a potent antioxidant, and inhibitor of a novel cell death pathway ferroptosis, Fer-1. Since SRF was recently identified to induce ferroptosis through the inactivation of glutathione peroxidase 4 (GPX4) and subsequent iron-dependent accumulation of ROS (*21*), we explored the possibility of EETs and/or DHETs protecting AC16 cells from ferroptotic cell death. We achieved this by inducing ferroptosis in AC16 cells with RAS-selective lethal 3 (RSL3), a small molecule inhibitor of GPX4 known to potently trigger ferroptosis, after preconditioning the cells with either a vehicle, EETs, DHETs, or Fer-1 (Supplementary Figure S3.1). And although we observed a very minor shift in $EC_{50}$ values in the presence of EETs and DHETs (0.76 uM vs 0.85 uM and 0.89 uM, respectively), no significant changes in cell viability were observed thereby eliminating the probability that EETs or DHETs protect against ferroptosis. Presumably, the cardioprotection against TKI toxicities elicited by EETs and DHETs together with Fer-1 mitigating cell injury in AC16 cells can be attributed to their reported antioxidant activity (*26-28*).

Proceeding, we further investigated the role of EETs and TKI toxicity using primary HCMs due to their similarity to the gene expression profile of human heart tissue (*20*). We first silenced *CYP2J2* gene expression then proceeded to condition the cells with exogenous 11,12-EET for up to one hour prior to TKI exposure. Compared to cells pre-conditioned with a vehicle

control, 11,12-EET attenuated cellular damage by 20-50% as measured by cell viability in primary HCMs (Figure 3.9 A-D). The scrambled siRNA control was protected by 11,12-EET as well but generally to a lesser degree. 11,12-EETs failed to protect cells against critical injury, however, suggesting the protective effect of EETs is most prominent when the injury is still reversible (Figure 3.10). We next determined whether overexpressing *CYP2J2* gene would mirror the protection seen by exogenous 11,12-EET. Despite achieving over 40,000-fold increase in gene expression (Figure 3.8), *CYP2J2* overexpression alone did not reverse TKI toxicity and interestingly, resulted in a more fragile cell phenotype as more detached cells were observed during normal handling (Figure 3.12). This, however, contrasted with what has been reported in the literature on the protective effects of CYP2J2 overexpression *(30-34).* For example, overexpressing *CYP2J2* in human pulmonary artery endothelial cells decreased pro-inflammatory cytokines following anoxia/reoxygenation injury to a similar extent observed by the addition of exogenous 11,12-EET (*29*). Increased EET levels have also been associated with increased CYP2J2 protein expression (*30*). Thus, it is possible that the observed null effect of *CYP2J2* overexpression against TKI toxicity was a result unaltered protein level which should be determined for future studies.

*CYP2J2* transcriptional activation was reported to closely resemble that of housekeeping genes due to a lack of a TATA promoter box and presence of four putative *Sp1* binding sites on the 5' flanking region (*31*). CYP2J2 mRNA and protein were also reported to be both highly and constitutively expressed in human heart further suggesting its role in regulating cellular maintenance akin to the function of housekeeping genes (*32*). This was further exemplified by Evangelista et al. where silencing *CYP2J2* expression and reducing enzyme activity in primary

HCMs resulted in over 1,000 differentially expressed genes in pathways involved in cardiac and electrophysiological dysfunction (*KCNA1, KCNA2, CACNA1B, etc)* (*18*). Therefore, modulating *CYP2J2* gene expression in either direction seems to result in deleterious effects in our cell model thereby potentially rationalizing the lack of cyto-protection observed for *CYP2J2* overexpression. To further investigate the cell-wide effect of CYP2J2 overexpression, however, future studies should include alternative gene delivery methods including viral transduction followed by RNA-sequencing pathway analysis.

Following on from our results that 11,12-EET protected against several TKI mediated toxicities, we sought to elucidate a potential pathway for EET mediated protection against TKIs. We performed RNA-sequencing in samples after exogenous EETs rescue in *CYP2J2* silenced HCMs against CBZ, SRF, and NLT toxicity to gain perspective into the dynamic changes of the transcriptome after treatment. RNA-seq data summary revealed 567, 441, and 234 uniquely expressed genes after rescuing the cells with exogenous 11,12 EETs following CBZ, SRF, and NLT treatment, respectively (Figure 3.13). We conducted differential expression analysis using an adjusted p-value of 0.05 and an absolute fold change of two as the cutoff criteria. This was followed by gene set enrichment analysis (GSEA) to identify overrepresented or underrepresented pathways between *CYP2J2* knockdown vs scrambled siRNA rescue groups.

The gene sets corresponding to hypertrophy and dilated cardiomyopathy from the KEGG database were significantly enriched in samples treated with CBZ and SRF after rescuing *CYP2J2* knockdown cells with 11,12-EET compared to the scrambled siRNA control suggesting these TKIs trigger a cardiomyopathic response in the primary HCMs when *CYP2J2* is compromised (Figures 3.15-16). Cardiomyopathy is a common disease that affects the contractability of heart

muscles. The most common type of cardiomyopathy includes dilated cardiomyopathy (DCM) which is a result of an enlarged heart chamber and hypertrophic cardiomyopathy (HCM) resulting from the thickening of the heart muscles. In either case, cell viability was rescued in the presence of exogenous 11,12-EET further highlighting the advantageous role of EETs against adverse cardiac remodeling. Interestingly, however, these pathways were not enriched after NLT treatment suggesting TKI cardiotoxicity is specific to the individual drug. The cardiotoxicity of the TKIs included in the panel ranged from no reported incidence of adverse cardiac events to black box warning for sudden death. The discrepancy between the toxicities that are exhibited by each TKI can be potentially explained by the pharmacokinetic parameters of the individual TKIs. TKIs are orally administered drugs and are highly protein bound (>90%). Numerous factors are involved that can be associated with variable response and toxicity of individual TKIs such as drug-drug interactions and genetic and environmental factors. An in-depth review of TKI clinical PK parameters and potential associated toxicities can be found in this review (*33*).

This study is not without limitations. We showed that exogenous 11,12-EET could rescue cell viability against various TKIs when *CYP2J2* expression is silenced in HCMs. However, due to the fragility of the primary HCMs, the present study could not interrogate other cellular pathways including, but not limited to, investigating levels of reactive oxygen species and caspase 3/7 activity. Most conventional and commercially available cellular assays were not compatible with our main cell model. The utilization of immortalized AC16 cells also had a major disadvantage in that the cells are derived, in part, from fibroblasts and consequently exhibited tumor-like properties with very low basal expression of *CYP2J2*. Since cardiomyocytes

are non-proliferative, any genetic mutations to force the proliferative phenotype results in a tumor-like phenotype with little resemblance to *in vivo* human cardiomyocytes. An alternative to our current cell model would be to use standardized cell lines such as rat cardiomyocytes (H9C2) or induced pluripotent stem cell (iPSC) derived cardiomyocytes. However, these solutions are not ideal either as H9C2 are non-human cells and the origin of most iPSC cardiomyocytes are embryonic cells or a heterogenous mixture of different cell types. Regardless of the various caveats, however, future studies should extend toward the utilization of other cardiac cell models to widen the breadth of investigation of TKI cardiotoxicity.

In summary, our study demonstrated an important role for *CYP2J2* and 11,12-EET in attenuating TKI toxicities in two human cardiomyocyte cell models. Pathways involved in hypertrophy and dilated cardiomyopathy were significantly enriched after CBZ and SRF treatment when *CYP2J2* expression was silenced compared to the control overall suggesting an important role for maintaining cardiac homeostasis by CYP2J2.

*Abbreviations*

AA, arachidonic acid; EETs, epoxyeicosatrienoic acids; TKI, tyrosine kinase inhibitor; RTK, receptor tyrosine kinase; AXT, axitinib; CBZ, cabozantinib; DHETs, di; ERL, erlotinib; GFT, gefitinib; LNV, Lenvatinib; IMT, imatinib; NLT, nilotinib; ROS, reactive oxygen species; SRF, sorafenib; SNT, sunitinib; PZO, pazopanib.

**Figures**

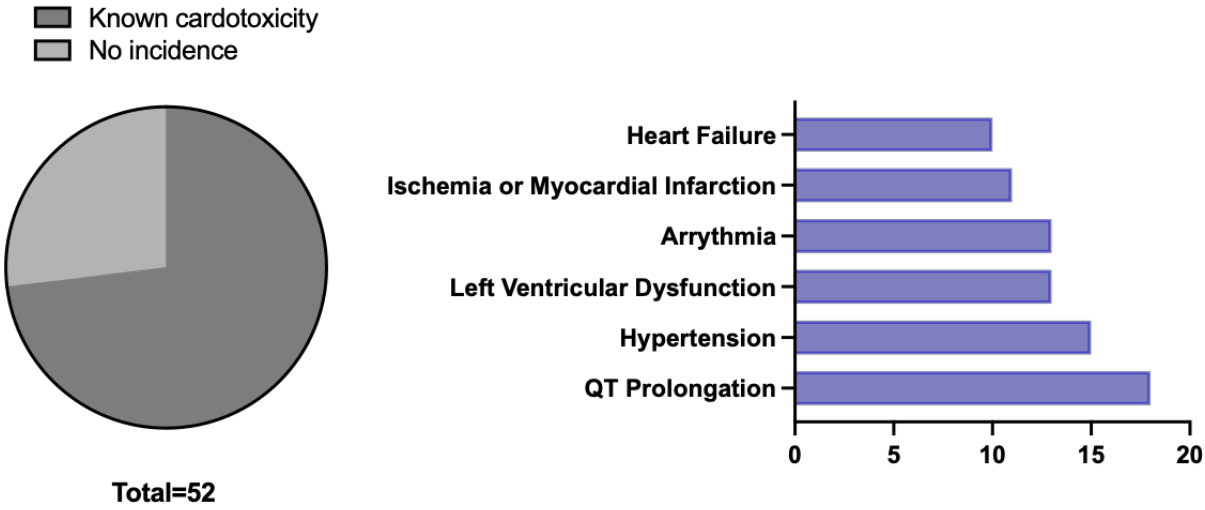


**Figure 3.1. Incidence of cardiotoxicity in 52 approved tyrosine kinase inhibitor class.** This figure was adapted from Jin et al. (2020) (*3*).

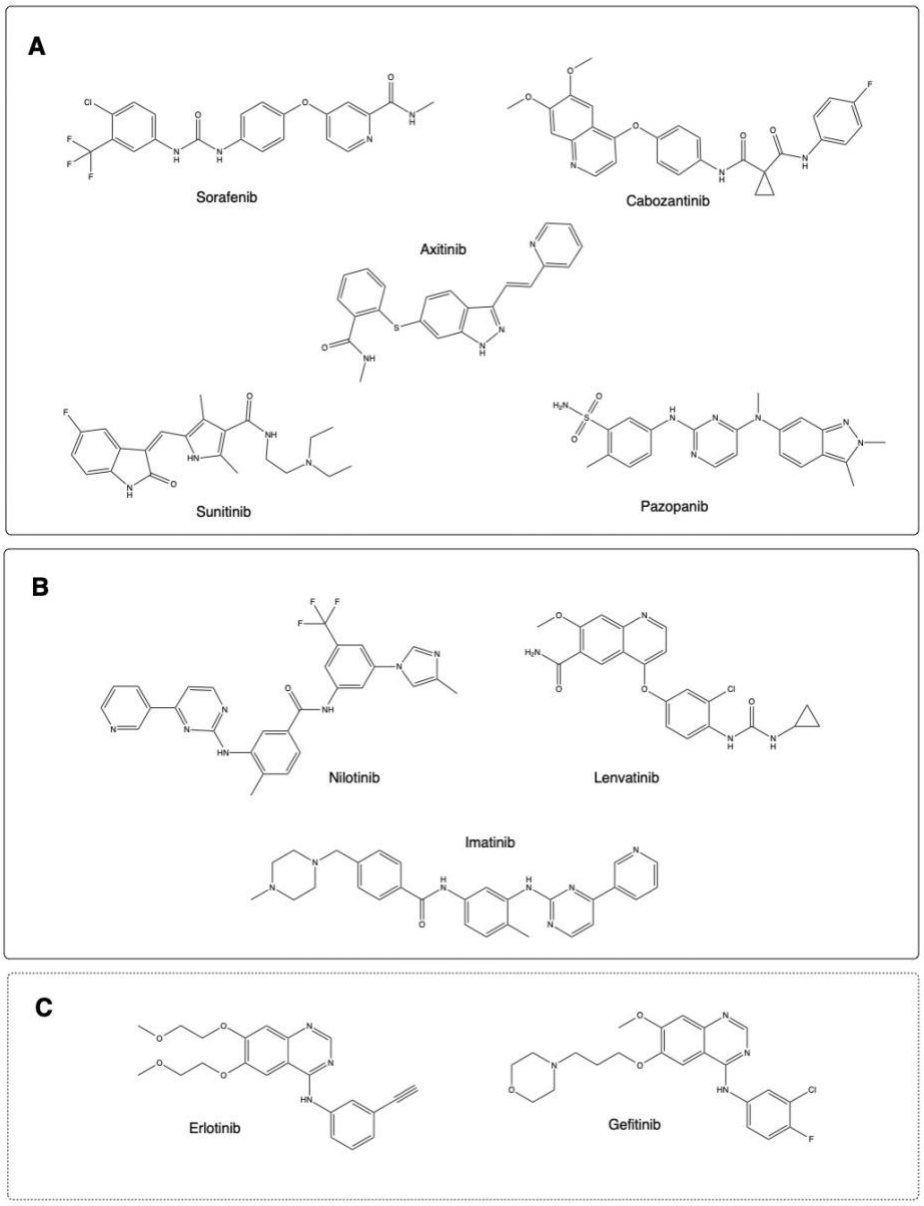


**Figure 3.2. Structure of TKIs.** A) Five approved TKIs in ccRCC associated with cardiotoxicity of varying degrees; B) TKIs with known cardiotoxicities; C) TKIs with minor or no reported incidence of cardiotoxicity.

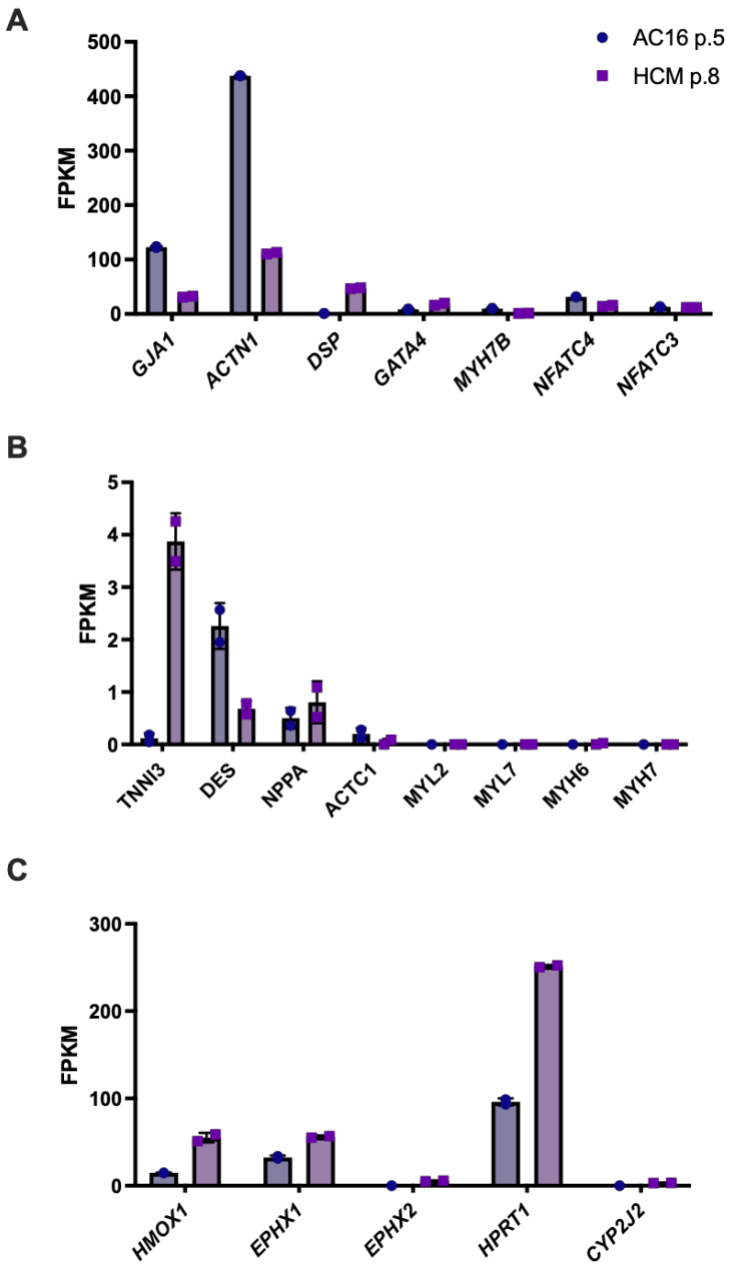


**Figure 3.3. Comparison of gene expression levels in primary human cardiomyocytes and immortal AC16 human cardiomyocytes to human heart tissue.** Panels A and B. Expression of cardiac markers; C. Expression of *HMOX-1, EPHX-1* and *-2, HPRT-1,* and *CYP2J2*.

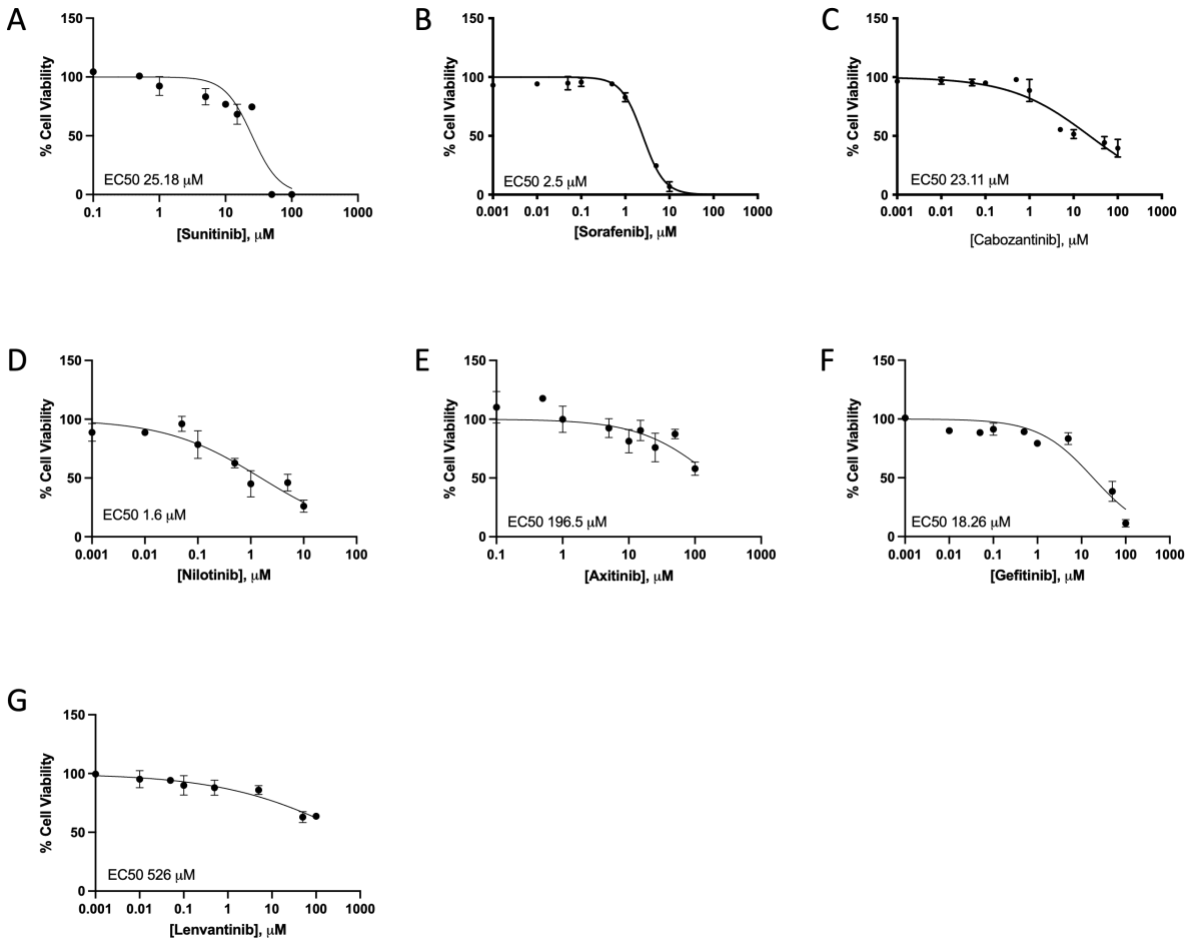


**Figure 3.4. TKI dose-response curves in primary human cardiomyocytes HCMs.** The cells were treated with a range of TKIs for 24 h then cell viability was measured (n=3). The $EC_{50}$ values were calculated using the Prism Graphpad software.

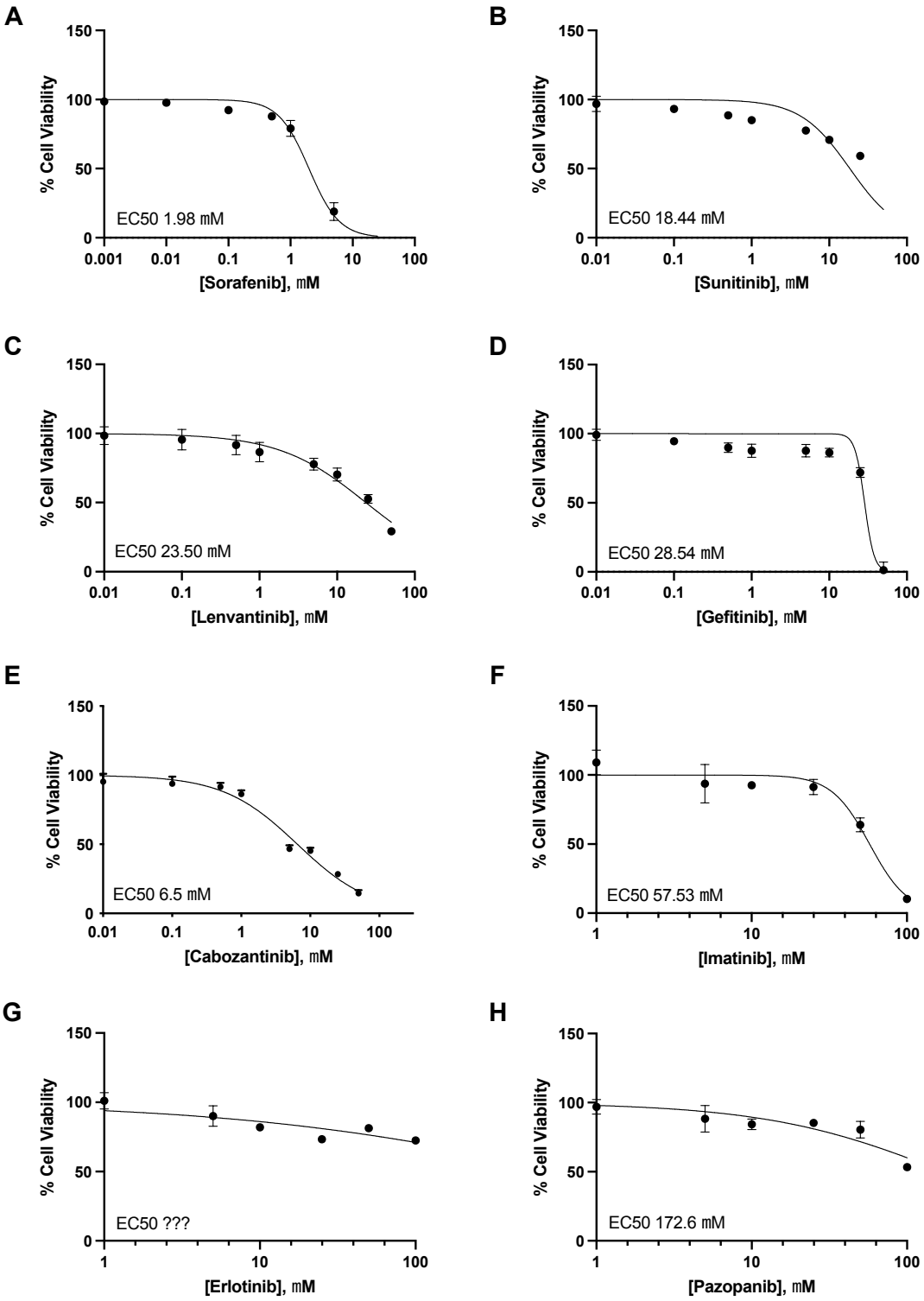


**Figure 3.5. TKI dose-response curve in AC16 immortal human cardiomyocytes.** The cells were treated with a range of TKIs for 24 h then cell viability was measured (n=3). The EC50 values were calculated using the Prism Graphpad software.

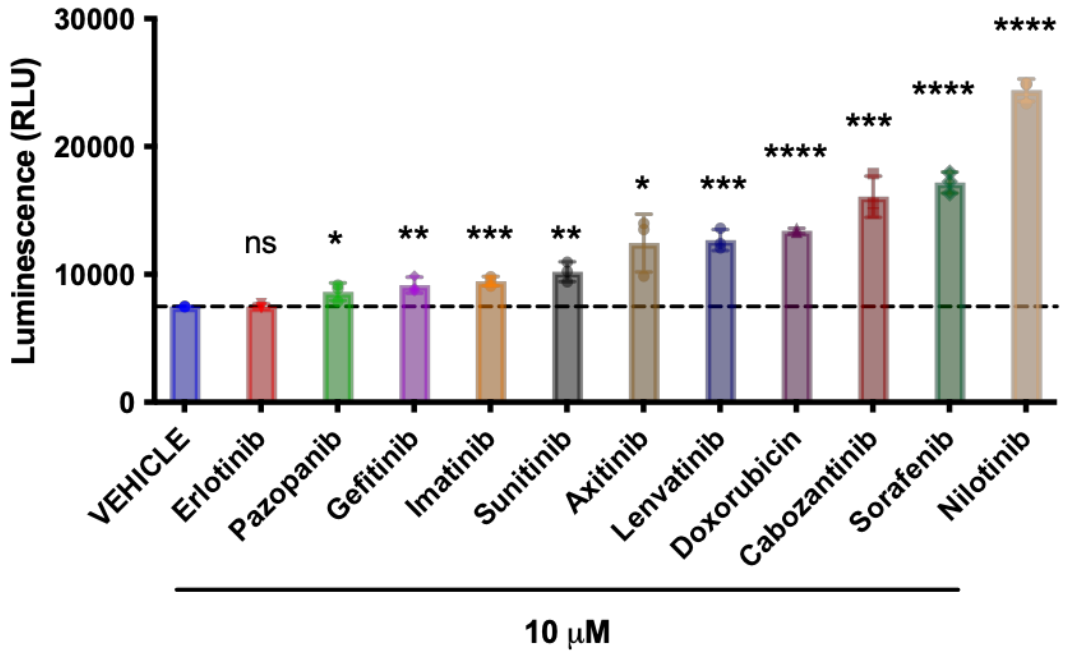


**Figure 3.6. Caspase 3/7 activity in immortal AC16 cardiomyocytes following 24 h of tyrosine kinase inhibitor exposure.** Statistical analyses were performed using an unpaired t-test between the vehicle treatment and TKIs using the Prism Graphpad software. *$p < 0.05$, **$p < 0.01$, ***$p < 0.001$, and ****$p < 0.0001$

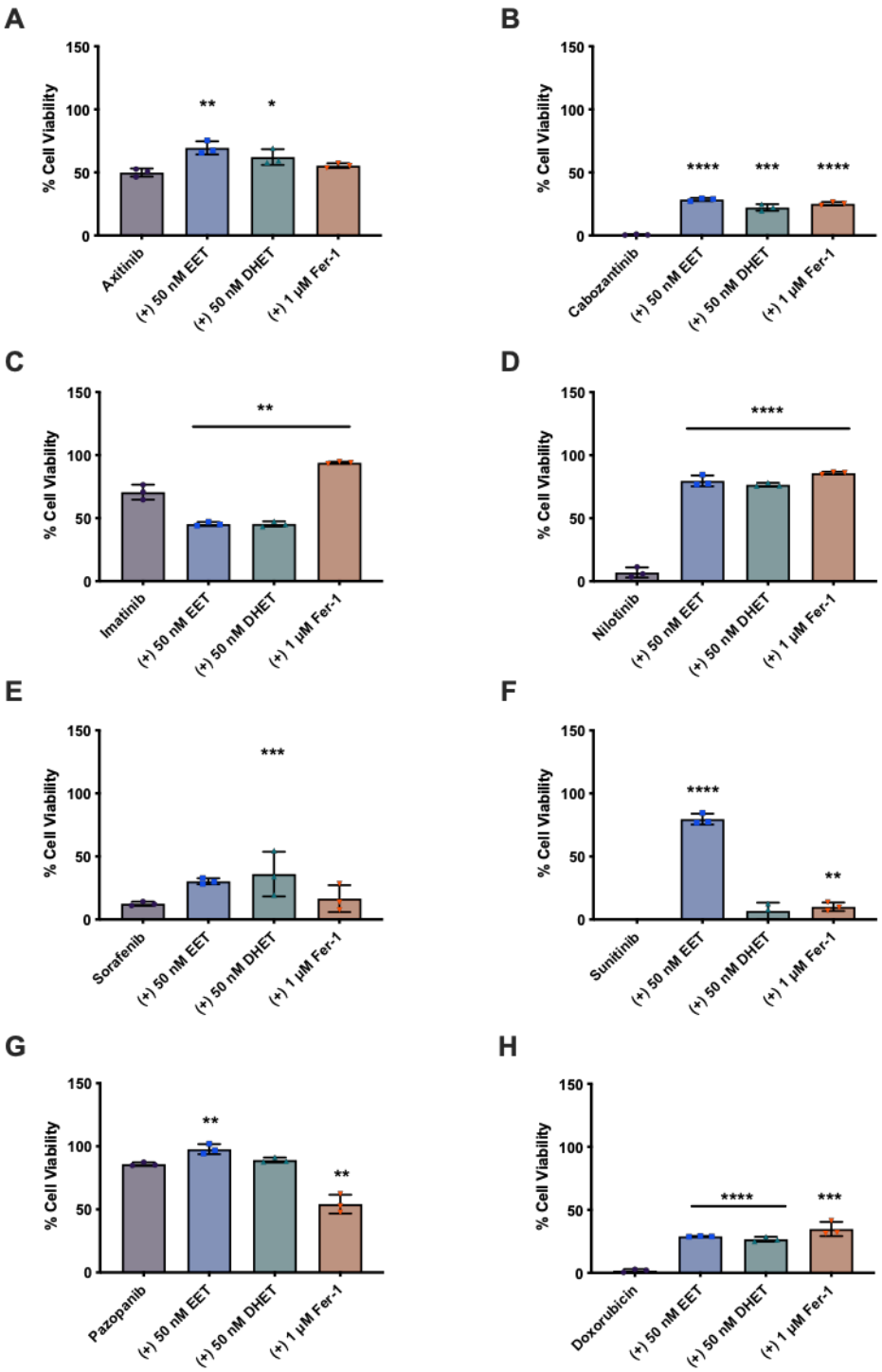


**Figure 3.7. Cell viability measured in AC16 cells exposed to TKIs or DOX prior to preconditioning with EETs, DHETs, and Fer-1.** The cells were pre-conditioned with EETs, DHETs, or Fer-1 for up to one hour prior to TKI treatment for 24 h followed by a cell viability assay. A) Axitinib; B) Cabozantinib; C) Imatinib; D) Nilotinib; E) Sorafenib; F) Sunitinib; G) Pazopanib; H) Doxorubicin. Statistical analyses were performed using an unpaired t-test using the Prism Graphpad software. *$p < 0.05$, **$p < 0.01$, ***$p < 0.001$, and ****$p < 0.0001$

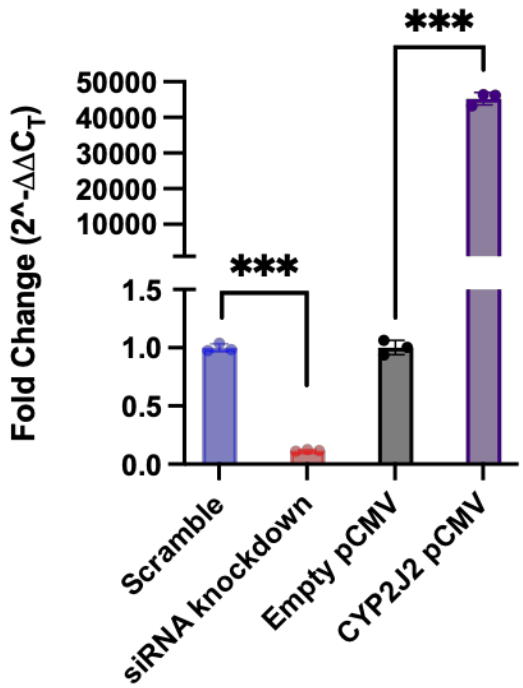


**Figure 3.8. *CYP2J2 g*ene silencing and overexpression in primary human cardiomyocytes.** Greater than 80% *CYP2J2* gene knockdown efficiency and approximately 40,000-fold gene overexpression was achieved and confirmed by RT-qPCR. *$p < 0.05$, **$p < 0.01$, ***$p < 0.001$, and ****$p < 0.0001$

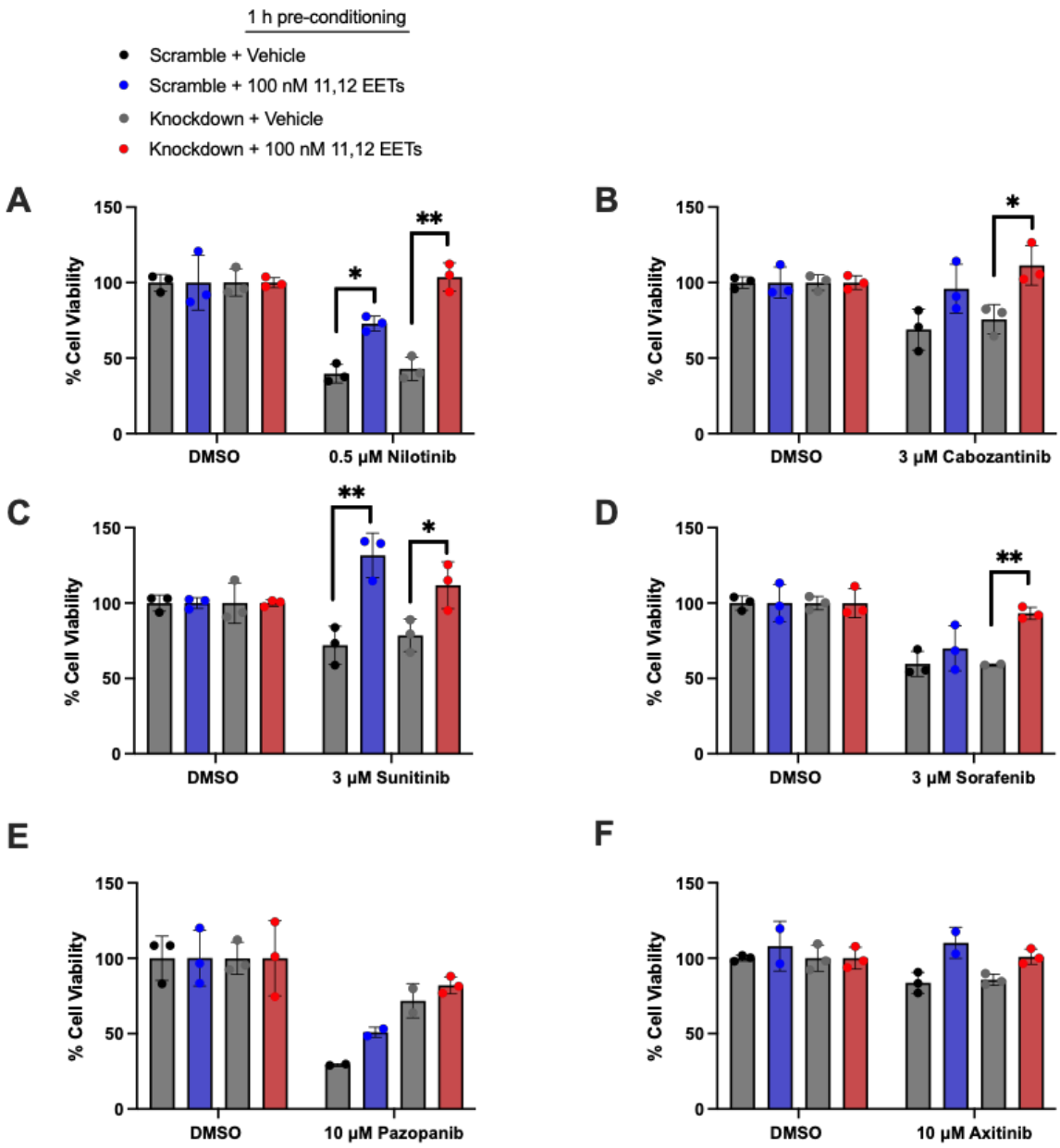


**Figure 3.9. Cell viability was rescued by 11,12-EETs following TKI treatment in primary cardiomyocytes.** The cells were pre-conditioned with 100 nM 11,12-EET for up to one hour prior to TKI treatment for 24 h followed by measurement of cell viability (n=3). A) Nilotinib; B) Cabozantinib; C) Sunitinib; D) Sorafenib; E) Pazopanib; F) Axitinib. *$p < 0.05$, **$p < 0.01$, ***$p < 0.001$, and ****$p < 0.0001$

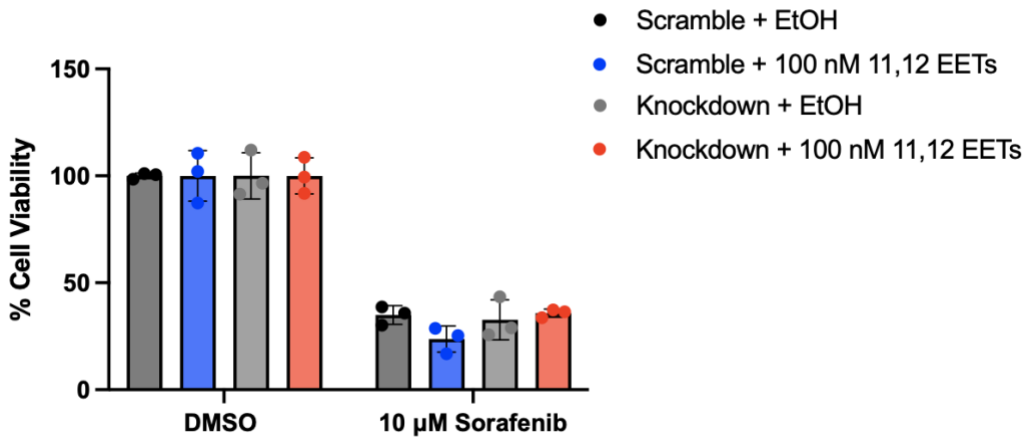


**Figure 3.10. 11,12-EETs failed to rescue cell viability following acute injury in primary cardiomyocytes.** The cells were pre-conditioned with 100 nM 11,12-EET for up to one hour prior to TKI treatment for 24 h followed by measurement of cell viability.

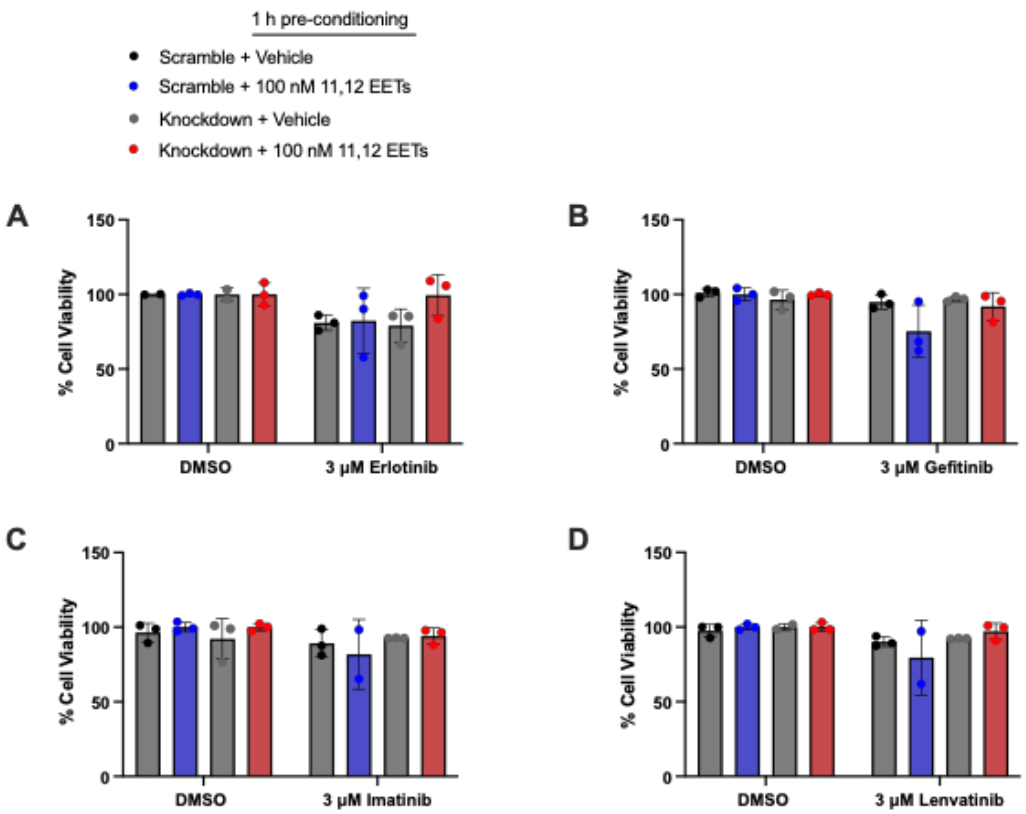


**Figure 3.11. was rescued by 11,12-EETs following TKI treatment in primary cardiomyocytes.** The cells were pre-conditioned with 100 nM 11,12-EET for up to one hour prior to TKI treatment for 24 h followed by measurement of cell viability (n=3). A) Erlotinib; B) Gefitinib; C) Imatinib; D) Lenvatinib.

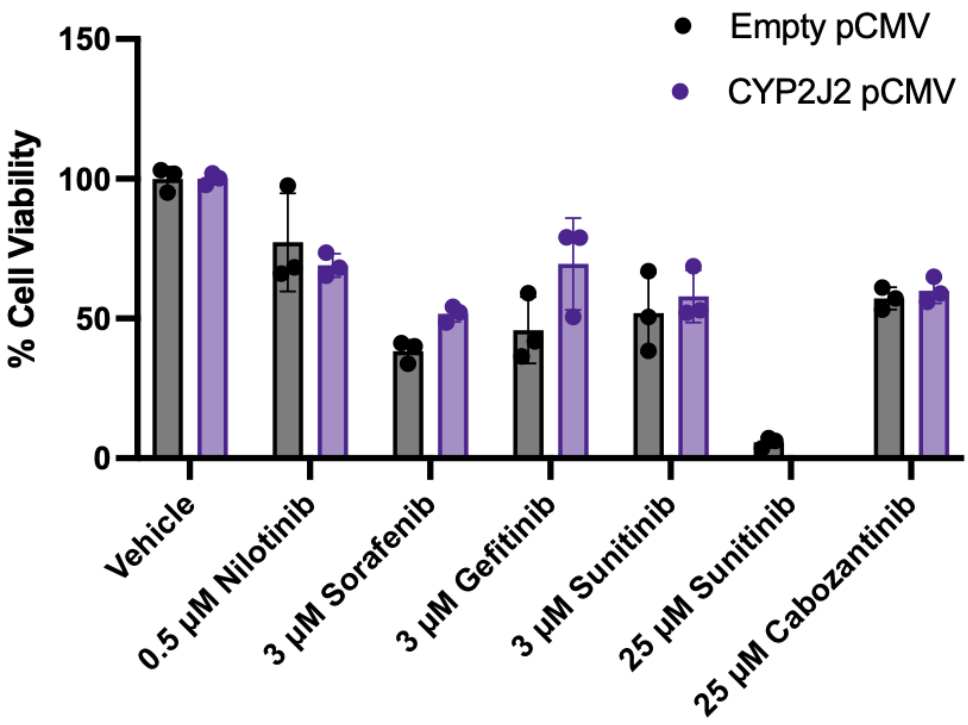


**Figure 3.12. *CYP2J2* overexpression did not rescue cells against TKI toxicity in primary cardiomyocytes.** CYP2J2 overexpression in primary human cardiomyocytes was achieved through reverse transfection of pCMV-CYP2J2 expression plasmid for 24 h. Once overexpression was achieved, the cells were treated with TKIs for 24 h prior to measure cell viability.

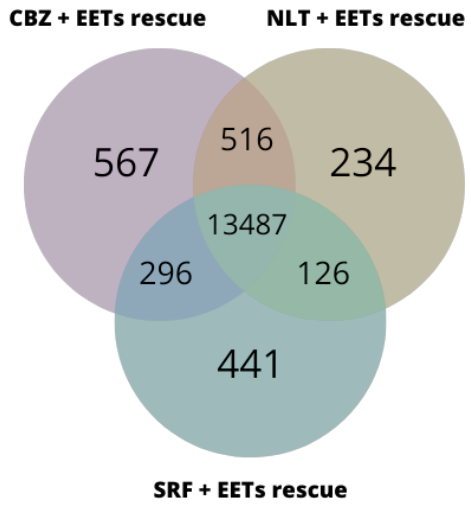


**Figure 3.13. Venn diagram representing the RNA-seq data summary of differentially expressed (DE) genes after exogenous 11,12-EET rescue against cabozantinib, nilotinib, and sorafenib toxicity in human cardiomyocytes.** *CYP2J2* expression was silenced in HCMS then the cells were pre-conditioned with 100 nM 11,12-EETs for up to one hour prior to TKI treatment. 567, 234, and 441 unique DE genes were identified after CBZ, NLT, and SRF treatment, respectively.

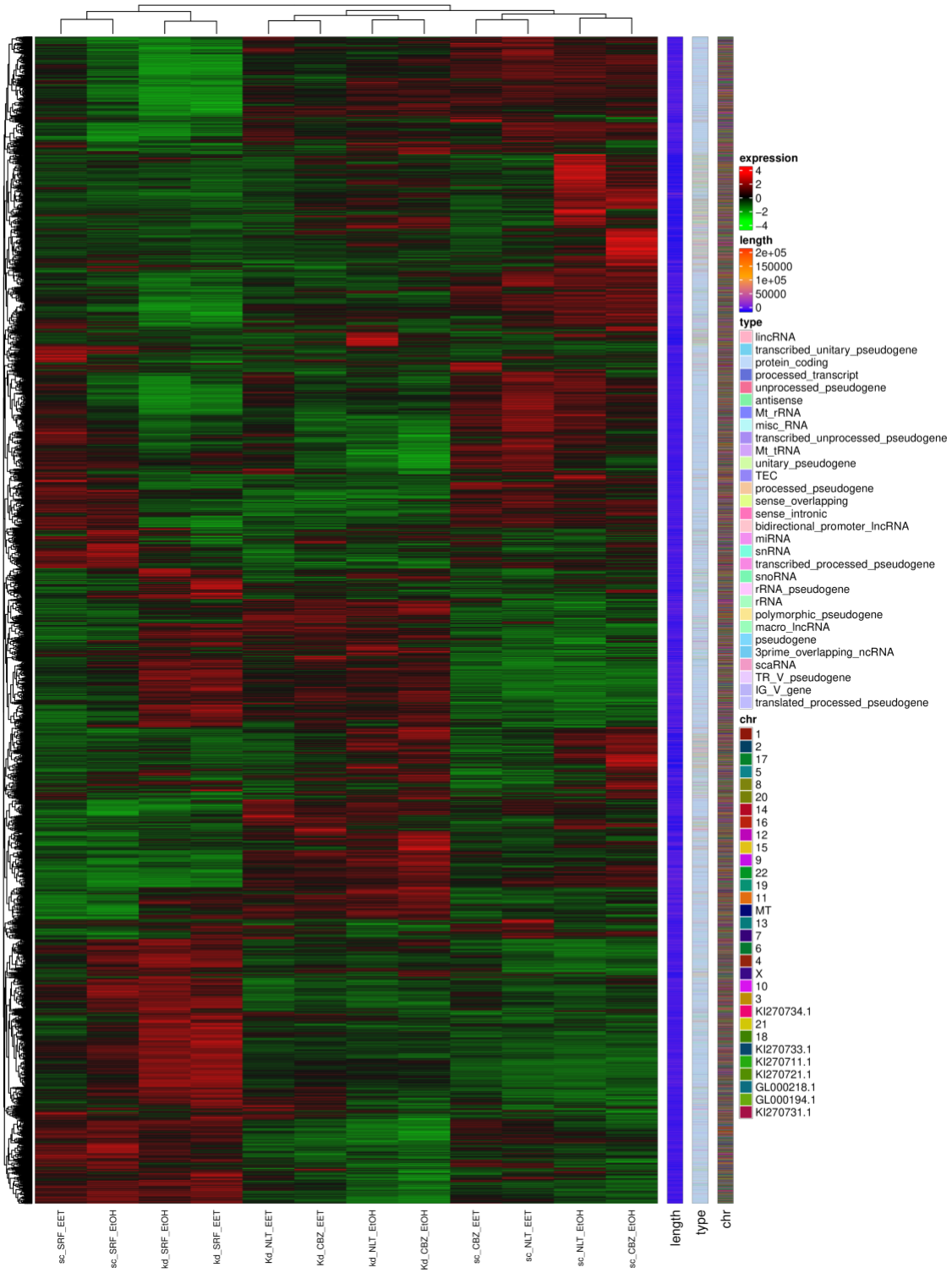


**Figure 3.14. Hierarchically clustered heatmap to visualize the expression pattern of differentially expressed genes across all experimental conditions.** Red refers to up-regulated genes and green refers to down-regulated genes. Each condition was sequenced as n=3 and represented as a single group.

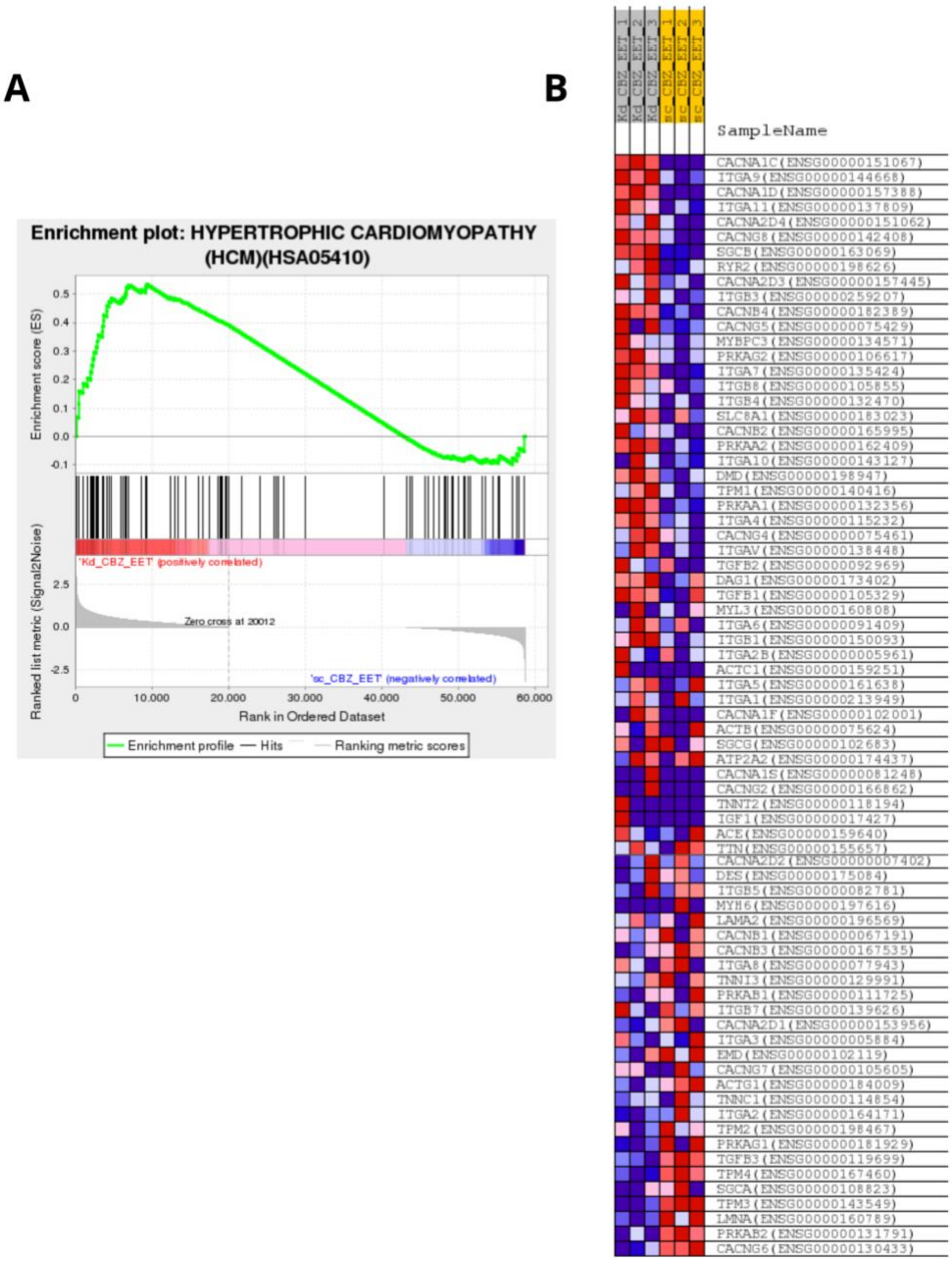


**Figure 3.15. Gene set enrichment analysis (GSEA) reveal differentially expressed genes that were identified between the *CYP2J2* silenced and scrambled siRNA groups after rescuing against CBZ toxicity with 11,12-EETs.** A) Enrichment plot for Hypertrophic Cardiomyopathy revealed this pathway was upregulated in the *CYP2J2* silenced group as compared to the scrambled siRNA control. B) Heatmap of positively and negatively enriched genes in the *CYP2J2* silenced group.

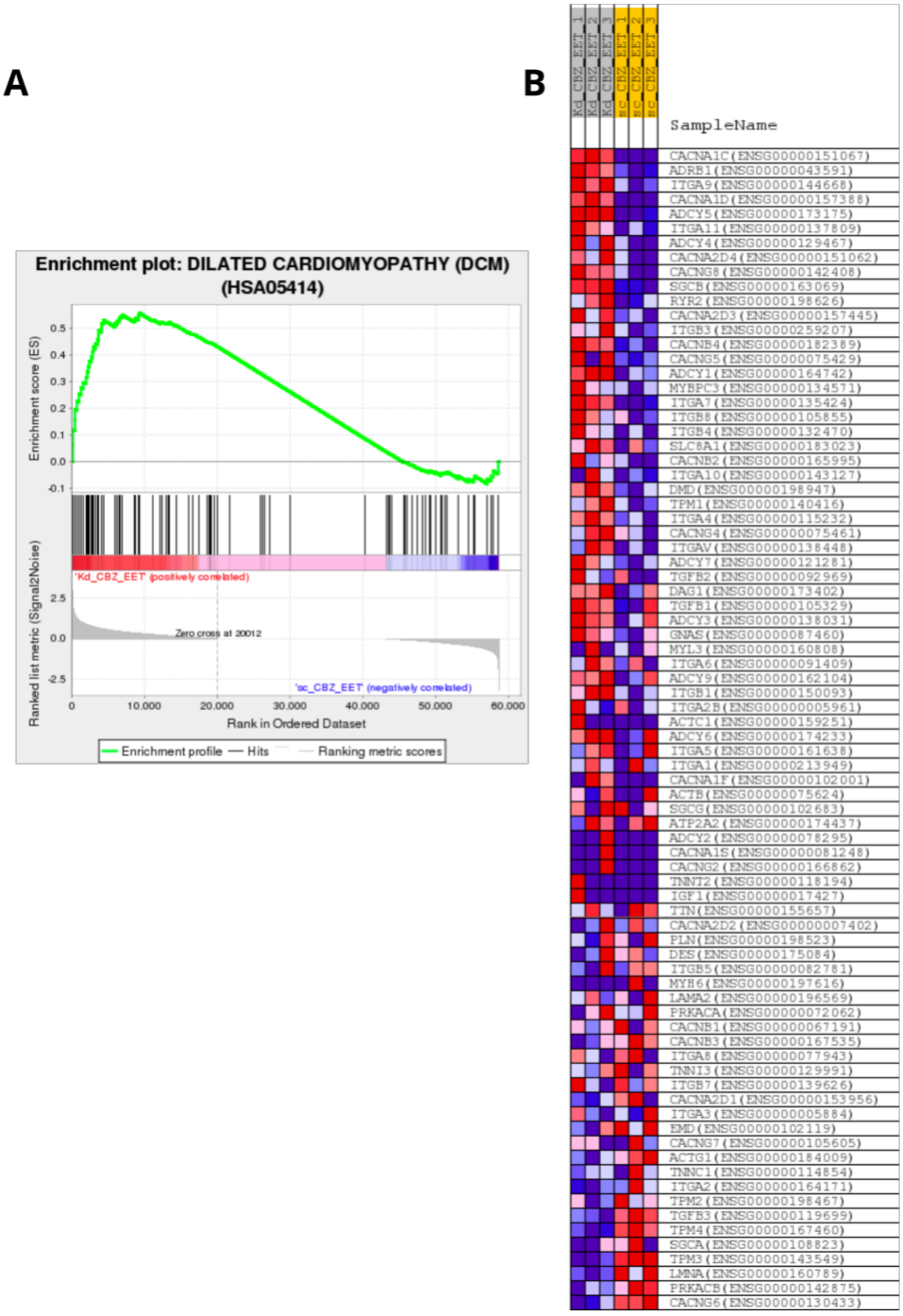


**Figure 3.16. Gene set enrichment analysis (GSEA) reveal differentially expressed genes that were identified between the *CYP2J2* silenced and scrambled siRNA groups after rescuing against CBZ toxicity with 11,12-EETs**. A) Enrichment plot for Dilated Cardiomyopathy revealed this pathway was upregulated in the *CYP2J2* silenced group as compared to the scrambled siRNA control. B) Heatmap of positively and negatively enriched genes in the *CYP2J2* silenced group.

## Tables

**Table I.** Adverse cardiac events of tyrosine kinase inhibitors.

| TKI | Targets | FDA approved indication | Cardiotoxicity | References |
|---|---|---|---|---|
| Axitinib (Inlyta) | VEGFRs† | Renal cell carcinoma (2012); First line in combination with pembrolizumab for RCC (2019) | Heart failure, hypertension | (*3, 34*) |
| Cabozantinib (Cabometyx) | B-RAF, MET, VEGFRs, AXL, RET, ROSI , C-KIT, TrkB, FLT-3 | Renal cell carcinoma (2016); Hepatocellular carcinoma (2019); Differentiated thyroid cancer (2021); First line in combination with nivolumab for RCC (2021) | Hypertension | (*3*) |
| Erlotinib (Tarceva) | EGFR† | Non-small cell lung cancer (2004); Pancreatic cancer (2005) | Ischemia or myocardial infarction (rare occurrence) | (*3, 34*) |
| Gefitinib (Iressa) | EGFR† | First-line for metastatic non-small cell lung cancer (2015) | None documented | (*1, 3*) |
| Imatinib (Glivec) | Bcr-Abl, PDGFRa, c-KIT | Gastrointestinal cancer (2008); Acute lymphoblastic leukemia (2013) | Left ventricular dysfunction, heart failure, hypertension | (*1, 3, 34*) |
| Lenvatinib (lenvima) | VEGFRs, FGFRs, PDGFRα, KIT, RET | Differentiated thyroid cancer (2015); Renal cell carcinoma (2016); Hepatocellular carcinoma (2018); Endometrial carcinoma (2019); First line in combination with pembrolizumab for RCC (2021) | QT interval prolongation, left ventricular dysfunction, heart failure, hypertension | (*3, 34*) |
| Nilotinib (Tasigna) | Bcr-Abl, PDGFRU, c-KIT, CSF-IR | Chronic myeloid leukemia (2007) | QT interval prolongation, ischemia, or myocardial infarction | (*1, 3, 34*) |
| Pazopanib (Votrient) | VEGFRs, PDGFR(Vß, FGFR, c-Kit, ltk, Lck, c-Fms | Renal cell carcinoma (2009); Soft tissue sarcoma (2012) | QT interval prolongation, left ventricular dysfunction, heart failure, hypertension, arrhythmia, ischemia, or myocardial infarction | (*3, 34*) |
| Sorafenib (Nexavar) | VEGFRs, B-RAF, CSF-IR, PDGFRß, KIT, FLT3, RET | Renal cell carcinoma (2005); Hepatocellular carcinoma (2007); Differentiated thyroid cancer (2013) | QT interval prolongation, ischemia or myocardial infarction, hypertension | (*1, 3, 34*) |
| Sunitinib (Sutent) | FLT3, CSF-I R, RET, PDGFRα/ß, VEGFRs, KIT | Gastrointestinal cancer (2006); Renal cell carcinoma (2006); Pancreatic cancer (2011) | QT interval prolongation, left ventricular dysfunction, heart failure, hypertension, arrhythmia, ischemia, or myocardial infarction | (*1, 3, 34*) |

†targeted therapy

## Supplementary Figures

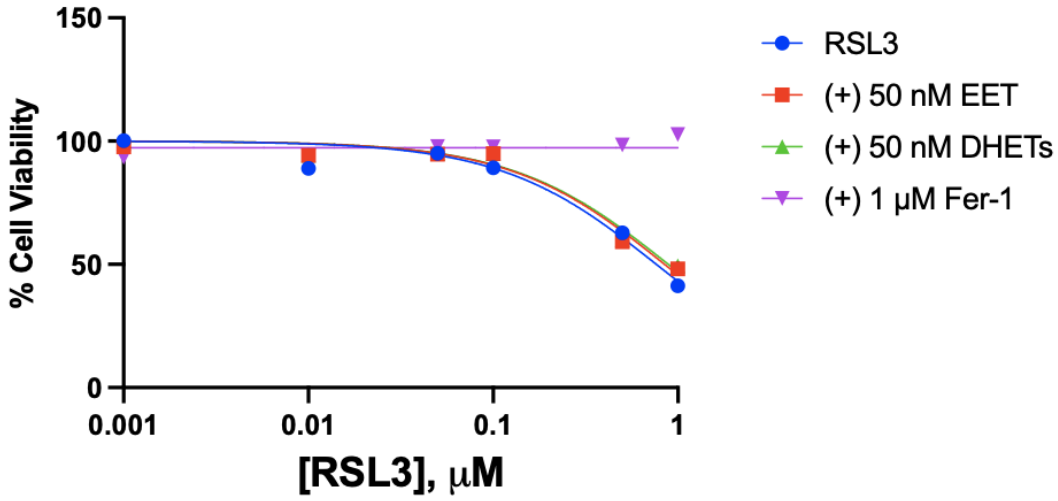


| | RSL3 | (+) 50 nM EET | (+) 50 nM DHETs | (+) 1 μM Fer-1 |
|---|---|---|---|---|
| Best-fit values | | | | |
| LogEC50 | -0.1166 | -0.07211 | -0.05159 | 616801 |
| HillSlope | -1.029 | -1.041 | -1.029 | -2.523e-006 |
| EC50 | 0.7645 | 0.8470 | 0.8880 | +infinity |

**Supplementary Figure 3.1.** EETs and DHETs do not protect against ferroptosis induced by RSL3 in AC16 cells.

**References**


1. M. Chaar, J. Kamta, S. Ait-Oudhia, Mechanisms, monitoring, and management of tyrosine kinase inhibitors–associated cardiovascular toxicities. *OncoTargets and therapy* **11**, 6227-6227 (2018).
2. G. S. Orphanos, G. N. Ioannidis, A. G. Ardavanis, Cardiotoxicity induced by tyrosine kinase inhibitors. *http://dx.doi.org/10.1080/02841860903229124* **48**, 964-970 (2009).
3. Y. Jin *et al.*, A Comprehensive Review of Clinical Cardiotoxicity Incidence of FDA-Approved Small-Molecule Kinase Inhibitors. *Frontiers in Pharmacology* **11**, 891-891 (2020).
4. M. H. Chen, R. Kerkelä, T. Force, Mechanisms of cardiac dysfunction associated with tyrosine kinase inhibitor cancer therapeutics. *Circulation* **118**, 84-95 (2008).
5. E. T. H. Yeh, C. L. Bickford, Cardiovascular complications of cancer therapy: incidence, pathogenesis, diagnosis, and management. *J Am Coll Cardiol* **53**, 2231-2247 (2009).
6. A. G. a. N. E. L. Howard Broder and Roberta, Chemotherapy and Cardiotoxicity. *Reviews in cardiovascular medicine* **9**, 75 , pmid = 18660728 , publisher = NIH Public Access (2008).
7. L. H. a. J. N. a. N. Z. a. S. H. G. a. M. C.-M. Mariana, Cardiotoxicity and Cardiac Monitoring Among Chemotherapy-Treated Breast Cancer Patients. *JACC: Cardiovascular Imaging* **11**, 1084-1093 , pmid = 30092967 , publisher = Elsevier (2018).
8. T. Aliwarga *et al.*, Enzymatic and free radical formation of cis- and trans-epoxyeicosatrienoic acids in vitro and in vivo. *Free Radical Biology and Medicine*, (2017).
9. T. Aliwarga, E. A. Evangelista, N. Sotoodehnia, R. N. Lemaitre, R. A. Totah, Regulation of CYP2J2 and EET Levels in Cardiac Disease and Diabetes. *International Journal of Molecular Sciences 2018, Vol. 19, Page 1916* **19**, 1916-1916 (2018).
10. J. Capdevila *et al.*, The oxidative metabolism of arachidonic acid by purified cytochromes P-450. *Biochemical and biophysical research communications* **101**, 1357-1363 (1981).
11. K. G. Proctor, J. R. Falck, J. Capdevila, Intestinal vasodilation by epoxyeicosatrienoic acids: arachidonic acid metabolites produced by a cytochrome P450 monooxygenase. *Circulation research* **60**, 50-59 (1987).
12. J. H. Capdevila, J. R. Falck, The arachidonic acid monooxygenase: from biochemical curiosity to physiological/pathophysiological significance. *Journal of lipid research* **59**, 2047-2062 (2018).
13. T. Aliwarga *et al.*, Enzymatic and free radical formation of cis- and trans-epoxyeicosatrienoic acids in vitro and in vivo. *Free Radical Biology and Medicine* **112**, 131-140 (2017).
14. E. A. Evangelista, R. N. Lemaitre, N. Sotoodehnia, S. A. Gharib, R. A. Totah, CYP2J2 expression in adult ventricular myocytes protects against reactive oxygen species toxicity. *Drug Metabolism and Disposition* **46**, 380-386 (2018).
15. J. D. Imig, Epoxyeicosanoids in Hypertension. *Physiological research* **68**, 695-695 (2019).
16. H. Qiu *et al.*, Soluble Epoxide Hydrolase Inhibitors and Heart Failure. *Cardiovascular Therapeutics* **29**, 99-111 (2011).

17. V. K. a. G. V. a. R. K. a. J. W. H. L. a. M. Q. H. a. H. I.-N. a. A. G. a. J. K. S. P. a. Aneesh, Site-directed deuteration of dronedarone preserves cytochrome P4502J2 activity and mitigates its cardiac adverse effects in canine arrhythmic hearts. *Acta Pharmaceutica Sinica B*, (2022).
18. E. A. Evangelista *et al.*, CYP2J2 Modulates Diverse Transcriptional Programs in Adult Human Cardiomyocytes. *Scientific Reports*, (2020).
19. Y. Benjamini, Y. Hochberg, Controlling the False Discovery Rate: A Practical and Powerful Approach to Multiple Testing. *Journal of the Royal Statistical Society: Series B (Methodological)* **57**, 289-300 (1995).
20. E. A. Evangelista, R. Kaspera, N. A. Mokadam, J. P. Jones, R. A. Totah, Activity, inhibition, and induction of cytochrome P450 2J2 in adult human primary cardiomyocytes. *Drug Metabolism and Disposition* **41**, 2087-2094 (2013).
21. C. L. Emma Lachaier 1 , Corinne Godin 1 , Zuzana Saidak 1 , Maxime Baert 2 , Momar Diouf 3 , Bruno Chauffert 4 , Antoine Galmiche. (Anticancer Research, 2014).
22. N. Bansal *et al.*, Strategies to prevent anthracycline-induced cardiotoxicity in cancer survivors. *Cardio-Oncology 2019 5:1* **5**, 1-22 (2019).
23. R. A. Clark *et al.*, Cardiotoxicity after cancer treatment: A process map of the patient treatment journey. *Cardio-Oncology* **5**, 1-11 (2019).
24. F. Ades *et al.*, Cardiotoxicity of systemic agents used in breast cancer. *Breast* **23**, 317-328 (2014).
25. J. Francis *et al.*, H & Reversible Cardiotoxicity With Tyrosine Kinase Inhibitors. *Clinical Advances in Hematology & Oncology* **8**, (2010).
26. L. Liu *et al.*, Epoxyeicosatrienoic Acids Attenuate Reactive Oxygen Species Level, Mitochondrial Dysfunction, Caspase Activation, and Apoptosis in Carcinoma Cells Treated with Arsenic Trioxide. *The Journal of Pharmacology and Experimental Therapeutics* **339**, 451-451 (2011).
27. D. Sacerdoti, P. Pesce, M. Di Pascoli, M. Bolognesi, EETs and HO-1 cross-talk. *Prostaglandins & Other Lipid Mediators* **125**, 65-79 (2016).
28. V. Samokhvalov *et al.*, PPARγ signaling is required for mediating EETs protective effects in neonatal cardiomyocytes exposed to LPS. *Frontiers in Pharmacology* **5**, 242-242 (2014).
29. J. Wang *et al.*, CYP2J2 and EETs Protect Against Lung Ischemia/Reperfusion Injury via Anti-in Vivo and in Vitro. *Cell Physiol Biochem* **35**, 2043-2054 (2015).
30. T. Aliwarga *et al.*, Higher Epoxyeicosatrienoic Acids in Cardiomyocytes-Specific CYP2J2 Transgenic Mice Are Associated with Improved Myocardial Remodeling. *Biomedicines*, (2020).
31. L. M. King *et al.*, Cloning of CYP2J2 gene and identification of functional polymorphisms. *Molecular pharmacology* **61**, 840-852 (2002).
32. S. Wu, C. R. Moomaw, K. B. Tomer, J. R. Falck, D. C. Zeldin, Molecular cloning and expression of CYP2J2, a human cytochrome P450 arachidonic acid epoxygenase highly expressed in heart. *The Journal of biological chemistry* **271**, 3460-3468 (1996).

33. D. H. Josephs, D. S. Fisher, J. Spicer, R. J. Flanagan, Clinical pharmacokinetics of tyrosine kinase inhibitors: Implications for therapeutic drug monitoring. *Therapeutic Drug Monitoring* **35**, 562-587 (2013).
34. S. A. Brown, J. C. Ray, J. Herrmann, Precision Cardio-Oncology: a Systems-Based Perspective on Cardiotoxicity of Tyrosine Kinase Inhibitors and Immune Checkpoint Inhibitors. *Journal of Cardiovascular Translational Research 2020 13:3* **13**, 402-416 (2020).

## Chapter 4

## Conclusion and Future Directions

The purpose of this dissertation was twofold: i) to characterize CYP2J2 expression in clear cell renal cell carcinoma (ccRCC) and ii) to investigate the cardioprotective nature of CYP2J2 and epoxyeicosatrienoic acids (EETs) against tyrosine kinase inhibitors (TKIs). To investigate the first half of the dissertation, we characterized CYP2J2, and other key enzymes involved in the CYP mediated arachidonic acid (AA) pathway using a multi-omics approach in matched ccRCC tumor tissues and histologically normal adjacent tissues (NAT). Through this investigation, we confirmed the mRNA and protein expressions of CYP2J2 were significantly elevated in ccRCC tumors compared to NAT which was consistent with literature reports (*1*). We also observed the significant downregulation of several key enzymes involved in the AA pathway in ccRCC tumors including the mRNA expressions of *CYP2C8,* several *CYP4* enzymes*,* phospholipase A2 enzymes, and *EPHX-2*, collectively referred to as leading-edge genes*.* The protein levels for most of the leading-edge genes were not significantly altered between the ccRCC tumor tissues and matched NAT except for soluble epoxide hydrolase (*EPHX-2)* in which protein levels were significantly decreased in tumor tissues.

Due to the observance of CYP2J2 overexpression and the downregulation of other CYPs involved in the AA pathway, we hypothesized that EETs levels would be increased in ccRCC tumors. And although we did show all four regioisomers of EETs were significantly increased in three ccRCC tumor and NAT pairs, EETs levels were either unchanged or downregulated in a different sample set containing three ccRCC and NAT pairs. Thus, a larger sample size is required in the future to validate the correlation between CYP2J2 overexpression and EET levels

in ccRCC tumors. All in all, we confirmed CYP2J2 overexpression in ccRCC and reported the AA pathway was significantly altered in ccRCC with several CYP enzymes significantly downregulated.

The discrepancy between CYP2J2 overexpression and downregulation of other CYPs identified in the AA pathway revealed a feature unique to CYP2J2 that is potentially attributable to its transcriptional regulation in ccRCC. Unlike the downregulated CYPs in ccRCC identified in this study, the promoter region of CYP2J2 consists of four Sp1 binding sites in the place of a TATA box. In cancer, post-translational modification, namely methylation, of Sp1 is critical for activating oncogenes (Sp1 demethylation) and silencing tumor suppressor genes (Sp1 methylation). DNA hypermethylation in ccRCC was revealed to have global transcriptomic consequences that was associated with poor prognosis (*2*). We therefore hypothesized that the DNA promoter region of CYP2J2 was demethylated in ccRCC compared to NAT resulting in the overexpression of CYP2J2. We confirmed the methylation of the DNA promoter region of CYP2J2 was lower in ccRCC tumors through a curated online database (UALCAN (*3*)). To determine the difference in DNA methylation in the promoter region, future work should perform ATAC-seq to map DNA methylation sites in ccRCC tumors and matched NAT. This would further confirm CYP2J2 is transcriptionally regulated via Sp1 binding in ccRCC which has not been reported in ccRCC.

The second half of this dissertation investigated the cardioprotective nature of CYP2J2 and EETs against TKI toxicity in primary human cardiomyocytes (HCMs). Previous investigations of CYP2J2 and EETs highlighted its role in preserving normal cardiac functions and/or reversing cardiotoxicity elicited by reactive oxygen species (ROS) or drugs (*4-6*). Therefore, we were

interested in determining if the addition of external EETs would protect human cardiomyocytes against TKI mediated damage. This was of particular interest as TKIs are first- and second-line drugs for many cancers including ccRCC yet the majority of TKIs on the market are associated with at least one adverse cardiac event. In our study, we demonstrate that the addition of external 11,12-EETs preserves cell viability against several TKIs in primary human cardiomyocytes. But due to the fragility of the cell line, we were unable to measure outputs other than cell viability such as ROS levels and caspase activity. Therefore, it would be of interest for future studies to identify and utilize different cell lines to broaden the breadth of investigation.

In conclusion, we investigated the role of CYP2J2 in two pathophysiological states—kidney cancer and drug induced cardiotoxicity. It appears the protective role of CYP2J2 and EETs is dependent on the context. For example, in cancer, CYP2J2 and EETs have been reported to promote tumorigenesis while in the heart, they are well documented to be protective. But rather than perceiving the duality of CYP2J2 as a double-edged sword, it is worthwhile to consider its relationship in cancer versus the heart as a delicate balancing act. In cancer, elevated levels of CYP2J2 appear to promote the tumor and thus, lower levels of CYP2J2 would be favored. However, in the heart, the opposite is true. Therefore, it would be of interest for future studies to further probe the duality of the role of CYP2J2 in cancer and the heart.

**References**


1. F. Zhang *et al.*, Identification of significant genes with prognostic influence in clear cell renal cell carcinoma via bioinformatics analysis. *Translational andrology and urology* **9**, 452-461 (2020).
2. M. M. a. E. Maher, Epigenetics of renal cell carcinoma: The path towards new diagnostics and therapeutics. *Genome Medicine* **2**, 1-10 (2010).
3. S. C. a. B. B. a. S. A. H. B. a. C. J. C. a. I. P.-R. a. B. V. S. K. C. a. S. V. Darshan, UALCAN: A Portal for Facilitating Tumor Subgroup Gene Expression and Survival Analyses. *Neoplasia (New York, N.Y.)* **19**, 649-658 , pmid = 28732212 , publisher = Neoplasia (2017).
4. A. V. Karkhanis *et al.*, Site-directed deuteration of dronedarone preserves cytochrome P4502J2 activity and mitigates its cardiac adverse effects in canine arrhythmic hearts. *Acta Pharmaceutica Sinica B*, (2022).
5. T. W. a. W. R. A. a. J. S. K. a. L. N. C. a. H. C. H. Aditi Das and Austin, CYP2J2 Molecular Recognition: A New Axis for Therapeutic Design. *Pharmacology & Therapeutics* **215**, 107601 , pmid = 32534953 , publisher = Pergamon (2020).
6. E. A. Evangelista, R. N. Lemaitre, N. Sotoodehnia, S. A. Gharib, R. A. Totah, CYP2J2 expression in adult ventricular myocytes protects against reactive oxygen species toxicity. *Drug Metabolism and Disposition* **46**, 380-386 (2018).